METHODS TO INCREASE THE EFFICIENCY OF PRECISE CRISPR GENOME EDITING

Der Fakultät für Lebenswissenschaften

der Universität Leipzig

eingereichte

D I S S E R T A T I O N

zur Erlangung des akademischen Grades

DOCTOR RERUM NATURALIUM

Dr. rer. nat.

vorgelegt

von Master of Science Biochemie Stephan Riesenberg

geboren am 02.06.1990 in Jena (Deutschland)

Leipzig, den 23.06.2020

THIS THESIS IS BASED ON THE FOLLOWING PUBLICATIONS:

1. **Targeting repair pathways with small molecules increases precise genome editing efficiency in pluripotent stem cells**
   S. Riesenberg and T. Maricic
   Nature Communications (2018)

2. **Simultaneous precise editing of multiple genes in human cells**
   S. Riesenberg, M. Chintalapati, D. Macak, P. Kanis, T. Maricic, and S. Pääbo
   Nucleic Acids Research (2019)

BIBLIOGRAPHISCHE DARSTELLUNG

Stephan Riesenberg

Methods to increase the efficiency of precise CRISPR genome editing

Fakultät für Lebenswissenschaften der Universität Leipzig

Angefertigt am Max Planck Institut für Evolutionäre Anthropologie Leipzig

Kumulative Dissertation

80 Seiten, 96 Literaturangaben, 21 Abbildungen, 9 Tabellen

Pluripotente Stammzellen haben das Potential, in unterschiedliche Zelltypen zu differenzieren und können genutzt werden, um organähnliche Mikrostrukturen zu generieren. Somit können molekulare Unterschiede verschiedenster künstlich differenzierter Gewebe, etwa zwischen Mensch und Schimpanse, anhand von pluripotenten Ausgangszellen untersucht werden. Da die Genome unserer nächsten ausgestorbenen Verwandten Neandertaler und Denisovaner aus konservierter DNA in alten Knochen sequenziert wurden, könnten ebenso Unterschiede zwischen Mensch und diesen Spezies oder dem letzten gemeinsamen Vorfahren untersucht werden. Dies erfordert jedoch die Generierung neandertalisierter Stammzellen durch künstliche Integration von Neandertalerallelen in humane Stammzellen, etwa durch die CRISPR Genomeditierungstechnik. Durch CRISPR kann ein DNA-Doppelstrangbruch an einer gewünschten Stelle im Genom eingefügt werden. Die zelluläre Reparatur des Doppelstrangbruchs ermöglicht dann die Editierung des Genoms. Basierend auf einer DNA-Matrize, die die gewünschte Modifikation trägt, kann das Genom an dieser Stelle präzise editiert werden. Die Effizienz präziser Editierung ist jedoch sehr niedrig im Vergleich zu unpräziser Reparatur. Um möglichst effizient neandertalisierte Stammzellen generieren zu können, wurden im Zuge dieser Doktorarbeit Methoden entwickelt, welche die präzise Genomeditierungseffizienz drastisch steigern. Zum einen wurde aus mehreren niedermolekularen Substanzen, welche mit Proteinen der DNA-Reparaturen interagieren, ein optimierter Mix entwickelt. Weiterhin konnte durch eine Mutation in einem zentralen Reparaturprotein die Effizienz für die Editierung eines einzelnen Gens auf 87% erhöht werden. Diese hohe Effizienz ermöglicht erstmals die präzise homozygote Editierung von vier Genen auf einmal in ein und derselben Zelle.

TABLE OF CONTENTS

SUMMARY 1

BACKGROUND 1

THESIS AIMS 4

RESULTS 5

Chapter 1 5

Chapter 2 6

CONCLUSIONS AND OUTLOOK 7

ZUSAMMENFASSUNG 8

HINTERGRUND 8

ZIELE DER DISSERTATION 12

ERGEBNISSE 12

Kapitel 1 12

Kapitel 2 13

SCHLUSSFOLGERUNGEN UND AUSBLICK 15

CHAPTER 1 PUBLICATION 16

‘Targeting repair pathways with small molecules increases precise genome editing efficiency in pluripotent stem cells’

CHAPTER 2 PUBLICATION 40

‘Simultaneous precise editing of multiple genes in human cells’

REFERENCES 63

ACKNOWLEDGEMENTS 69

CURRICULUM VITAE 70

DECLARATION OF INDEPENDENCE 78

AUTHOR CONTRIBUTION STATEMENT 79

SUMMARY

BACKGROUND

Embryonic stem cells (ESCs) and induced pluripotent stem cells (iPSCs) are both pluripotent, i.e. they have the potential to differentiate into different cell types. While ESCs need to be initially extracted from the blastocycst, iPSCs can be generated from differentiated cells like fibroblast by expression of the four transcription factors Oct4, Sox2, Klf4, and c-Myc (Takahashi and Yamanaka, 2006; Robinton and Daley, 2012). It has been shown that human iPSCs (hiPCSs) can be differentiated into all three germ layers and specific cell types (Murry and Keller, 2008), including hematopoetic stem cells, cardiomyocytes, dopaminergic neurons, immature pancreatic cells, and new differentiation protocols are constantly developed. Also, hESCs and hiPSCs have been used to generate miniaturized simplified organs called organoids including but not limited to those resembling the brain, gut, kidney and pancreas (Kaushik et al., 2018). Consequently, hiPSCs are a valuable tool to model different cell types and hold great promise for personalized disease treatment as they can be used to convert patient derived hiPSCs into cell types the body has lost or is unable to produce due to disease. They are also useful for comparisons between species. For example, brain organoids have been used to identify developmental differences between humans and great apes (Mora-Bermudez et al., 2016).

The genomes of the great apes and the genomes our closest extinct relatives, Neandertal and Denisovan, sequenced from DNA preserved in ancient bones allow us to infer what the genome of the last common ancestor of the modern human and those ancient humans looked like. The genetic changes acquired on the modern human lineage from this last common ancestor are what defines us as modern humans from a genomic perspective. With respect to the proteome, we differ by only 96 amino acid changes in 87 proteins that became fixed among modern humans during the half million years since we share a common ancestor with Neandertals and Denisovans (Prüfer et al., 2014). Genome editing techniques could be used to introduce such ancestral alleles and thus ancestralize hESCs or hiPSCs, which could then be differentiated into cell types or organoids of interest and thus allow investigation of molecular and cellular phenotypes of an extinct species. This could help elucidate what makes modern humans special by finding genetic causes or predispositions that in contrast to Neandertals allowed our species to successfully populate the

planet, live in complex societies, and constantly push for technical development. Unfortunately, state-of-the-art genome editing techniques are still not good enough to introduce many changes in the genome. Improvement of editing efficiencies is therefore a prerequisite to be able to study stem cells ancestralized for many alleles. It would obviously also be helpful in the study of any other biological phenomenon that relies on variants in multiple genes.

In genome editing, nucleases are used to cut a cellular genomic target of interest. Cellular repair of the DNA double-strand break (DSB) can then result in the modification of the target. The most widely used targetable nucleases are Zinc Finger Nucleases (ZNFs), Transcription Activator-like Effector Nucleases (TALENs), and Clustered Regularly Interspaced Short Palindromic Repeats Nucleases (CRISPR) (LaFountaine et al., 2015). ZNFs have three to six zinc finger protein domains that each recognize a specific three base pair sequence to bind the sequence of interest. TALENs consist of a series of four different TALE domains that can bind to guanine, adenine, cytosine, or thymine, respectively. While zinc finger protein domains or TALE domains are needed to guide the nuclease to the genomic sequence of interest, both ZNFs and TALENs are fused to a FokI domain that cleaves DNA if a FokI dimer is present. Thus, two closely spaced ZNFs or TALENs on opposite DNA strands are needed to introduce a DSB. In CRISPR Cas9 editing the Cas9 nuclease is directed to the genomic target by a guide RNA (gRNA) which carries a 20-nt sequence complementary to the sequence of interest. In contrast to ZNFs and TALENs, where proteins bind to DNA to guide the nuclease to the target sequence, CRISPR uses RNA to bind the target DNA. Consequently, CRISPR-Cas9 genome editing is preferable over ZNFs and TALENs, because no protein needs to be designed and RNA can be chemically synthesized in a cost effective way.

CRISPR is derived from bacteria and archea where they provide a form of acquired immunity against viruses. Bacterial genomes carry sequences of viral DNA from previous viral infections called ‘spacers’ which are a located in the CRISPR locus where they are separated by short repetitive sequences (Jiang and Marraffini, 2015). The CRISPR locus is transcribed and processed into pre-CRISPR RNA (pre-crRNA). Another short RNA called the trans-activating CRISPR RNA (tracRNA) hybridizes to the repetitive sequences in the pre-crRNA. RNase III cleavage then separates the crRNA/tracRNA hybrids that each now form a gRNA. *Cas* nuclease binds to the gRNA forming an active ribonucleoprotein that can cut DNA that is complementary to the spacer

sequence of the gRNA, if a protospacer adjacent motif (PAM) is present. Various prokaryotes have evolved many different CRISPR systems that are classified in six types based on *cas* gene content, mechanism of crRNA biogenesis and gRNA structure, as well as targeting mechanism (Makarova et al., 2018). The CRISPR system from S. *pyogenes* is relatively simple as only the Cas9 protein and a gRNA is needed for targeting of sequences adjacent to a PAM of the sequence NGG (Sapranauskas et al., 2011). Also, other comparably simple CRISPR enzymes like Cas12a (Cpf1) that rely on a TTTN PAM have been described (Zetsche et al., 2015). Such simple CRISPR systems can be used as tools outside of their original prokaryotic context for editing of genomes of yeast, plants, and animals, including humans (Cong et al., 2013; Khatodia et al., 2016).

Unfortunately, Cas9 might also cut off-target sequences when only few mismatches to its on-target sequence are present. While mismatches distant from the PAM are more prone to allow off-target cleavage, mismatches in the 8-10 nt 'seed region' next to the PAM almost always block Cas9 cleavage (Hsu et al., 2013). The Cas9 nuclease has two nuclease domains called HNH and RuvC. Inactivating one of those (D10A for RuvC, H840A for HNH) generates Cas9 enzymes that can only cleave one strand of the double stranded DNA. A single such Cas9 nickase only cuts one strand, but two close cuts on opposing DNA strands by two different Cas9 nickases produce a staggered DSB. Since it is very unlikely to have two off-target cuts in close proximity, and repair of potential off-target DNA nicks is very efficient and error-free, Cas9 double nicking can by employed to drastically reduce off-target DSBs (Shen et al., 2014).

DSBs are repaired by three competing pathways; Non-homologous End Joining (NHEJ), its backup pathway alternative NHEJ often referred to as Microhomology-mediated end joining (MMEJ), and homology directed repair (HDR) that uses the intact homologous sister chromatid as template (Nussenzweig and Nussenzweig, 2007; Williams and Schumacher, 2016). When a targeted DNA DSB is introduced by CRISPR-Cas9 repair of the DSB can edit the genome at this position. While NHEJ and MMEJ are error-prone and can introduce insertions or deletions (indels), HDR can be hijacked to precisely introduce a mutation of interest by providing a homologous exogenous DNA donor which carries the desired mutation. In NHEJ, the DSB is bound by Ku70/80 and DNA-dependent protein kinase catalytic subunit (DNA-PKcs). Subsequently, DNA-PKcs phosphorylates itself and downstream repair proteins that are recruited to the DSB, which is then sealed by DNA ligase 4 after processing of the DNA ends (Shrivastav

et al., 2008). If NHEJ is compromised, MMEJ can act as a backup repair pathway (Sfeir and Symington, 2015). A prerequisite for HDR is 5' resection of the DNA ends by the MRN (MRE11/RAD50/NBS1) complex, CtIP, and exonuclease 1, generating 3' overhangs on both sides of the DSB. The overhangs are then coated and stabilized by RPA. Stimulated by BRCA2, RPA-coated single stranded DNA forms of a RAD51 nucleoprotein filament that can bind a homologous DNA template. Following DNA synthesis by a polymerase this finally results in precisely repaired DNA as a crossover or non-crossover product (Shrivastav et al., 2008). Thus, HDR is competing with NHEJ and MMEJ and precise genome editing efficiencies, especially in hPSCs, are therefore usually low, ranging from 0.5-15% (Gonzalez et al., 2014; Yu et al., 2015). Consequently, precise HDR-dependent editing of more than one target gene has not yet been reported in animal cells. To overcome this, researches have tried to inhibit NHEJ to increase HDR efficiency but increases were at best moderate and the efficacy of inhibition of proteins involved in NHEJ by small molecules was inconsistent in the published literature (Greco et al., 2016).

THESIS AIMS

I aimed to develop methods to increase HDR efficiency to enable robust and efficient precise genome editing of a gene of interest and possibly simultaneous precise editing of multiple genes. In particular, these methods should allow future work that will revert nucleotide substitutions in genes that are fixed or almost fixed among present-day humans but occur in the ancestral, ape-like states in the Neandertal and Denisovan genomes back to their ancestral states. Obviously, such methods would also substantially reduce time and labor in many other areas of research.

RESULTS

Chapter 1

To increase HDR efficiency in CRISPR Cas9 genome editing, we tested the effect of 12 small molecules which target proteins of repair pathways on the efficiency of genome editing using Cas9 nuclease editing or Cas9D10A double nickase editing. The DNA-PKcs inhibitor NU7026 increased HDR for both Cas9 and Cas9D10A. Further, we found ATM-kinase activator Trichostatin A, inhibitor of Neddylation of CtIP MLN4924, and RPA-p53 interaction inhibitor NSC15520 to be enhancers of HDR with Cas9D10A. We then combined these compounds in the 'CRISPY mix', which is comprised of NU7026 (20μM), Trichostatin A (0.01μM), MLN4924 (0.5μM), NSC 15520 (5μM). The CRISPY mix achieves a 2.8-7.2-fold increase in HDR with Cas9D10A and 2.3-4-fold with Cas12a (Cpf1). This allows introduction of an intended nucleotide substitution in almost 50% of chromosomes and the introduction of a gene fragment encoding for a BFP in 27% of cells, the highest HDR efficiency in hiPSCs reported at the time of the study. CRISPY mix-treated edited cells had a normal karyotype and cell survival was only mildly reduced to 75%. Interestingly, the CRISPY mix increases HDR efficiency with staggered cuts and 5' overhangs (Cas9D10A and Cpf1) but not blunt cuts (Cas9), which suggests that these two types of cuts engage different repair pathways. While it is effective in three human and one chimpanzee stem cell lines tested, components of the CRISPY mix do not always increase HDR in HEK293, K562, CD4+ T cells, CD34+ progenitor cells, or primary human epidermal keratinocytes, suggesting that the repair pathways used are cell-type specific. Thus, a screen of small molecules is needed to optimize HDR in each cell type. A related patent has been filed (EP 17 165 784.4 | PCT/EP2018/059173, pending).

Chapter 2

In the study presented in chapter 1, inhibition of DNA-PKcs by NU7026 increased HDR efficiency moderately in most tested cell types regardless of the CRISPR enzyme used. Others showed that a lysine to arginine mutation at position 3753 in the DNA-PKcs protein increases homologous recombination in Chinese hamster ovary cells to 2- to 3-fold above those achieved when DNA-PKcs was completely absent (Shrivastav et al., 2008). We thus introduced the K3753R DNA-PKcs mutation (KR) in a hiPSC line carrying doxycycline inducible Cas9D10A and compared editing efficiency of 14 different genes in cells expressing wildtype or mutated DNA-PKcs. The KR mutation increased HDR for all targeted genes between 1.6- and 6.8-fold (average 3.3-fold) reaching up to 81% HDR. For a few genes the majority of genome editing events were deletions with microhomologies. We used Cas9 instead of Cas9D10A to introduce different break patterns and possibly different tendencies for MMEJ. When using Cas9, MMEJ decreased for all three genes and HDR could be drastically increased for two of them resulting in up to 87% HDR – the highest HDR efficiency described to date in animal cells. The HDR increase by KR mutation is independent of cell type (hiPSCs, HEK293, K562) and CRISPR enzyme used (Cas9D10A, Cas9, Cpf1). For simultaneous edits of three genes, a third of single cell-derived colonies carried the intended edits on all six chromosomes, and simultaneous editing of up to four genes (eight chromosomes) could be achieved in 6% of colonies. Cell survival decreased with number of genes targeted. The number of translocations per metaphase after bleomycin treatment, which introduces random DSBs, is not increased in KR cells (8% wildtype vs. 4% KR). Also, cells grown for three months with the KR mutation have a normal karyotype. We further determined the mutation rate of cells expressing DNA-PKcs wildtype or KR by whole genome sequencing of the DNA-PKcs wildtype ancestor cell line, the descendent cell line with the KR mutation, and triple edit clone of the KR line. The number of mutations fixed per passage in the genome is 21 in wildtype cells and 7 in KR cells. Importantly, we thus show that genome stability is not compromised and is potentially even better in KR cells.

Finally, we show that a novel DNA-PKcs inhibitor M3814 enhances HDR to an extent similar to the KR mutation in hiPSCs and K562 cells, and thus allows transient almost absolute HDR of CRISPR-induced DSB. Two related patents have been filed (EP 17 203 591.7, EP 18 215 071.4 | PCT/EP2018/059173, pending).

CONCLUSIONS AND OUTLOOK

I have achieved a drastic increase in precise genome editing efficiency by supplying the targeted cell with small molecules that enhance HDR and block competing repair pathways. I further accomplished the simultaneous precise editing of up to four genes when the key repair protein DNA-PKcs is mutated in the active site. In recent collaborations, I have used these methods to ancestralize 27 genes in stem cells. In most cases these were single gene edits. In future projects, successfully ancestralized hPSCs will be used for comparative analysis of human and ancestralized cells after differentiation into a variety of cell types and in organoids. Further exciting applications that could benefit from my methods are high-throughput genome-wide-association-screen validation of medically important alleles, disease modelling and drug screens, and simplified production of tailor-made animal models. In the future, I strive to develop methods to increase efficiencies of multiplexed precise genome editing even further to allow us to generate a hPSC line ancestralized for the whole proteome.

ZUSAMMENFASSUNG

HINTERGRUND

Embryonale Stammzellen (ESCs) und induzierte pluripotente Stammzellen (iPSCs) haben das Potenzial in verschiedene Zelltypen zu differenzieren. Während ESCs zunächst aus der Blastozyste extrahiert werden müssen, können iPSCs aus differenzierten Zellen wie Fibroblasten durch Expression der vier Transkriptionsfaktoren Oct4, Sox2, Klf4 und c-Myc erzeugt werden (Takahashi und Yamanaka, 2006; Robinton und Daley, 2012). Humane iPSCs (hiPCSs) können in alle drei Keimschichten, aber auch spezifische Zelltypen, einschließlich hämatopoetischer Stammzellen, Kardiomyozyten, dopaminerger Neuronen und unreifer Pankreaszellen, differenziert werden (Murry und Keller, 2008). Außerdem können aus hESCs und hiPSCs miniaturisierte vereinfachte Organe, sogenannte Organoide, die beispielsweise Gehirn, Darm, Niere oder Bauchspeicheldrüse ähneln, erzeugt werden (Kaushik et al., 2018). Auch können von Patienten stammende hiPSCs in Zelltypen umgewandelt werden, die aufgrund einer Krankheit abgestorben sind oder nicht mehr produziert werden können. Weiterhin können Stammzellen für Vergleichsstudien zwischen Arten genutzt werden. Beispielsweise wurden Gehirnorganoide verwendet, um Entwicklungsunterschiede zwischen Menschen und Menschenaffen zu identifizieren (Mora-Bermudez et al., 2016).

Die Genome der Menschenaffen und die Genome unserer nächsten ausgestorbenen Verwandten, Neandertaler und Denisovaner, welche aus in alten Knochen konservierter DNA sequenziert wurden, lassen auf das Genom des letzten gemeinsamen Vorfahren des modernen Menschen und dieser Urmenschen schließen. Die genetischen Veränderungen, die sich seit diesem letzten gemeinsamen Vorfahren auf der Evolutionslinie des modernen Menschen angereichert haben, sind die genetische Grundlage der Eigenschaften des modernen Menschen. Dabei unterscheiden wir uns in Bezug auf das Proteom nur durch 96 Aminosäureveränderungen in 87 Proteinen, die während der halben Million Jahre, seit wir einen gemeinsamen Vorfahren mit Neandertalern und Denisovanern haben, beim modernen Menschen fixiert wurden (Prüfer et al., 2014). Solche anzestralen Allele könnten durch Genomeditierungstechniken in hESCs oder hiPSCs eingefügt werden. Diese anzestralisierten Stammzellen könnten dann in gewünschte Zelltypen oder Organoide differenziert werden und somit die Untersuchung molekularer und zellulärer

Phänotypen einer ausgestorbenen Spezies ermöglichen. Eventuell könnten so genetische Ursachen oder Veranlagungen gefunden werden, die es unserer Spezies im Gegensatz zu Neandertalern ermöglichten, den Planeten erfolgreich zu bevölkern, in komplexen Gesellschaften zu leben und ständig auf technische Entwicklung zu drängen. Vorhandene Methoden zur Genomeditierung sind immer noch nicht effizient genug, um mehrere Veränderungen im Genom einzufügen. Die Erhöhung der Editierungseffizienz ist daher eine Grundvoraussetzung, um Stammzellen untersuchen zu können, die für viele Allele anzestralisiert wurden. Auch andere biologische Phänomene, die auf Veränderungen in mehreren Genen beruhen, könnten mit Hilfe solcher verbesserter Methoden untersucht werden.

Bei der Genomeditierung werden mit Hilfe von Nukleasen zielgerichtet gewünschte zelluläre Genomsequenzen geschnitten. Die zelluläre Reparatur des DNA-Doppelstrangbruchs (DSB) kann dann zur Modifikation der Zielsequenz führen. Die am häufigsten verwendeten zielgerichteten Nukleasen sind Zinkfinger-Nukleasen (ZNFs), Transkriptionsaktivator-ähnliche Effektor-Nukleasen (TALENs) und Clustered Regularly Interspaced Short Palindromic Repeats Nukleasen (CRISPR) (LaFountaine et al., 2015). ZNFs haben drei bis sechs Zinkfingerproteindomänen, die jeweils eine spezifische Sequenz mit drei Basenpaaren erkennen, um die Zielsequenz zu binden. TALENs bestehen aus einer Reihe von vier verschiedenen TALE-Domänen, die an Guanin, Adenin, Cytosin bzw. Thymin binden können. Während Zinkfingerproteindomänen oder TALE-Domänen benötigt werden, um die Nuklease zur Zielsequenz zu führen, werden sowohl ZNFs als auch TALENs an eine FokI-Domäne fusioniert, die nur DNA schneiden kann, wenn ein FokI-Dimer vorhanden ist. Um einen DSB zu generieren, werden daher zwei eng beieinander liegende ZNFs oder TALENs auf gegenüberliegenden DNA-Strängen benötigt. Bei CRISPR-Cas9 wird die Cas9-Nuklease durch eine guide-RNA (gRNA), die eine zur Zielsequenz komplementäre 20-nt-Sequenz trägt, zur genomischen Zielsequenz geführt. Bei ZNFs und TALENs wird die DNA-Zielsequenz durch Proteininteraktion gebunden, während bei CRISPR die Interaktion durch RNA erfolgt. Folglich ist CRISPR-Cas9 den ZNFs und TALENs vorzuziehen, da kein Protein hergestellt werden muss und RNA auf kostengünstige Weise chemisch synthetisiert werden kann.

CRISPR kommt ursprünglich aus Bakterien und Archaeen, in denen es eine Form der erworbenen Immunität gegen Viren darstellt. Bakteriengenome tragen Sequenzen viraler DNA aus früheren Virusinfektionen, die als "Spacer" bezeichnet werden und sich im CRISPR-Locus befinden, wo

sie durch kurze repetitive Sequenzen getrennt sind (Jiang und Marraffini, 2015). Der CRISPR-Locus wird transkribiert und zu pre-CRISPR-RNA (pre-crRNA) weiterverarbeitet. Eine andere kurze RNA, die als transaktivierende CRISPR-RNA (tracRNA) bezeichnet wird, hybridisiert mit den repetitiven Sequenzen in der pre-crRNA. Nachfolgender Verdau durch RNase III trennt dann die crRNA/tracRNA-Hybride, die jeweils eine gRNA bilden. Die *Cas*-Nuklease bindet an die gRNA und bildet so ein aktives Ribonukleoprotein, das die zur Spacersequenz der gRNA komplementäre DNA schneiden kann. Zusätzlich muss die zu schneidende Sequenz an ein kurzes Protospacer-Nachbarmotiv (PAM) angrenzen. Unter den Prokaryoten gibt es viele verschiedene CRISPR-Systeme, die basierend auf den *cas*-Genen, dem Mechanismus der crRNA-Biogenese und der gRNA-Struktur sowie dem Targeting-Mechanismus in sechs Typen eingeteilt werden (Makarova et al., 2018). Das CRISPR-System von S. *pyogenes* ist relativ einfach aufgebaut, da nur das Cas9-Protein und eine gRNA zum Finden der Zielsequenz benötigt wird, die an eine PAM der Sequenz NGG angrenzt (Sapranauskas et al., 2011). Außerdem wurden andere vergleichsweise einfache CRISPR-Enzyme wie Cas12a (Cpf1) beschrieben, die eine TTTN-PAM benötigen (Zetsche et al., 2015). Solche einfachen CRISPR-Systeme können als Werkzeuge außerhalb ihres ursprünglichen prokaryotischen Kontexts zur Genomeditierung von Hefen, Pflanzen und Tieren, einschließlich Menschen, verwendet werden (Cong et al., 2013; Khatodia et al., 2016).

Cas9 kann aber auch ungewünschte Sequenzen (Off-Target) schneiden, die der Zielsequenz sehr ähnlich sind. Sequenzen mit Basenfehlpaarungen distal zur PAM sind besonders anfällig für unerwünschtes Schneiden durch Cas9, während Fehlpaarungen in der Nähe der PAM einen falschen Schnitt meist verhindern (Hsu et al., 2013). Die Cas9-Nuklease hat zwei Nuklease-Domänen, die als HNH und RuvC bezeichnet werden. Die Inaktivierung einer dieser Domänen (D10A für RuvC, H840A für HNH) erzeugt Cas9-Enzyme, die nur einen Strang der doppelsträngigen DNA schneiden können. Eine einzelne solche Cas9-Nickase schneidet nur einen Strang, aber zwei nahe liegende Schnitte auf gegenüberliegenden DNA-Strängen durch zwei verschiedene Cas9-Nickasen erzeugen einen DSB mit DNA-Überhängen. Da es sehr unwahrscheinlich ist, dass zwei Schnitte außerhalb der Zielsequenz in unmittelbarer Nähe auftreten und die Reparatur potenzieller DNA-Einzelsstrangschnitte außerhalb des Ziels sehr effizient und fehlerfrei ist, kann das doppelte Einzelstrangschneiden durch Cas9-Nickasen unerwünschte DSB außerhalb der Zielsequenz drastisch reduzieren (Shen et al ., 2014).

DSB werden von der Zelle durch drei konkurrierende Reparaturwege geschlossen; non-homologous end joining (NHEJ), dessen Ersatz alternatives NHEJ, das häufig als microhomology-mediated end joining (MMEJ) bezeichnet wird, und homology directed repair (HDR), bei der das intakte homologe Schwesterchromatid als Vorlage verwendet wird (Nussenzweig und Nussenzweig, 2007; Williams und Schumacher, 2016). Wenn ein gezielter DSB durch CRISPR-Cas9 eingefügt wird, kann die Reparatur des DSB das Genom an dieser Position modifizieren. Während NHEJ und MMEJ fehleranfällig sind und Insertionen oder Deletionen (Indels) einfügen können, kann HDR ausgenutzt werden, um eine Zielmutation präzise einzufügen, indem ein homologer exogener DNA-Donor mit der gewünschten Mutation bereitgestellt wird. Bei NHEJ wird der DSB durch Ku70 80 und DNA-dependent protein kinase catalytic subunit (DNA-PKcs) gebunden. Anschließend phosphoryliert DNA-PKcs sich selbst und nachgeschaltete Reparaturproteine, die zum DSB rekrutiert werden, der dann durch DNA Ligase 4 geschlossen wird (Shrivastav et al., 2008). Wenn NHEJ blockiert ist, kann MMEJ als Ersatzreparaturmechanismus fungieren (Sfeir und Symington, 2015). Voraussetzung für HDR ist die 5'-Resektion der DNA-Enden durch den MRN-Komplex (MRE11/RAD50/NBS1), CtIP, und Exonuklease 1, wodurch auf beiden Seiten des DSB 3'-Überhänge entstehen. Die Überhänge werden dann durch RPA gebunden und stabilisiert. Durch BRCA2 stimuliert bildet die mit RPA beladene einzelsträngige DNA ein RAD51-Nukleoproteinfilament, das eine homologe DNA-Matrize binden kann. Nach der DNA-Synthese durch eine Polymerase führt dies schließlich zu präzise reparierter DNA als Crossover- oder Nicht-Crossover-Produkt (Shrivastav et al., 2008). Durch die Konkurrenz von HDR mit NHEJ und MMEJ ist die präzise Genomeditierungseffizienz durch HDR normalerweise gering und liegt zwischen 0,5 und 15% in hPSCs (Gonzalez et al., 2014; Yu et al., 2015). Folglich konnte nie mehr als ein Zielgen durch präzise HDR abhängige Genomeditierung in Tierzellen verändert werden. Um die HDR-Effizienz zu steigern, wurde z.B. versucht, NHEJ durch niedermolekulare Substanzen zu blockieren. Die HDR-Steigerung war jedoch nur mäßig und in verschiedenen Studien nicht klar reproduzierbar (Greco et al., 2016).

ZIELE DER DISSERTATION

Ziel dieser Arbeit war es, Methoden zu entwickeln, um die HDR-Effizienz bei der Genomeditierung zu steigern. Dabei wollte ich die robuste und effiziente präzise Editierung eines Zielgens und möglicherweise das gleichzeitige präzise Editieren mehrerer Zielgene erreichen. Insbesondere sollen diese Methoden zukünftige Arbeiten ermöglichen, bei denen Mutationen, die beim heutigen Menschen fixiert oder fast fixiert sind, aber im menschenaffenähnlichen Zustand in Neandertaler- und Denisovaner-Genomen vorkommen, wieder anzestralisiert und dann auf zellulärer Ebene verglichen werden können. Effizientere Methoden zur präzisen CRISPR-Genomeditierung würden auch in vielen anderen Forschungsbereichen von großem Nutzen sein.

ERGEBNISSE

Kapitel 1

Um die HDR-Effizienz bei der CRISPR-Cas9 Genomeditierung zu erhöhen, haben wir die Wirkung von 12 niedermolekularen Substanzen, die mit Proteinen aus Reparaturwegen interagieren, auf die Genomeditierungseffizienz mit Hilfe der Cas9-Nuklease oder der Cas9D10A-Doppel-Nickase getestet. Der DNA-PKcs-Inhibitor NU7026 steigerte die HDR sowohl für Cas9 als auch für Cas9D10A. Weiter fanden wir, dass der ATM-Kinase-Aktivator Trichostatin A, Inhibitor der Neddylierung von CtIP MLN4924, und der RPA-p53-Interaktionsinhibitor NSC15520 die HDR mit Cas9D10A steigern. Wir haben diese Substanzen dann im „CRISPY-Mix“ kombiniert, das aus NU7026 (20 µM), Trichostatin A (0,01 µM), MLN4924 (0,5 µM), NSC 15520 (5 µM) besteht. Der CRISPY-Mix erzielt mit Cas9D10A einen 2,8- bis 7,2 -fachen Anstieg der HDR und mit Cas12a (Cpf1) einen 2,3- bis 4 -fachen Anstieg. Dies ermöglicht die Einführung einer gewünschten Nukleotidsubstitution in fast 50% der Chromosomen und die Einführung eines Genfragments, das für ein fluoreszierendes Protein kodiert, in 27% der Zellen. Dies war zum Zeitpunkt der Studienveröffentlichung die höchste beschriebene HDR-Effizienz in hiPSCs. Mit CRISPY-Mix behandelte editierte Zellen hatten einen normalen Karyotyp und das Zellüberleben war nur geringfügig auf 75% reduziert. Interessanterweise erhöht der CRISPY-Mix die HDR-Effizienz bei DSB mit 5‘-DNA-Überhängen (Cas9D10A und Cpf1), jedoch nicht bei DSB ohne

Überhänge (Cas9). Dies deutet darauf hin, dass diese beiden Schnittarten unterschiedliche Reparaturwege aufweisen. Während der CRISPY-Mix in drei getesteten humanen und einer Schimpansen-Stammzelllinie wirksam ist, erhöhen dessen Komponenten nicht immer die HDR in HEK293-, K562-, CD4 + T-Zellen, CD34 + -Vorläuferzellen und primären humanen epidermalen Keratinozyten, was darauf hindeutet, dass die verwendeten Reparaturwege zelltypspezifisch sind. Um die HDR in einem gewünschten Zelltyp zu optimieren, ist daher ein dem Zelltyp entsprechendes Screening niedermolekularer Substanzen zu empfehlen. Im Zusammenhang mit dieser Studie wurde ein entsprechendes Patent angemeldet (EP 17 165 784.4 | PCT / EP2018 / 059173, ausstehend).

Kapitel 2

In der in Kapitel 1 vorgestellten Studie erhöhte die Inhibition von DNA-PKcs durch NU7026 die HDR-Effizienz in den meisten getesteten Zelltypen unabhängig vom verwendeten CRISPR-Enzym moderat. Andere Forscher zeigten, dass eine Mutation von Lysin zu Arginin an Position 3753 im DNA-PKcs-Protein die homologe Rekombination in Ovarialzellen des chinesischen Hamsters auf das 2- bis 3-fache über jene Effizienz erhöht, die erreicht wurde, wenn DNA-PKcs vollständig fehlt (Shrivastav et al., 2008). Wir fügten daher die K3753R-DNA-PKcs-Mutation (KR) in eine hiPSC-Linie ein, die Doxycyclin-induzierbares Cas9D10A trägt und verglichen die Editiereffizienz von 14 verschiedenen Genen in Zellen, die Wildtyp- oder mutiertes DNA-PKcs exprimieren. Die KR-Mutation erhöhte die HDR für alle Zielgene 1,6- bis 6,8 -fach (durchschnittlich 3,3 -fach) und erreichte bis zu 81% HDR. Bei einigen Genen waren die meisten DSB-Reparaturereignisse Deletionen mit Mikrohomologien. Daher haben wir Cas9 anstelle von Cas9D10A verwendet, um unterschiedliche DNA-Bruchmuster und möglicherweise unterschiedliche Tendenzen für MMEJ einzuführen. Bei Verwendung von Cas9 verringerte sich MMEJ für alle drei Gene und HDR konnte für zwei von ihnen drastisch erhöht werden, was zu einer HDR von bis zu 87% führte - der höchsten HDR-Effizienz, die bisher in tierischen Zellen beschrieben wurde. Die HDR-Steigerung durch die KR-Mutation ist unabhängig vom Zelltyp (hiPSCs, HEK293, K562) und dem verwendeten CRISPR-Enzym (Cas9D10A, Cas9, Cpf1). Nach gleichzeitiger Editierung von drei Genen trug ein Drittel der von Einzelzellen abgeleiteten Zellkolonien die beabsichtigten Mutationen auf allen sechs Chromosomen. Bei 6% der

Zellkolonien konnten eine gleichzeitige Editierung von bis zu vier Genen (acht Chromosomen) erreicht werden. Das Zellüberleben nahm mit der Anzahl der gleichzeitig editierten Gene ab. Die Anzahl der chromosomalen Translokationen pro Metaphase nach Bleomycin-Behandlung, die zufällige DSBs einfügt, ist in KR-Zellen nicht erhöht (8% Wildtyp gegenüber 4% KR). Außerdem behalten Zellen einen normalen Karyotyp, nachdem sie drei Monate lang mutiertes DNA-PKcs exprimiert haben. Ferner haben wir die Mutationsrate von Zellen, die DNA-PKcs-Wildtyp oder KR exprimieren, durch Sequenzierung des vollständigen Genoms der DNA-PKcs-Wildtyp-Vorläuferzelllinie, der daraus abgeleiteten Zelllinie mit der KR-Mutation und des Dreifacheditierungs-Klons der KR-Linie bestimmt. Die Anzahl der pro Passage im Genom fixierten Mutationen beträgt 21 in Wildtypzellen und 7 in KR-Zellen. Somit haben wir gezeigt, dass die Genomstabilität in KR-Zellen nicht beeinträchtigt und möglicherweise sogar verbessert ist.

Schließlich zeigen wir, dass der neuartige DNA-PKcs-Inhibitor M3814 transient eine nahezu absolute HDR von CRISPR-induziertem DSB ermöglicht, da er HDR in einem ähnlichen Ausmaß wie die KR-Mutation in hiPSCs und K562-Zellen steigert. Im Zusammenhang mit dieser Studie wurden zwei entsprechende Patente angemeldet (EP 17 203 591.7, EP 18 215 071.4 | PCT / EP2018 / 059173, ausstehend).

SCHLUSSFOLGERUNGEN UND AUSBLICK

Durch einen Mix aus niedermolekularen Substanzen, welche die HDR aktivieren und konkurrierende Reparaturwege in der Zelle blockieren, konnte ich die präzise Genomeditierungseffizienz drastisch steigern. Weiterhin konnte ich durch eine Mutation im aktiven Zentrum des Schlüsselreparaturproteins DNA-PKcs die gleichzeitige präzise Editierung von bis zu vier Zielgenen erreichen. Im Zuge dieser Arbeit und laufender Kooperationen habe ich mit Hilfe dieser Methoden 27 Gene in Stammzellen anzestralisiert. In den meisten Fällen handelte es sich um einzelne Genänderungen. In zukünftigen Projekten sollen erfolgreich anzestralisierte hPSCs zur vergleichenden Analyse von menschlichen und anzestralisierten Zellen nach Differenzierung in verschiedene Zelltypen und in Organoide verwendet werden. Weiterhin könnten die genomweite Assoziations-Screening-Validierung von medizinisch wichtigen Allelen, die Modellierung von Krankheiten und Wirkstoff-Screenings sowie die vereinfachte Erstellung maßgeschneiderter Tiermodelle von meinen Methoden profitieren. In Zukunft werde ich versuchen, die Effizienz der gleichzeitigen präzisen Genomeditierung noch weiter zu steigern, um beispielsweise eine für das gesamte Proteom anzestralisierte hPSC-Linie zu generieren.

CHAPTER 1

Targeting repair pathways with small molecules increases precise genome editing efficiency in pluripotent stem cells

S. Riesenberg (corresponding) and T. Maricic

Nature Communications (2018)

nature COMMUNICATIONS

ARTICLE

DOI: 10.1038/s41467-018-04609-7 OPEN

Targeting repair pathways with small molecules increases precise genome editing in pluripotent stem cells

Stephan Riesenberg[1] & Tomislav Maricic[1]

A now frequently used method to edit mammalian genomes uses the nucleases CRISPR/Cas9 and CRISPR/Cpf1 or the nickase CRISPR/Cas9n to introduce double-strand breaks which are then repaired by homology-directed repair using DNA donor molecules carrying desired mutations. Using a mixture of small molecules, the "CRISPY" mix, we achieve a 2.8- to 7.2-fold increase in precise genome editing with Cas9n, resulting in the introduction of the intended nucleotide substitutions in almost 50% of chromosomes or of gene encoding a blue fluorescent protein in 27% of cells, to our knowledge the highest editing efficiency in human induced pluripotent stem cells described to date. Furthermore, the CRISPY mix improves precise genome editing with Cpf1 2.3- to 4.0-fold, allowing almost 20% of chromosomes to be edited. The components of the CRISPY mix do not always increase the editing efficiency in the immortalized or primary cell lines tested, suggesting that employed repair pathways are cell-type specific.

[1] Department of Evolutionary Genetics, Max-Planck-Institute for Evolutionary Anthropology, Deutscher Pl. 6, 04103 Leipzig, Germany. Correspondence and requests for materials should be addressed to S.R. (email: stephan.riesenberg@eva.mpg.de)

Embryonic stem cells (ESCs) and induced pluripotent stem cells (iPSCs) have the potential to differentiate into many types of adult cells and have become an important tool, e.g., for disease modeling, drug development, and tissue repair[1,2]. Stem cells are especially powerful in combination with the ability to precisely and efficiently edit DNA with the CRISPR technology. Often, multiple edits are required to test sets of variant alleles (e.g., epistatic interaction that may be associated with a certain disease), but this requires development of methods that increase the editing efficiency of stem cells.

The bacterial nuclease CRISPR/Cas9 is now frequently used to accurately cut chromosomal DNA sequences in eukaryotic cells. The resulting DNA double-strand breaks (DSBs) are repaired by two competing pathways: non-homologous end joining (NHEJ) and homology-directed repair (HDR) (Fig. 1). In NHEJ, the first proteins to bind the cut DNA ends are Ku70/Ku80, followed by DNA protein kinase catalytic subunit (DNA-PKcs)[3]. The kinase phosphorylates itself and other downstream effectors at the repair site, which results in joining of the DNA ends by DNA ligase IV[4]. If this canonical NHEJ is repressed, the alternative NHEJ pathway becomes active[5], which, among other proteins, requires Werner syndrome ATP-dependent helicase. HDR is initiated when the MRN complex binds to the DSB[3]. In this case, DNA endonuclease RBBP8 (CtIP) removes nucleotides at the 5′-ends. Further resection produces long 3′ single-stranded DNA (ssDNA) overhangs on both sides of the DNA break[4]. These are coated and stabilized by the replication protein A (RPA) complex, followed by generation of a RAD51 nucleoprotein filament[3]. RAD52 facilitates replacement of RPA bound to ssDNA with RAD51 and promotes annealing to a homologous donor DNA[6]. Subsequent DNA synthesis results in precisely repaired DNA. In HDR, the protein kinase ataxia telangiectasia mutated (ATM) has a major role in that it phosphorylates at least 12 proteins involved in the pathway[3].

As NHEJ of Cas9-induced DSBs is error prone and frequently introduces short insertions and deletions (indels) at the cut site, it is useful for knocking out a targeted gene. In contrast, HDR allows precise repair of a DSB by using a homologous donor DNA. If the donor DNA provided in the experiment carries mutations, these will be introduced into the genome (precise genome editing). Repair with homologous ssDNA or double-stranded DNA (dsDNA) has been suggested to engage different pathways[7]. We will refer to targeted nucleotide substitutions using ssDNA donors (ssODNs) as "TNS" and targeted insertion of cassettes using dsDNA donors as knock-ins, respectively. In order to introduce a DSB, Cas9 requires the nucleotide sequence NGG (a "PAM" site) in the target DNA. Targeting of Cas9 is further determined by a guide RNA (gRNA) complementary to 20 nucleotides adjacent to the PAM site. However, the Cas9 may also cut the genome at sites that carry sequence similarity to the gRNA[8]. One strategy to reduce such off-target cuts is to use a mutated Cas9 that introduces single-stranded nicks instead of DSBs (Cas9n)[9]. Using two gRNAs to introduce two nicks on opposite DNA strands in close proximity to each other (double nicking) will result in a staggered DSB at the desired location, while reducing the risk of off-target DSBs, because two nicks close enough to cause a DSB are unlikely to occur elsewhere in the genome. Another strategy is to use Cpf1[10], a nuclease that introduces staggered cuts near T-rich PAM sites and causes less off-target DSBs than Cas9[11,12].

Efficiencies of TNS in human stem cells range from 15% down to as low as 0.5%[13,14] making the isolation of edited homozygous clones challenging. Several studies have tried to increase precise genome-editing efficiency by promoting HDR or decreasing NHEJ. Synchronization of cells to the S or G_2/M phase when homologous recombination occurs increases TNS efficiency in HEK cells (from 26% to 38%), human primary neonatal fibroblast (undetectable to 0.6%), and human ESCs (hESCs) (undetectable to 1.6%)[15], and knock-in efficiency in hESCs (from 7% to 41% after sorting)[16]. Improved knock-in efficiency was also achieved in HEK cells by suppressing repair proteins like Ku70/80 and DNA ligase IV with small interfering RNA (from 5% to 25%) or

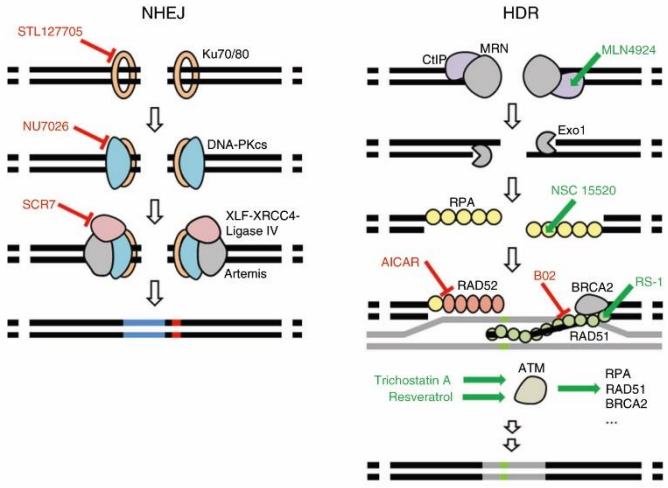

Fig. 1 Small molecules described or anticipated to target key proteins of NHEJ and HDR. Proteins are labeled with black text and inhibitors and enhancing small molecules are marked red and green, respectively. STL127705, NU7026, or SCR7 have been described to inhibit Ku70/80, DNA-PK, or DNA ligase IV, respectively. MLN4924, RS-1, Trichostatin A, or Resveratrol have been described to enhance CtIP, RAD51, or ATM, respectively. NSC 15520 has been described to block the association of RPA to p53 and RAD9. AICAR is an inhibitor of RAD52 and B02 is an ihibitor of RAD51. For simplicity, some proteins and protein interactions are not depicted

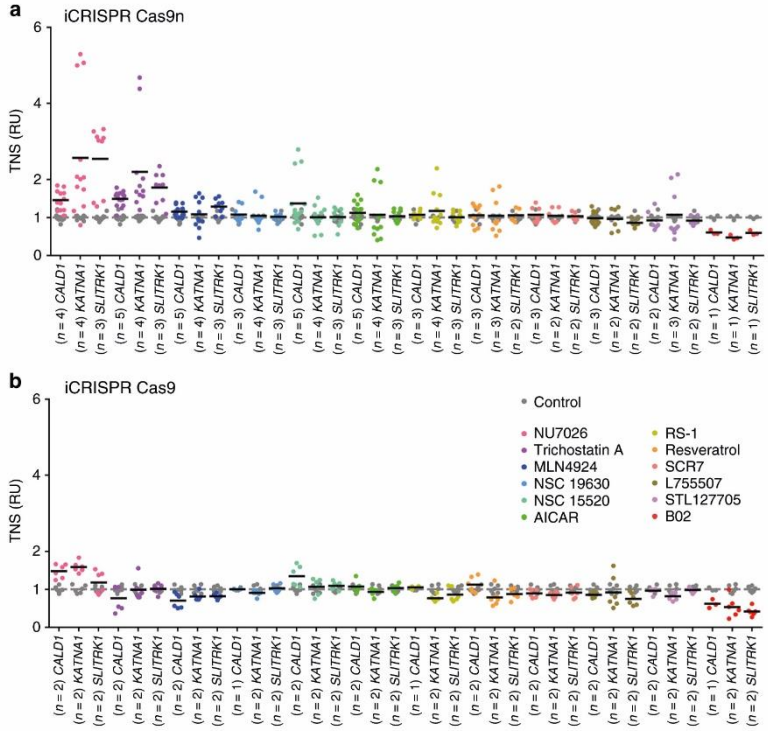

Fig. 2 Effects of small molecules on targeted nucleotide substitution (TNS) efficiency in iCRISPR hiPSCs. Shown are TNS efficiencies in *CALD1*, *KATNA1* and *SLITRK1* with Cas9n (**a**) and Cas9 (**b**) in 409-B2 iCRISPR hiPSCs. TNS efficiency is given in relative units (RU) with the mean of controls set to 1 to account for varying efficiency in different loci. Shown are technical replicates of *n* independent experiments. Data from Fig. 3 and Supplementary Fig. 3 are included. Gray and black bars represent the mean of the control and the respective small molecule, respectively. Concentrations used were 20 μM NU7026, 0.01 μM Trichostatin A, 0.5 μM MLN4924, 1 μM NSC 19630, 5 μM NSC 15520, 20 μM AICAR, 1 μM RS-1, 1 μM Resveratrol, 1 μM SCR7, 5 μM L755507, 5 μM STL127685, and 20 μM B02. Mean absolute percentages of TNS and indels of all technical replicates are shown in Supplementary Table 4

by coexpression of adenovirus type 5 proteins 4E1B55K and E4orf6, which mediate degradation of DNA ligase IV among other targets (from 5% to 36%)[17].

Several small molecules have been used to increase precise genome editing in various cell lines[16–26] (Supplementary Table 1). In summary, inhibitors of DNA-PK (NU7026 and NU7441) tend to increase precise genome-editing efficiency in different cell lines, while the effects of SCR7, L755507, and RS-1 are not consistent between cell lines. In this study, we systematically screen several small molecules and find a small-molecule mix that additively increases TNS and gene fragment insertion efficiency in pluripotent stem cells, when a DSB with 5′-overhangs is introduced with Cas9n double nicking or Cpf1 and a donor DNA is provided as ssODN. We also find that small molecules can have non-identical and even opposite effects on precise genome-editing efficiencies in different cell types, possibly explaining the inconsistencies reported in the literature.

Results

Individual small-molecule effects on editing efficiency. Here we test the above as well as other small molecules with respect to their efficiency to induce TNS in human iPSCs (hiPSCs). We identified additional molecules interacting with repair proteins listed in the REPAIRtoire database[27] by literature and database (ChEMBL[28]) search. The additional molecules we test, which have been described to either block NHEJ/alternative NHEJ or to activate or increase the abundance of proteins involved in HDR/damage-dependent signaling (Fig. 1 and Supplementary Table 2), are as follows: NU7026, Trichostatin A, MLN4924, NSC 19630, NSC 15520, AICAR, Resveratrol, STL127685, and B02.

We tested these molecules in hiPSC lines that we generated that carry doxycycline-inducible Cas9 (iCRISPR-Cas9) and Cas9 nickase with the D10A mutation (iCRISPR-Cas9n) integrated in their genomes[13]. After the delivery of gRNA (duplex of chemically synthesized crRNA and tracrRNA) and ssODN, cells were treated with small molecules for 24 h, expanded, their DNA was collected, targeted loci sequenced, and editing efficiency quantified (Supplementary Fig. 1 and Supplementary Fig. 2).

We tested the effect of different concentrations of each molecule on TNS in the three genes *CALD1*, *KATNA1*, and *SLITRK1* in 409B2 iCRISPR-Cas9n hiPSCs. For further experiments we used the concentration that gave the highest frequency of TNS, or if two or more concentrations gave a similarly high frequency we chose the lowest concentration (Supplementary

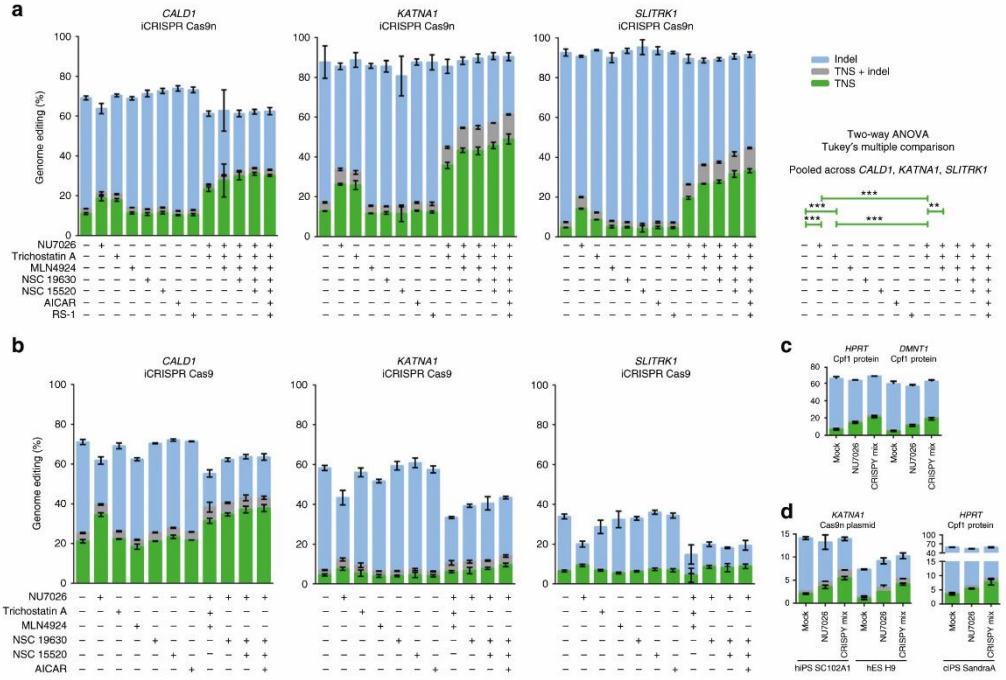

Fig. 3 Impact of small-molecule combinations on targeted nucleotide substitution (TNS) efficiency in iPSCs and hESCs. Shown are TNS efficiencies in *CALD1*, *KATNA1*, and *SLITRK1* with Cas9n and Cas9, and in *HPRT* and *DNMT1* with Cpf1. Small molecules have an additive effect on TNS efficiency with Cas9n (**a**) but not with Cas9 (**b**) in the 409-B2 iCRISPR hiPSC lines. TNS of *HPRT* and *DNMT1* in 409-B2 hiPSCs with recombinant Cpf1 was increased using the CRISPY mix as well (**c**). Using the CRISPY mix, TNS efficiency was also increased in SC102 A1 hiPSCs and H9 hESCs with plasmid-delivered Cas9n-2A-GFP (GFP-FACS enriched), and in chimpanzee SandraA ciPSCs with recombinant Cpf1 (**d**). Shown are TNS, TNS + indels, and indels with green, gray, or blue bars, respectively. Error bars show the SD of three technical replicates for **a**, **b**, and **c**, and two technical replicates for **d**. Concentrations used were 20 μM of NU7026, 0.01 μM of Trichostatin A, 0.5 μM MLN4924, 1 μM NSC 19630, 5 μM NSC 15520, 20 μM AICAR, and 1 μM RS-1. CRISPY mix indicates a small-molecule mix of NU7026, Trichostatin A, MLN4924, and NSC 15520. Statistical significances of TNS efficiency changes was determined using a two-way ANOVA and Tukey's multiple comparison pooled across the three genes *CALD1*, *KATNA1*, and *SLITRK1*. Genes and treatments were treated as random and fixed effect, respectively. *P*-values are adjusted for multiple comparison (**$P \leq 0.01$, ***$P \leq 0.001$). Overall, there was a clear treatment effect ($F(12, 24) = 32.954$, $P \leq 0.001$)

Fig. 3). Dependent on the targeted gene, we found that NU7026 increased TNS 1.5- to 2.5-fold in Cas9n cells (Fig. 2a and Supplementary Table 4) and 1.2- to 1.6-fold in Cas9 cells (Fig. 2b and Supplementary Table 4). Trichostatin A increased TNS 1.5- to 2.2-fold in Cas9n cells, whereas no increase was seen in Cas9 cells. MLN4924 increased TNS 1.1- to 1.3-fold in Cas9n cells, whereas it slightly reduced TNS in Cas9 cells. NSC 15520 increased TNS of *CALD1* 1.4-fold and 1.3-fold in Cas9n and Cas9 cells, respectively, but had no effect on TNS of *KATNA1* and *SLITRK1*. NSC 19630, AICAR, RS-1, Resveratrol, SCR7, L755507, and STL127685 showed no clear effect on TNS frequency in the three genes in Cas9n cells and had no effect or decreased TNS in Cas9 cells. B02 reduced TNS in all three genes in both cell lines (Fig. 2).

Additive effect of small molecules. To test whether combinations of these compounds enhance TNS, we combined compounds that individually increased TNS for at least one gene in Cas9n cells and never decreased TNS. Those are NU7026, Trichostatin A, MLN4924, NSC 19630, NSC 15520, AICAR, and RS-1. The results are shown in Fig. 3a, b. Treatment with NU7026 or Trichostatin A resulted in 2.3- or 1.8-fold higher TNS in Cas9n cells (Tukey's pair-wise post-hoc comparisons: $p < 0.001$) (Fig. 3a) and combinations of NU7026 and Trichostatin A resulted in 1.3 to 1.6 times higher TNS than with either compound alone ($p < 0.001$). Addition of MLN4924 to the mix of NU7026 and Trichostatin A lead to an additional 1.3-fold increase in TNS ($p < 0.01$). Further addition of NSC 15520 slightly increased the mean TNS in Cas9n cells, without reaching statistical significance. Addition of NSC 19630, AICAR, and RS-1 had no measurable effect on TNS. We conclude that the mix of small molecules that increases the frequency of TNS with Cas9n the most (although we admittedly could not test all combinatorial possibilities) is a combination of NU7026 (20 μM), Trichostatin A (0.01 μM), MLN4924 (0.5 μM), and NSC 15520 (5 μM). This "CRISPY" nickase mix results in an increase of TNS of 2.8-fold (from 11% to 31%) for *CALD1*, 3.6-fold (from 12.8% to 45.8%) for *KATNA1*, and 6.7-fold (from 4.7% to 31.6%) for *SLITRK1* in the iCRISPR 409-B2 iPSC line (NSC 19630 has no effect on TNS efficiency).

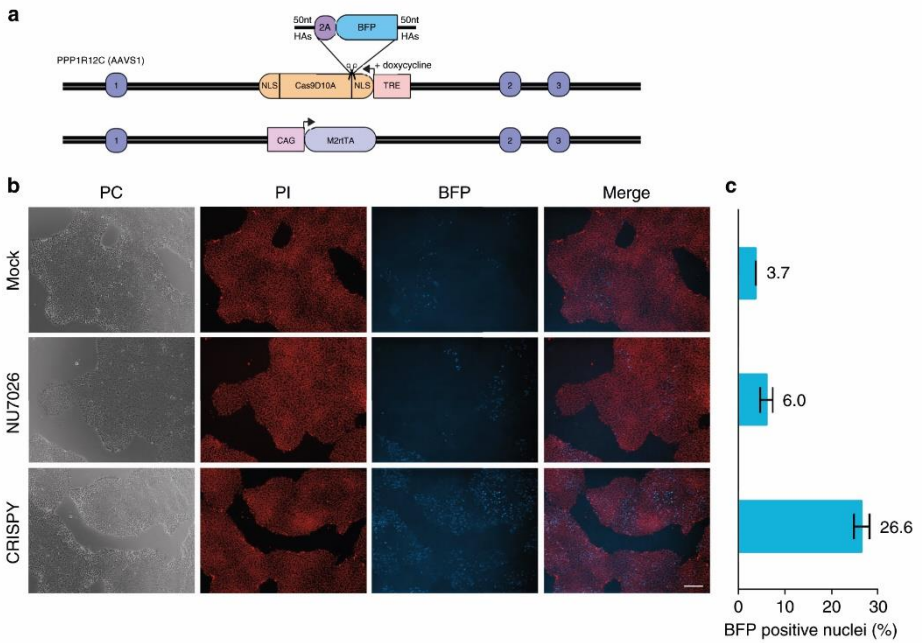

Fig. 4 Impact of the CRISPY mix on gene fragment insertion efficiency in iCRISPR hiPSCs. Shown is the insertion efficiency of a gene fragment coding for a blue fluorescent protein (BFP) in the heterozygous AAVS1 iCRISPR locus using a single-stranded DNA donor in 409-B2 iCRISPR-Cas9n hiPSCs. The design of the mtagBFP2[30] ssODN donor and the iCRISPR system is shown in **a**. We inserted a 871 nt (including 50 nt homology arms) sequence coding for a 2A-self cleaving peptide in front of a blue fluorescent protein (BFP), directly after the N-terminal nuclear localization signal sequence (NLS) of the Cas9n in the heterozygous AAVS1 iCRISPR locus[13]. If the sequence is inserted, doxycycline will lead to expression of nucleus-imported BFP. Representative images of the mock, NU7026, and CRISPY mix treatment, after 7 days of BFP expression are shown in **b** as phase contrast (PC), propidium iodide nuclei staining (PI), mtagBFP2 expression (BFP), and merge of PI and BFP. Two images (× 50 magnification, white size bar 200 µm) from each of three technical replicates for the respective treatments were used to quantify the percentage of cells with BFP insertion using ImageJ (**c**)

When we used Cas9, which introduces blunt-ended DSBs, no significant effect was seen when adding other small molecules in addition to NU7026 (Fig. 3b). In contrast, the CRISPY mix together with Cpf1 ribonucleoprotein, which produces staggered DNA cuts, introduced by electroporation in 409-B2 hiPSCs, increased TNS 2.9-fold for *HPRT* and 4.0-fold for *DNMT1* (Fig. 3c). Addition of only NU7026 increased TNS 2.1-fold for *HPRT* and 2.4-fold for *DNMT1*. To test whether the CRISPY mix increases TNS in other pluripotent stem cell lines, we edited the gene *KATNA1* in SC102A1 hiPSCs and H9 hESCs using Cas9n plasmid electroporation and *HPRT* in chimpanzee iPSCs using Cpf1 ribonucleoprotein. TNS increased 2.6-fold, 2.8-fold, and 2.3-fold, respectively, and the increase was bigger than when using NU7026 alone (Fig. 3d).

Next, we tested the toxicity of each small-molecule and molecule combinations including the CRISPY mix on iCRISPR 409-B2 hiPSCs using a resazurin assay[29]. After *KATNA1* editing with Cas9n double nicking and CRISPY mix treatment for 24 h cells showed a viability of 75% compared with no small-molecule treatment, with no additive toxic effect of its components (Supplementary Fig. 4A). Importantly, when we simulated five rounds of editing, each round consisting of passaging cells with the lipofection reagent and CRISPY mix followed with 3 days of recovery, the cells had a healthy karyotype with no numerical or large-scale chromosomal aberrations as shown by trypsin-induced Giemsa staining (Supplementary Fig. 4B).

Furthermore, we tested whether the CRISPY mix can also increase efficiency of insertion of a gene fragment. We inserted a 871 nt (including 50 nt homology arms) sequence encoding a 2A-self cleaving peptide in front of an enhanced blue fluorescent protein (BFP)[30] in the AAVS1 iCRISPR locus (Fig. 4a and Supplementary Table 3). If the sequence is inserted, doxycycline will lead to expression of nucleus-imported BFP. Nuclei positive for BFP increased 7.1-fold (26.6%) compared with the no-CRISPY control (3.7%), whereas NU7026 alone lead to an increase of 1.6-fold (6%) (Fig. 4b, c) showing that the CRISPY mix increases efficiency of insertion of a gene fragment in hiPSCs.

Non-identical small-molecule effects in different cell types. Finally, we tested whether the CRISPY mix or other combinations of its comprising small molecules increase the efficiency of TNS in non-pluripotent cells. We edited the *HPRT* gene with Cpf1 in two immortalized cell lines (HEK293, K562) and primary cells ($CD4^+$ T cells, $CD34^+$ progenitor cells, and primary human epidermal keratinocytes (HEKa)). TNS percentages are shown in Supplementary Fig. 5 and corresponding cell viabilities after small-molecule treatments are shown in Supplementary Fig. 6. Whereas MLN4924 decreases TNS efficiency in all of those cell lines, other CRISPY components have effects that can differ in different cell lines. NU7026 is the only single small molecule that clearly increases TNS in HEK293 (3.0-fold), K562 cells (4.0-fold),

$CD4^+$ T (3.0-fold), and $CD34^+$ progenitor cells (1.7-fold). However, it decreases TNS in HEKa cells (3.1-fold) (Supplementary Fig. 5). The TNS increase was even higher when the CRISPY mix without MLN4924 was used (6.6-fold and 2.6-fold) in primary $CD4^+$ T cells and $CD34^+$ progenitor cells, respectively (Supplementary Fig. 5B). Admittedly, the achieved TNS efficiencies for $CD34^+$ progenitor cells were very low (increase of 0.24% to 0.63%) and for the other cells lines around 5% with small-molecule treatment, which suggest that the targeted *HPRT* locus is difficult to edit with the donor we used. The treatment with this mix decreased the cell viability to 59 and 65% compared with the electroporation control for $CD4^+$ T cells and $CD34^+$ progenitor cells, respectively (Supplementary Fig. 6B).

Discussion

Previously, it has been shown that types of cuts introduced by distinct CRISPR enzymes engage different repair pathways, because 5′-overhanging ends yielded higher levels of HDR than 3′-overhangs or blunt ends[7]. This is in line with our observation that Trichostatin A and MLN4924 increase TNS with 5′-overhang-inducing Cas9n and Cpf1 but have no TNS increasing effect with blunt end-inducing Cas9.

In pluripotent stem cells, NU7026, Trichostatin A, MLN4924, and NSC 15520 (CRISPY mix components) increase TNS with Cas9n and Cpf1 when applied either singly or together (Figs 2a and 3a, c and d). NU7026 inhibits DNA-PK (Fig. 1), a major complex in NHEJ pathway[3], and has been previously shown to increase knock-in efficiency in hiPSCs[25]. Trichostatin A activates an ATM-dependent DNA-damage signaling pathway[31]. MLN4924 inhibits the Nedd8-activating enzyme and has been shown to inhibit the neddylation of CtIP, which leads to an increase of the extent of DNA end resection at strand breaks, thereby promoting HDR[32] by leaving ssDNA stabilized by RPA that can undergo recombination. NSC 15520 prevents the association of RPA with p53 and RAD9[33,34], possibly increasing the abundance of RPA available, which could favor HDR. Although RAD51 is obviously important for classical homologous recombination with dsDNA[3], it is possible that RAD52, rather than RAD51, could be responsible for HDR with ssDNA donors, as RAD52 is needed for annealing of ssDNA[6]. Our observation that inhibition of RAD52 by AICAR has no effect on TNS efficiency, while inhibition of RAD51 by B02 halved it, suggests that RAD51 and not RAD52 is important for precise editing with ssODN of both blunt and 5′-staggered ends in hiPSCs. This is in contrast to Bothmer et al.[7] who described that knockdown of RAD51 has no effect on precise editing with ssODN in U2OS cells. RS-1, SCR7, and L755507 for which there are conflicting reports on their capacity to increase precise genome editing (Supplementary Table 1) showed no measurable effect in our hands on TNS neither in the Cas9 or the Cas9n hiPSCs.

Although the CRISPY mix increases TNS more than any individual component it comprised in all four pluripotent stem cell lines tested (three human and one chimpanzee) (Fig. 3a, c, and d), this is not the case for other cell lines tested (Supplementary Fig. 5). In fact, our results (Fig. 3. and Supplementary Fig. 5) show that small molecules and their combinations can have opposite effects on TNS in different cell lines. This could be due to that cell lines rely on different repair proteins or repair pathways.

In line with this interpretation are studies that show that hESCs and iPSCs possess very high DNA repair capacity that decreases after differentiation[35,36]. CtIP expression and proteins levels, and consequently the relative length of resection of DSBs are increased in iPSCs[37], thereby promoting HDR initiation. CtIP levels can be further artificially increased by inhibiting its neddylation through MLN4924. Our results show that treatment with MLN4924 alone or in a small-molecule mix increases HDR efficiencies when using Cas9n double nicking or Cpf1 in ESCs and iPSCs (Figs 2a, 3a, c, d), whereas it decreases HDR efficiencies in the immortalized and primary cell lines tested (Supplementary Fig 5). Jimeno et al.[32] showed that cell protein neddylation not only affects the choice between NHEJ and HDR, but also controls the balance between different HDR subpathways, as MLN4924 treatment reduced the gene conversion efficiency, whereas it increased single-strand annealing efficiency[32]. It is tempting to speculate that pluripotent stem cells, but not the tested non-pluripotent cells, can efficiently utilize an HDR subpathway that is characterized by CtIP-dependent hyper-resection when confronted with a staggered CRISPR-enzyme-induced DSB and supplied with ssODN. Cell-type-specific reliance on different repair pathways may also explain some of the inconsistencies between studies (Supplementary Table 1), e.g., the DNA ligase IV inhibitor SCR7 and RAD51 enhancer RS-1 increase precise genome editing in some cell types but not in others. Thus, it may be necessary to screen small molecules for their effects on CRISPR editing in each cell type of interest.

In summary, we show that CRISPY mix of small molecules increases TNS in all four pluripotent stem cell lines we tested, after a DSB with 5′-overhangs was introduced with a Cas9n or Cpf1 and a donor DNA was provided as ssODN. We also show that none of the tested small molecules clearly increased TNS in all cell types, which supports the idea of cell-type-specific mechanisms of DNA repair. This suggests that for increasing precise editing efficiency in a cell type of interest the corresponding small-molecule screen needs to be carried out.

Methods

Cell culture. Stem cell lines cultured for this project included human 409-B2 hiPSC (female, Riken BioResource Center) and SC102A1 hiPSC (male, BioCat GmbH), chimpanzee SandraA ciPSC (female, Mora-Bermúdez et al.[38]), as well as H9 hESC (female, WiCell Research Institute, Ethics permit AZ 3.04.02/0118). Stem cell lines were grown on Matrigel Matrix (Corning, 35248) and mTeSR1 (Stem Cell Technologies, 05851) with mTeSR1 supplement (Stem Cell Technologies, 05852) was used as culture media. Non-pluripotent cell types and their respective media used were as follows: HEK293 (ECACC, 85120602) with Dulbecco's modified Eagle's medium/F-12 (Gibco, 31330-038) supplemented with 10% fetal bovine serum (FBS) (SIGMA, F2442) and 1% NEAA (SIGMA, M7145); K562 (ECACC, 89121407) with Iscove's modified Dulbecco's media (ThermoFisher, 12440053) supplemented with 10% FBS; $CD4^+$ T (HemaCare, PB04C-1) with RPMI 1640 (ThermoFisher, 11875-093) supplemented with 10% FBS and activated with Dynabeads Human T-Activator (CD3/CD28) (ThermoFisher, 11131D); $CD34^+$ progenitor (HemaCare, M34C-1) with StemSpan SFEM (Stem Cell, 09600) supplemented with StemSpan CC110 (Stem Cell, 02697); and HEKa (Gibco, C0055C) with Medium 154 (ThermoFisher, M154500) and Human Keratinocyte Growth Supplement (ThermoFisher, S0015). Cells were grown at 37 °C in a humidified incubator gassed with 5% CO_2. Media was replaced every day for stem cells and every second day for non-pluripotent cell lines. Cell cultures were maintained 4–6 days until ~ 80% confluency and subcultured at a 1:6 to 1:10 dilution. Adherent cells were dissociated using EDTA (VWR, 437012 C). The media was supplemented with 10 μM Rho-associated protein kinase (ROCK) inhibitor Y-27632 (Calbiochem, 688000) after cell splitting for one day in order to increase cell survival.

Generation and validation of iCRISPR cell lines. 409-B2 hiPSCs were used to create an iCRISPR-Cas9 line as described by Gonzalez et al.[13] (GMO permit AZ 54-8452/26). In brief, the iCRISPR system was introduced using two transcription activator-like effector nucleases targeting the AAVS1 locus and two donors that are responsible for doxycycline-inducible Cas9 expression, namely Puro-Cas9 donor and AAVS1-Neo-M2rtTA. Each inserted cassette has a either a puromycin or a geneticin resistance gene, in order to select for colonies, which have inserted both iCRISPR cassettes. For the production of iCRISPR-Cas9n line Puro-Cas9 donor was subjected to site-directed mutagenesis with the Q5 mutagenesis kit to introduce the D10A mutation (New England Biolabs, E0554S). Primers were ordered from IDT (Coralville, USA) and are shown in Supplementary Table 3. Expression of the pluripotency markers SOX2, OCT-4, TRA1-60, and SSEA4 in iCRISPR lines

was validated using the PSC 4-Marker immunocytochemistry kit (Molecular Probes, A24881) (Supplementary Fig. 7). Quantitative PCR was used to confirm doxycycline-inducible Cas9 or Cas9n expression and digital PCR was used to exclude off-target integration of the iCRISPR cassettes (Supplementary Fig. 8).

Small molecules. Commercially available small molecules used in this study were NU7026 (SIGMA, T8552), Trichostatin A (SIGMA, T8552), MLN4924 (Adooq BioScience, A11260), NSC 19630 (Calbiochem, 681647), NSC 15520 (ChemBridge, 6048069), AICAR (SIGMA, A9978), RS-1 (Calbiochem, 553510), Resveratrol (Selleckchem, S1396), SCR7 (XcessBio, M60082-2s), L755507 (TOCRIS, 2197), B02 (SIGMA, SML0364), and STL127685 (Vitas-M). STL127685 is a 4-fluorophenyl analog of the non-commercially available STL127705. Stocks of 15 mM (or 10 mM for NU7026) were made using dimethylsulfoxide (DMSO) (Thermo Scientific, D12345). Solubility is a limiting factor for NU7026 concentration. Suitable working solutions for different concentrations were made so that addition of each small molecule accounts for a final concentration of 0.08% (or 0.2% for NU7026) DMSO in the media. Addition of all small molecules would lead to a final concentration of 0.7% DMSO.

Design of gRNAs and ssODNs. We chose to introduce one desired mutation in three genes *CALD1*, *KATNA1*, and *SLITRK1* back to the state of the last common ancestor of human and Neanderthal[39]. gRNA pairs for editing with the Cas9n nickase were selected to cut efficiently at a short distance from the desired mutation and from the respective partnering gRNA. The efficiency was estimated with the sgRNA scorer 1.0 tool[40] as a percentile rank score. Donor ssODNs for nickase editing were designed to have the desired mutation and Cas9-blocking mutations to prevent re-cutting of the locus and had 50 nt homology arms upstream and downstream of each nick (Supplementary Fig. 2). gRNA of the nickase gRNA pair that cuts closer to the desired mutation was used for Cas9 nuclease editing together with a 90 nt ssODN centered at the desired mutation and containing a Cas9-blocking mutation (Supplementary Fig. 2). ssODNs for editing of *HPRT* and *DNMT1* using Cpf1 were designed to contain a blocking mutation near the PAM site and an additional mutation near the cut. gRNAs (crRNA and tracR) and ssODN were ordered from IDT (Coralville, USA). ssODNs and crRNA targets are shown in Supplementary Table 3.

Lipofection of oligonucleotides. Cells were incubated with media containing 2 µg/ml doxycycline (Clontech, 631311) 2 days prior to lipofection. Lipofection (reverse transfection) was done using the alt-CRISPR manufacturer's protocol (IDT) with a final concentration of 7.5 nM of each gRNA and 10 nM of the respective ssODN donor. In brief, 0.75 µl RNAiMAX (Invitrogen, 13778075) and the respective oligonucleotides were separately diluted in 25 µl OPTI-MEM (Gibco, 1985-062) each and incubated at room temperature for 5 min. Both dilutions were mixed to yield 50 µl of OPTI-MEM including RNAiMAX, gRNAs and ssODNs. The lipofection mix was incubated for 20–30 min at room temperature. During incubation cells were dissociated using EDTA for 5 min and counted using the Countess Automated Cell Counter (Invitrogen). The lipofection mix, 100 µl containing 25,000 dissociated cells in mTeSR1 supplemented with Y-27632, 2 µg/ml doxycycline and the respective small molecule(s) to be tested were thoroughly mixed and put in 1 well of a 96-well plate covered with Matrigel Matrix (Corning, 35248). Media was exchanged to regular mTeSR1 media after 24 h.

Ribonucleoprotein electroporation. The recombinant *A.s.* Cpf1 protein and electroporation enhancer was ordered from IDT (Coralville, USA) and nucleofection was done using the manufacturer's protocol, except for the following alterations. Nucleofection was done using the B-16 program (or U-14 for $CD34^+$ progenitor cells) of the Nucleofector 2b Device (Lonza) in cuvettes for 100 µl Human Stem Cell nucleofection buffer (Lonza, VVPH-5022), or Human T Cell nucleofection buffer for $CD4^+$ T cells (Lonza, VPA-1002), and Human CD34 Cell nucleofection buffer for $CD34^+$ progenitor cells (Lonza, VPA-1003), containing 1 million cells of the respective lines, 78 pmol electroporation enhancer, 0.3 nmol gRNA, 200 pmol ssODN donor (600 pmol for $CD4^+$ T cells), and 252 pmol Cpf1. Cells were counted using the Countess Automated Cell Counter (Invitrogen).

Fluorescence-associated cell sorting. Introduction of 2 µg plasmid DNA (pSpCas9n(BB)-2A-GFP (PX461) was a gift from Feng Zhang Addgene 48140[41]) into cells not expressing Cas9 inducably was done using the B-16 program of the Nucleofector 2b Device (Lonza) in cuvettes for 100 µl Human Stem Cell nucleofection buffer (Lonza, VVPH-5022) containing 1 million of either SC102A1 hiPSC or H9 hESC. Cells were counted using the Countess Automated Cell Counter (Invitrogen). Twenty-four hours after nucleofection, cells were dissociated using Accutase (SIGMA, A6964), filtered to obtain a single-cell solution, and subjected to fluorescence-associated cell sorting (FACS) for green fluorescent protein (GFP)-expressing cells. During sorting with the BD FACSAria III (Becton-Dickinson) cells were kept at 4 °C in mTeSR1 supplemented with Y-27632. 48 h after sorting cells were subjected to lipofection with gRNAs, ssODNs, and treatment with small molecules.

Illumina library preparation and sequencing. Three days after lipofection cells were dissociated using Accutase (SIGMA, A6964), pelleted, and resuspended in 15 µl QuickExtract (Epicentre, QE0905T). Incubation at 65 °C for 10 min, 68 °C for 5 min, and finally 98 °C for 5 min was performed to yield ssDNA as a PCR template. Primers for each targeted loci containing adapters for Illumina sequencing were ordered from IDT (Coralville, USA) (see Supplementary Table 3). PCR was done in a T100 Thermal Cycler (Bio-Rad) using the KAPA2G Robust PCR Kit (Peqlab, 07-KK5532-03) with supplied buffer B and 3 µl of cell extract in a total volume of 25 µl. The thermal cycling profile of the PCR was: 95 °C 3 min; 34 × (95° 15 s, 65 °C 15 s, 72 °C 15 s); 72 °C 60 s. P5 and P7 Illumina adapters with sample-specific indices were added in a second PCR reaction[42] using Phusion HF MasterMix (Thermo Scientific, F-531L) and 0.3 µl of the first PCR product. The thermal cycling profile of the PCR was: 98 °C 30 s; 25 × (98° 10 s, 58 °C 10 s, 72 °C 20 s); 72 °C 5 min. Amplifications were verified by size separating agarose gel electrophoresis using EX gels (Invitrogen, G4010-11). The indexed amplicons were purified using Solid Phase Reversible Immobilization (SPRI) beads[43]. Double-indexed libraries were sequenced on a MiSeq (Illumina) giving paired-end sequences of 2 × 150 bp. After base calling using Bustard (Illumina), adapters were trimmed using leeHom[44].

CRISPResso analysis. CRISPresso[45] was used to analyze sequencing data from CRISPR genome-editing experiments for percentage of wild type, TNS, indels, and mix of TNS and indels. Parameters used for analysis were "-w 20," "–min_identity_score 70," and "–ignore_substitutions" (analysis was restricted to amplicons with a minimum of 70% similarity to the wild type sequence and to a window of 20 bp from each gRNA; substitutions were ignored, as sequencing errors would be falsly characterized as NHEJ events).

Statistical analysis. Significances of changes in TNS efficiencies were determined using a two-way analysis of variance and Tukey's multiple comparison pooled across the three genes *CALD1*, *KATNA1*, and *SLITRK1*. Genes and treatments were treated as random and fixed effect, respectively. Hence, we tested the effect of treatment against its interaction with gene[46]. Analysis included three technical replicates for each gene. We checked for whether the assumptions of normally distributed and homogeneous residuals were fulfilled by visual inspection of a QQ-plot[47] and residuals plotted against fitted values[48]. These indicated residuals to be roughly symmetrically distributed but with elongated tails (i.e., too large positive and negative residuals) and no obvious deviations from the homogeneity assumption. *P*-values are adjusted for multiple comparison. Statistical analysis was done using R.

Resazurin assay. 409-B2 iCRISPR-Cas9n hiPSCs were either seeded with or without editing reagents (RNAiMax, gRNA, and ssODN donor for *KATNA1* editing) as described in "Lipofection of oligonucleotides" (25,000 cells per 96 wells). Non-pluripotent cell lines were either seeded without editing reagents or electroporated with editing reagents as decribed in "Ribonucleoprotein electroporation" (50,000 cells per 96 wells). The media was supplemented with small molecules or combinations of small molecules, and each condition was carried out in duplicate. After 24 h, media was aspirated and 100 µl fresh media together with 10 µl resazurin solution (Cell Signaling, 11884) was added. Resazurin is converted into fluorescent resorfin by cellular dehydrogenases and resulting fluorescence (exitation: 530–570 nm, emission: 590–620 nm) is considered as a linear marker for cell viability[29]. Cells were incubated with resazurin at 37 °C. The redox reaction was measured every hour by absorbance readings using a Typhoon 9410 imager (Amershamn Biosciences). After 5 h (12 h for CD34 + progenitor cells) the absorbance scan showed a good contrast without being saturated, and was used to quantify the absorbance using ImageJ and the "ReadPlate" plugin. Duplicate wells with media and resazurin, but without cells, were used a blank.

Microscopy and image analysis. 409-B2 iCRISPR-Cas9n hiPSCs were electroporated with gRNAs and the BFP single-stranded oligo (Fig. 4a, 330 ng) in two technical replicates for either mock, NU7026, and CRISPY mix treatment. Media was supplemented with 2 µg/ml doxycycline (Clontech, 631311) for 7 days, to allow expression of nuclear imported BFP in precisely edited cells. Then, cells were fixed with 4% formaldehyde in Dulbecco's phosphate-buffered saline (DPBS) (ThermoFisher, A24881) for 15 min, permeablized with 1% saponin in DPBS (ThermoFisher, A24881) supplemented with 100 µg/ml RNAseA (ThermoFisher, EN0531) and 40 µg/ml propidium iodide (ThermoFisher, P3566) for 45 min at 37 °C, and washed three times with DPBS. Nucleic acid intercalating propidium iodide was used to counterstain nuclei. A fluorescent microscope Axio Observer Z (Zeiss) was used to aquire two images (× 50 magnification), from each of three technical replicates for the respective treatments, consisting of the following: phase contrast, HcRed channel (BP 580–604 nm, BS 615 nm, BP 625–725 nm, 10.000 ms), and 4',6-diamidino-2-phenylindole channel (BP 335–383 nm, BS 395 nm, BP 420–470 nm, 20,000 ms). Images were blinded and BFP-positive nuclei were counted using the Adobe Photoshop CS5 counting tool. Propidium iodide-positive nuclei were quantified using ImageJ by dividing the area of nuclei (default threshold) with the mean area of a single nuclei.

Karyotyping. Microscopic analysis of the karyotype was done after trypsin-induced Giemsa staining. The analysis was carried out according to international quality guidelines (ISCN 2016: An International System for Human Cytogenetic Nomenclature[49]) by the "Sächsischer Inkubator für klinische Translation" (Leipzig, Germany).

Data availability. Data available on request from the authors.

Received: 6 December 2017 Accepted: 14 May 2018
Published online: 04 June 2018

References

1. Robinton, D. A. & Daley, G. Q. The promise of induced pluripotent stem cells in research and therapy. *Nature* **481**, 295–305 (2012).
2. Mandai, M. et al. Autologous induced stem-cell-derived retinal cells for macular degeneration. *N. Engl. J. Med.* **376**, 1038–1046 (2017).
3. Shrivastav, M., De Haro, L. P. & Nickoloff, J. A. Regulation of DNA double-strand break repair pathway choice. *Cell Res.* **18**, 134–147 (2008).
4. Dueva R. & Iliakis G. Alternative pathways of non-homologous end joining (NHEJ) in genomic instability and cancer. *Transl. Cancer Res* **2**, 163–177 (2013).
5. Nussenzweig, A. & Nussenzweig, M. C. A backup DNA repair pathway moves to the forefront. *Cell* **131**, 223–225 (2007).
6. Grimme, J. M. et al. Human Rad52 binds and wraps single-stranded DNA and mediates annealing via two hRad52-ssDNA complexes. *Nucleic Acids Res.* **38**, 2917–2930 (2010).
7. Bothmer A. et al. Characterization of the interplay between DNA repair and CRISPR/Cas9-induced DNA lesions at an endogenous locus. *Nature Commun.* **8**, 13905 (2017).
8. Fu, Y. et al. High-frequency off-target mutagenesis induced by CRISPR-Cas nucleases in human cells. *Nat. Biotechnol.* **31**, 822–826 (2013).
9. Shen, B. et al. Efficient genome modification by CRISPR-Cas9 nickase with minimal off-target effects. *Nat. Methods* **11**, 399–402 (2014).
10. Zetsche, B. et al. Cpf1 is a single RNA-guided endonuclease of a class 2 CRISPR-Cas system. *Cell* **163**, 759–771 (2015).
11. Kim, D. et al. Genome-wide analysis reveals specificities of Cpf1 endonucleases in human cells. *Nat. Biotechnol.* **34**, 863–868 (2016).
12. Kleinstiver, B. P. et al. Genome-wide specificities of CRISPR-Cas Cpf1 nucleases in human cells. *Nat. Biotechnol.* **34**, 869–874 (2016).
13. Gonzalez, F. et al. An iCRISPR platform for rapid, multiplexable, and inducible genome editing in human pluripotent stem cells. *Cell Stem Cell* **15**, 215–226 (2014).
14. Yu, C. et al. Small molecules enhance CRISPR genome editing in pluripotent stem cells. *Cell Stem Cell* **16**, 142–147 (2015).
15. Lin, S., Staahl, B. T., Alla, R. K. & Doudna, J. A. Enhanced homology-directed human genome engineering by controlled timing of CRISPR/Cas9 delivery. *eLife* **3**, e04766 (2014).
16. Yang, D. et al. Enrichment of G2/M cell cycle phase in human pluripotent stem cells enhances HDR-mediated gene repair with customizable endonucleases. *Sci. Rep.* **6**, 21264 (2016).
17. Chu, V. T. et al. Increasing the efficiency of homology-directed repair for CRISPR-Cas9-induced precise gene editing in mammalian cells. *Nat. Biotechnol.* **33**, 543–548 (2015).
18. Maruyama, T. et al. Increasing the efficiency of precise genome editing with CRISPR-Cas9 by inhibition of nonhomologous end joining. *Nat. Biotechnol.* **33**, 538–542 (2015).
19. Singh, P., Schimenti, J. C. & Bolcun-Filas, E. A mouse geneticist's practical guide to CRISPR applications. *Genetics* **199**, 1–15 (2015).
20. Pinder, J., Salsman, J. & Dellaire, G. Nuclear domain 'knock-in' screen for the evaluation and identification of small molecule enhancers of CRISPR-based genome editing. *Nucleic Acids Res.* **43**, 9379–9392 (2015).
21. Song, J. et al. RS-1 enhances CRISPR/Cas9- and TALEN-mediated knock-in efficiency. *Nat. Commun.* **7**, 10548 (2016).
22. Zhang, J. P. et al. Efficient precise knockin with a double cut HDR donor after CRISPR/Cas9-mediated double-stranded DNA cleavage. *Genome Biol.* **18**, 35 (2017).
23. Greco, G. E. et al. SCR7 is neither a selective nor a potent inhibitor of human DNA ligase IV. *DNA Repair* **43**, 18–23 (2016).
24. Robert, F., Barbeau, M., Ethier, S., Dostie, J. & Pelletier, J. Pharmacological inhibition of DNA-PK stimulates Cas9-mediated genome editing. *Genome Med.* **7**, 93 (2015).
25. Suzuki, K. et al. In vivo genome editing via CRISPR/Cas9 mediated homology-independent targeted integration. *Nature* **540**, 144–149 (2016).
26. Wang, K. et al. Efficient generation of orthologous point mutations in pigs via CRISPR-assisted ssODN-mediated homology-directed repair. *Mol. Ther. Nucleic Acids* **5**, e396 (2016).
27. Milanowska, K. et al. REPAIRtoire–a database of DNA repair pathways. *Nucleic Acids Res.* **39**, D788–D792 (2011).
28. Bento, A. P. et al. The ChEMBL bioactivity database: an update. *Nucleic Acids Res.* **42**, D1083–D1090 (2014).
29. O'Brien, J., Wilson, I., Orton, T. & Pognan, F. Investigation of the Alamar Blue (resazurin) fluorescent dye for the assessment of mammalian cell cytotoxicity. *Eur. J. Biochem.* **267**, 5421–5426 (2000).
30. Subach, O. M., Cranfill, P. J., Davidson, M. W. & Verkhusha, V. V. An enhanced monomeric blue fluorescent protein with the high chemical stability of the chromophore. *PLoS ONE* **6**, e28674 (2011).
31. Lee, J. S. Activation of ATM-dependent DNA damage signal pathway by a histone deacetylase inhibitor, trichostatin A. *Cancer Res. Treat.* **39**, 125–130 (2007).
32. Jimeno, S. et al. Neddylation inhibits CtIP-mediated resection and regulates DNA double strand break repair pathway choice. *Nucleic Acids Res.* **43**, 987–999 (2015).
33. Glanzer, J. G., Liu, S. & Oakley, G. G. Small molecule inhibitor of the RPA70 N-terminal protein interaction domain discovered using in silico and in vitro methods. *Bioorg. Med. Chem.* **19**, 2589–2595 (2011).
34. Glanzer, J. G. et al. A small molecule directly inhibits the p53 transactivation domain from binding to replication protein A. *Nucleic Acids Res.* **41**, 2047–2059 (2013).
35. Blanpain, C., Mohrin, M., Sotiropoulou, P. A. & Passegue, E. DNA-damage response in tissue-specific and cancer stem cells. *Cell Stem Cell* **8**, 16–29 (2011).
36. Rocha, C. R., Lerner, L. K., Okamoto, O. K., Marchetto, M. C. & Menck, C. F. The role of DNA repair in the pluripotency and differentiation of human stem cells. *Mutat. Res.* **752**, 25–35 (2013).
37. Gomez-Cabello, D., Checa-Rodriguez, C., Abad, M., Serrano, M. & Huertas, P. CtIP-specific roles during cell reprogramming have long-term consequences in the survival and fitness of induced pluripotent stem cells. *Stem Cell Rep.* **8**, 432–445 (2017).
38. Mora-Bermudez, F. et al. Differences and similarities between human and chimpanzee neural progenitors during cerebral cortex development. *eLife* **5**, e18683 (2016).
39. Prüfer, K. et al. The complete genome sequence of a Neanderthal from the Altai Mountains. *Nature* **505**, 43–49 (2014).
40. Chari, R., Mali, P., Moosburner, M. & Church, G. M. Unraveling CRISPR-Cas9 genome engineering parameters via a library-on-library approach. *Nat. Methods* **12**, 823–826 (2015).
41. Ran, F. A. et al. Genome engineering using the CRISPR-Cas9 system. *Nat. Protoc.* **8**, 2281–2308 (2013).
42. Kircher, M., Sawyer, S. & Meyer, M. Double indexing overcomes inaccuracies in multiplex sequencing on the Illumina platform. *Nucleic Acids Res.* **40**, e3 (2012).
43. Meyer, M. & Kircher, M. Illumina sequencing library preparation for highly multiplexed target capture and sequencing. *Cold Spring Harb. Protoc.* **2010**, https://doi.org/10.1101/pdb.prot5448 (2010).
44. Renaud, G., Stenzel, U. & Kelso, J. leeHom: adaptor trimming and merging for Illumina sequencing reads. *Nucleic Acids Res.* **42**, e141 (2014).
45. Pinello, L. et al. Analyzing CRISPR genome-editing experiments with CRISPResso. *Nat. Biotechnol.* **34**, 695–697 (2016).
46. Zar, J. H. *Biostatistical Analysis*. (Prentice Hall: 1999).
47. Field A. *Discovering Statistics using SPSS*. (Sage Publications, 2005).
48. Quinn G. P. & Keough, M. J. *Experimental Designs and Data Analysis for Biologists*. (Cambridge Univ. Press, 2002).
49. International Standing Committee on Human Cytogenomic Nomenclature, McGowan-Jordan, J., Simons, A., Schmid, M. *ISCN: An International System for Human Cytogenomic Nomenclature* (Karger, 2016).

Acknowledgements

We thank Malgorzata Santel for assistance with FACS sorting, Anna Kirstein for experimental help in validation of the iCRISPR cell lines, Roger Mundry for help with statistical analysis, and Heidrun Holland for karyotyping. Furthermore, we thank Antje Weimann and Barbara Schellbach for DNA sequencing, and Adrian Briggs and especially Svante Pääbo for comments on the manuscript and helpful discussions. This work was supported by the Max Planck Society and by the NOMIS Foundation.

Author contribution

S.R. conceived the idea. S.R. and T.M planned the experiments. S.R. performed the experiments. S.R. and T.M. wrote the paper.

Additional information

Supplementary Information accompanies this paper at https://doi.org/10.1038/s41467-018-04609-7.

Competing interests: A related patent application on compounds for increasing genome-editing efficiency has been filed (patent applicant: Max Planck Society, inventors: S.R. and T.M., application number: EP17203591.7, PCT/EP2018/059173, status: pending).

Reprints and permission information is available online at http://npg.nature.com/reprintsandpermissions/

Publisher's note: Springer Nature remains neutral with regard to jurisdictional claims in published maps and institutional affiliations.

SUPPLEMENTARY INFORMATION

Targeting repair pathways with small molecules increases precise genome editing in pluripotent stem cells

Riesenberg et al.

Supplementary Figures and Tables

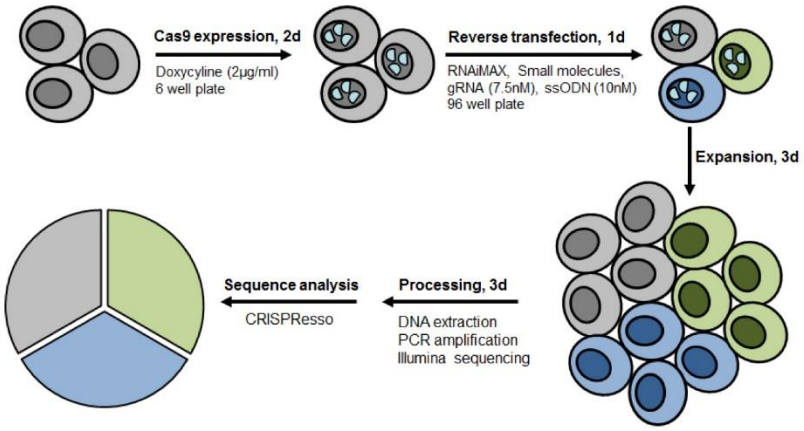

Supplementary Fig. 1: Genome editing and analysis flowchart. 409-B2 iCRISPR hiPSCs are treated with 2µg/ml doxycycline for 2 days to induce Cas9 or Cas9n expression. Reverse transfection with RNAiMAX, gRNA (7.5nM each), ssODN donor (10nM) and the small molecules to be evaluated is carried out in a 96 well plate for 1 day. Cells are then expanded for 3 days with regular media change. After harvest follows DNA extraction, PCR amplification of targeted loci, Illumina sequencing and CRISPResso[1] sequence analysis for amount of indels and targeted nucleotide substitutions (TNS).

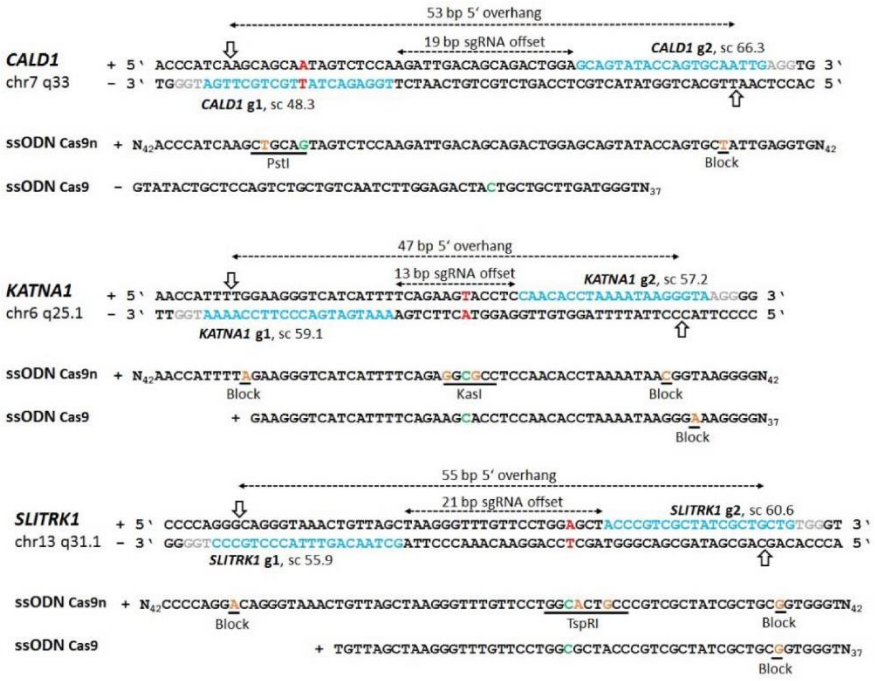

Supplementary Fig. 2: Design of gRNAs and ssODN for targeted nucleotide substitution (TNS) of human *CALD1*, *KATNA1* and *SLITRK1*. Shown are the respective loci of *CALD1*, *KATNA1* and *SLITRK1* together with the gRNAs and their efficiency score (sc) (sgRNA scorer 1.0[2]) used for DSB generation. The PAM site is grey, the target sequence is blue and the base to be changed is red. The point of nick by Cas9n or DSB by Cas9 is indicated by an arrow. Whereas both guides are used for editing with Cas9n, *CALD1* g1, *KATNA1* g2 and *SLITRK1* g2 are used for editing with Cas9. The respective ssODN for editing with both Cas9 variants are also shown. Desired mutation is marked green and additional mutations are orange. ‚Block' indicates a Cas9-blocking mutation to prevent re-cutting oft the locus. All Cas9n donors have 50nt homology arms after the nicks while all Cas9 donors are 90nt in total with the desired mutation centered in the middle. The full sequences are shown in Supplementary Table 3.

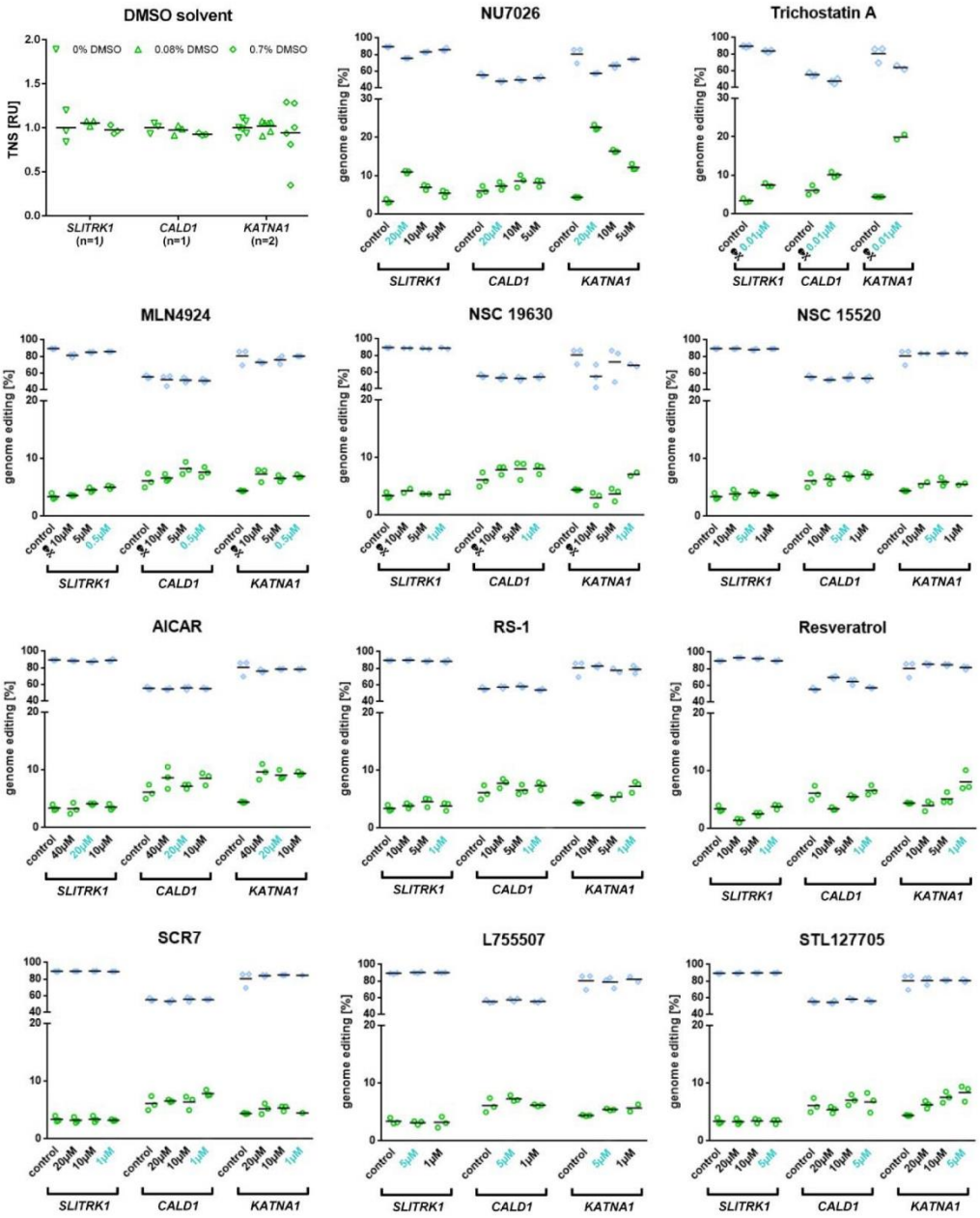

Supplementary Fig. 3: First screen for solvent effect and influence of different small molecule concentrations on genome editing in iCRISPR hiPSCs. Shown are genome editing efficiencies in *CALD1, KATNA1* and *SLITRK1* in 409-B2 iCRISPR-Cas9n hiPSCs. Targeted Nucleotide Substitutions (TNS) are green and indels are blue. Each symbol represents a technical replicate. The respective means are shown as a black line. Each skull indicates cell death of up to around 20% determined by phase contrast light microscopy. All cells died with 1µM and 0.1µM Trichostatin A. Concentrations chosen for further experiments are marked with turquoise.

A **Acute toxicity**

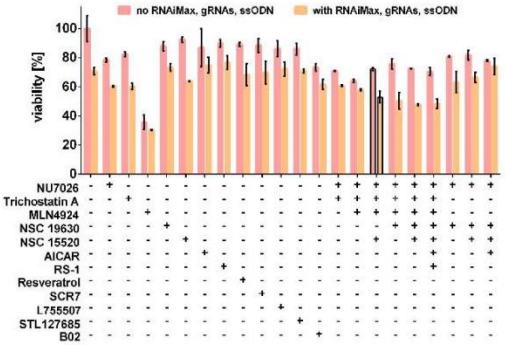

B **Long-term genotoxicity**

5x (1 day passaging with mock or CRISPY mix, and RNAiMax; 3 days recovery)

sample	metaphases	band number	gray shades	healthy karyotype (46,XX)
mock (bulk)	20	400	3	20/20
CRISPY (bulk)	25	450	3	25/25
mock clone 1	25	400	3	21/25 (4 polyploid)
mock clone 2	25	450	3	25/25
mock clone 3	25	450	3	25/25
mock clone 4	25	450	3	25/25
mock clone 5	25	400	3	25/25
CRISPY clone 1	25	400	3	25/25
CRISPY clone 2	25	400	3	25/25
CRISPY clone 3	25	400	3	25/25
CRISPY clone 4	25	400	3	22/25 (3 polyploid)
CRISPY clone 5	25	400	3	25/25

Supplementary Fig. 4: Toxicity of the CRISPY mix and its components. A resazurin assay from 409-B2-iCRISPR-Cas9n cells after 24h incubation with the small molecules and combinations from Fig. 2 and 3, with (orange) and without RNAiMax, gRNA and ssODNs (pink), is shown in (A). Resazurin is converted into fluorescent resorfin by cellular dehydrogenases and resulting fluorescence (Exitation: 530-570nm, Emission: 590-620nm) is considered as a marker for cell viability[3]. Resorfin absorption (610±30nm) of normally passaged cells without small molecule treatment and RNAiMax, gRNAs, and ssODN is set to 100% cell viability. The CRISPY mix is highlighted with black borders and is slightly toxic with no additive toxic effect of its components. Error bars show the standard deviation of two technical replicates. Karyotype analysis after five rounds of passaging the cells together with the CRISPY mix and mock treatment is shown in (B). At least 20 metaphases of the bulk and five clones of each conditions were analysed using trypsin-induced Giemsa staining. No numerical or large scale chromosomal aberrations, except for a small subset of metaphases from two single clones corresponding to CRISPY mix (3 of 25 metaphases polyploid) and mock treatment (4 of 25 metaphases polyploid), were identified.

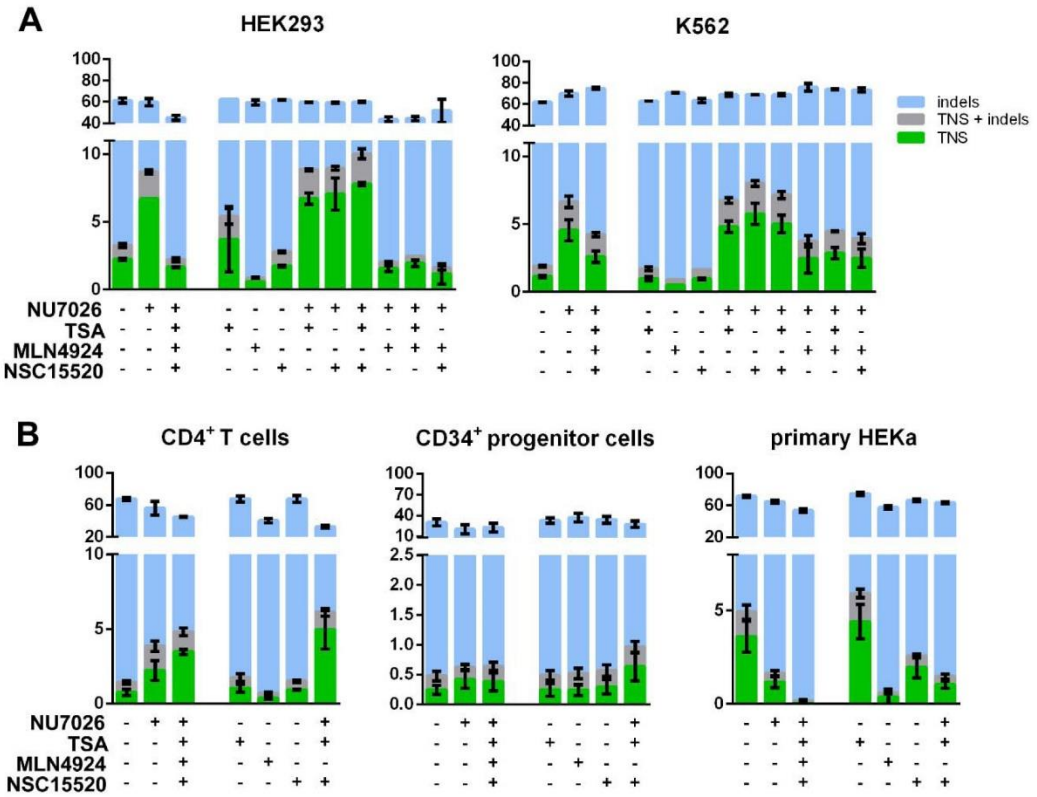

Supplementary Fig. 5: Impact of the CRISPY mix and small molecule combinations on Targeted Nucleotide Substitution (TNS) efficiency in non-pluripotent cell types. Shown are TNS efficiencies in *HPRT* with electroporated Cpf1 ribonucleoprotein and ssODN. All possible combinations for the CRISPY mix components are shown for HEK293 and K562 cells (A). While NU7026 increases TNS efficiency, TSA and NSC15520 have no clear effect, and MLN4924 has a clear disruptive effect in immortalized cell lines. MLN4924 has a disruptive effect on TNS efficiency in primary cells as well (B). The CRISPY mix without MLN4924 has a higher effect on TNS efficiency than NU7026 alone in $CD4^+$ T and $CD34^+$ progenitor cells. In primary Human Epidermal Keratinocytes (HEKa) also NU7026 and NSC15520 have a disruptive effect on TNS efficiency. Shown are TNS, TNS + indels, and indels with green, grey or blue bars, respectively. Error bars show the standard deviation of two independent experiments for HEK293 and K562 cells, three independent experiments for $CD4^+$ T cells, two technical replicates for each of four independent experiments for $CD34^+$ progenitor cells, and two technical replicates for each of two independent experiments for primary HEKa cells.

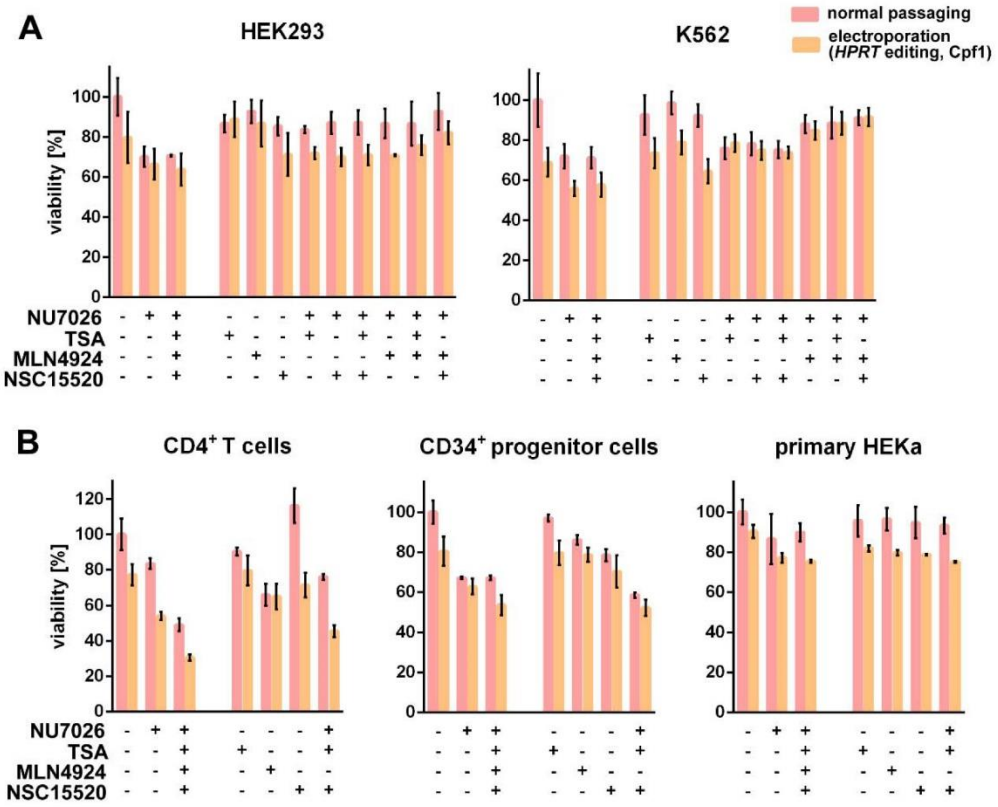

Supplementary Fig. 6: Impact of the CRISPY mix and small molecule combinations on cell viability in non-pluripotent cell types. Results of resazurin assays for cell viability after 24h incubation with the small molecules and combinations from Supplementary Fig. 5 are shown for HEK293, and K562 cells (A) and $CD4^+$ T, $CD34^+$ progenitor, and primary HEKa cells (B). Resazurin is converted into fluorescent resorfin by cellular dehydrogenases and resulting fluorescence (Exitation: 530-570nm, Emission: 590-620nm) is considered as a marker for cell viability[3]. Resorfin absorption (610±30nm) of normally passaged cells without small molecule treatment is set to 100% cell viability. Shown are viability after small molecule treatment following normal passaging (pink) and editing of *HPRT* using electroporated Cpf1 ribonucleoprotein and ssODN (orange), respectively. Error bars show the standard deviation of three independent experiments.

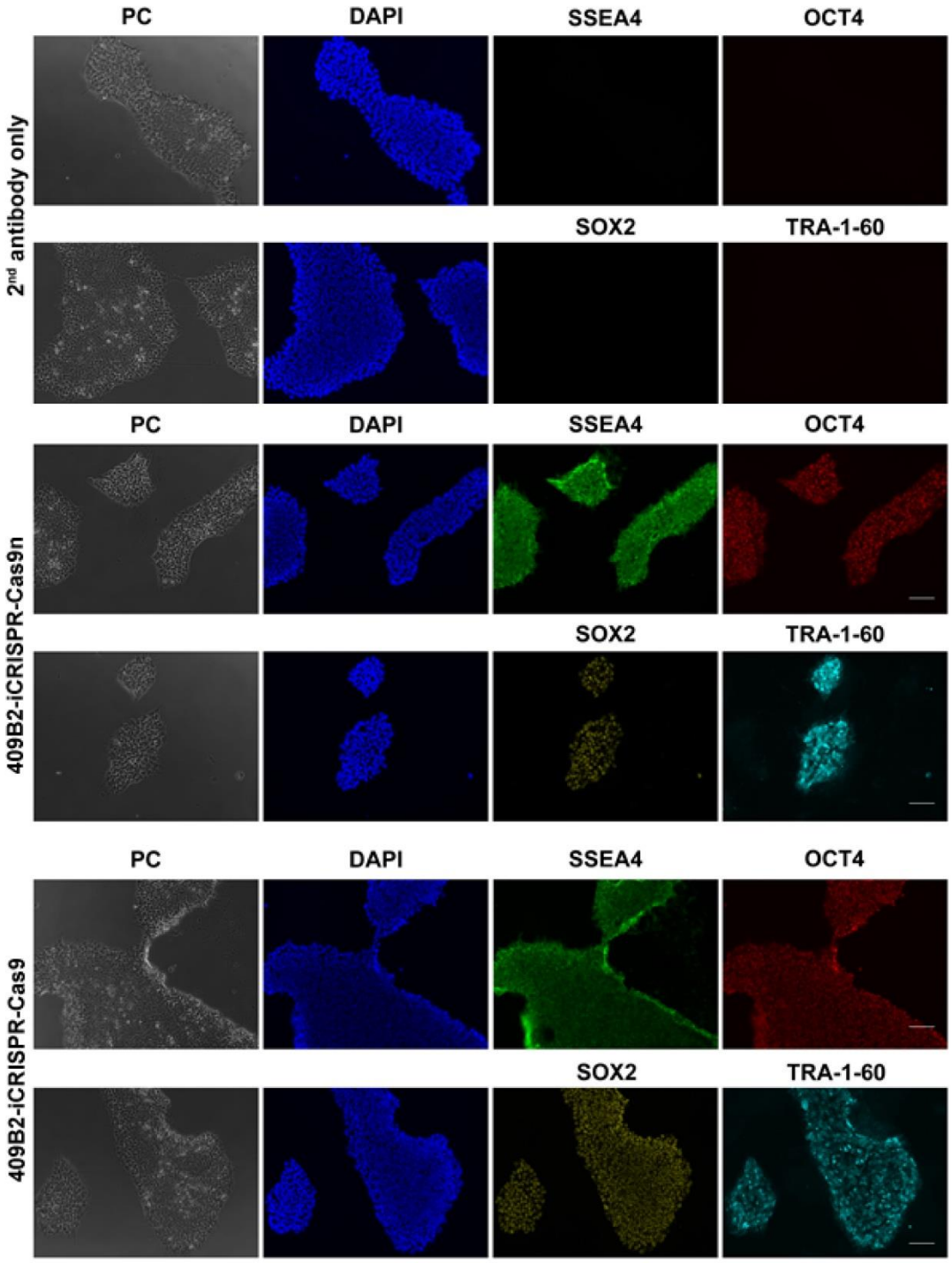

Supplementary Fig. 7: Expression of pluripotency markers in 409-B2 iCRISPR cell lines. Representative images of the phase contrast (PC), nuclei stain DAPI (blue), and pluripotency markers SSEA4 (green), OCT4 (red), SOX2 (yellow) and TRA-1-60 (turquoise) are shown. Images were equally adjusted for brightness using Adobe Photoshop CS5 with regard to the negative control. Magnification 10x, size bar 100 µM.

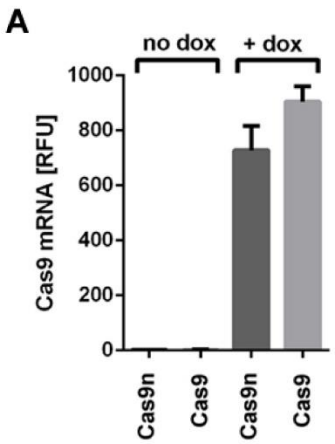

B

ratio of copy number (Fam/Hex)

	cell line	
amplicon	**Cas9n**	**Cas9**
Neo backbone	0.02	0.03
M2rtTA	0.54	0.57
Puro backbone	0.08	0.05
Cas9n/Cas9	0.50	0.46

Supplementary Fig. 8: Confirmation of inducible Cas9/Cas9n expression and absent off-target integration. Cas9 or Cas9n expression can be induced by doxycycline in 409-B2 iCRISPR cell lines (A) as shown by qPCR. Cells were treated without doxycyline or with 2µg/ml doxycycline for two days. The Cas9 mRNA level is inferred from qPCR of cDNA as relative fluorescence units (RFU). Values were normalized to *GAPDH* levels. Error bars show the standard deviation of two technical replicates each. The iCRISPR cassettes are heterozygously introduced in the AAVS1 locus and off-target integration of the iCRISPR cassettes or the plasmid backbone is absent (B) as shown by ddPCR. Presented values of the copy number ratio (Fam-insert/Hex-genomic control) are means of three technical replicates. PCR primer and dye probe sequences are shown in Supplementary Table 3.

Supplementary Table 1: Inconsistencies between studies using small molecules to increase CRISPR Precise Genome Editing (PGE). PGE percentages with an asterisk have been estimated from figures. Non significant precise genome editing changes are labelled with ns.

Targeted protein	Small molecule	Concentration [µM]	Cell type	Locus/Gene	Donor	PGE increase [%]	PGE increase [fold]	Reference
Ligase IV	**SCR7**	1	A549	*TSG101*	dsODN	n.a. (gel)	1.8	Maruyama et al. 2015[4]
		1	MelJuSo	*TSG101*	dsODN	n.a. (gel)	19.1	Maruyama et al. 2015[4]
		1000	mouse embryos	*Kell*	ssODN	28.6 to 58.3	2	Maruyama et al. 2015[4]
		1000	mouse embryos	*Igkc*	ssODN	5 to 22.7	4.5	Maruyama et al. 2015[4]
		1	HEK293A	*LMNA*	dsODN	10 to 11.5*	1.2	Pinder et al. 2015[5]
		1	HEK293/TRL	AAVS1	dsODN	5 to 25	5	Chu et al. 2015[6]
		50	mouse embryos	*Tex15*	ssODN	5.8 to 56.2	10	Singh et al. 2015[7]
		80	rabbit embryos	*RLL*	dsODN	ns		Song et al. 2015[8]
		1	hPSCs	GFP	dsODN	ns		Yang et al. 2015[9]
		200	human pre-B Rhe	pGG49	dsODN	ns (NHEJ decrease)		Greco et al. 2016[10]
		1	hiPSCs	*CTNNB1*	dsODN	ns		Zhang et al. 2017[11]
		1	hiPSCs	*PRDM14*	dsODN	ns		Zhang et al. 2017[11]
DNA-PK	**NU7026**	30	HEK293	GFP	dsODN	3 to 7.6	2.5	Suzuki et al. 2016[12]
	NU7441	2	MEFs	*TP53*	ssODN	3 to 10*	10	Robert et al. 2015[13]
		2	HEK293/TRL	GFP	dsODN	1.9 to 3.8	2	Robert et al. 2015[13]

		2	hiPSCs	*CTNNB1*	dsODN	13 to 16*	1.2	Zhang et al. 2017[11]
		2	hiPSCs	*PRDM14*	dsODN	ns		Zhang et al. 2017[11]
RAD51	**RS-1**	7,5	rabbit embryos	*RLL*	dsODN	4.4 to 26.1	5.9	Song et al. 2015[8]
		7,5	rabbit embryos	*CFTR*	dsODN	12.5 to 30	2.4	Song et al. 2015[8]
		10	HEK293A	*LMNA*	dsODN	3.5 to 21*	6	Pinder et al. 2015[5]
		10	U2OS	*LMNA*	dsODN	1.9 to 2.4*	1.3	Pinder et al. 2015[5]
		1	PFF	*APP*	ssODN	ns		Wang et al. 2016[14]
		10	hiPSCs	*CTNNB1*	dsODN	ns		Zhang et al. 2017[11]
		10	hiPSCs	*PRDM14*	dsODN	ns		Zhang et al. 2017[11]
β3-adrenergic receptor ?	**L755507**	5	mouse ESCs	*Nanog*	dsODN	17.7 to 33.3	2	Yu et al. 2015[15]
		5	hiPSCs	*SOD1*	ssODN	0.35 to 3.13	9	Yu et al. 2015[15]
		5	HeLa	*ACTA2*	dsODN	1 to 2*	2	Yu et al. 2015[15]
		5	HEK293A	*LMNA*	dsODN	ns		Pinder et al. 2015[5]
		5	hiPSCs	*CTNNB1*	dsODN	ns		Zhang et al. 2017[11]
		5	hiPSCs	*PRDM14*	dsODN	ns		Zhang et al. 2017[11]

Supplementary Table 2: Overview of the small molecules evaluated in this study. Literature references with an asterisk indicate the small molecule as a CRISPR-Cas effector. Abbreviations: alternative NHEJ (Alt-NHEJ), damage dependent signaling (DDS).

Pathway	Protein targeted	Protein function	Small molecule	Small molecule function	Reference
NHEJ	**Ku70/80**	First proteins to bind to DNA ends	**STL127685**	4-fluorophenyl analog of a Ku70/80 inhibitor	Weterings et al. 2016[16]
	DNA-PK	Complex of Ku70/80 and DNA-PKcs, DNA-PKcs phosphorylates itself and downstream effectors at the repair site	**NU7026**	DNA-PK inhibitor	Suzuki et al. 2016*[12]
	Ligase IV	End-processing ligation	**SCR7**	Ligase IV inhibitor	Maruyama et al. 2015*[4]
Alt-NHEJ (NHEJ)	**WRN helicase**	DNA unwinding	**NSC 19630**	WRN helicase inhibitor	Aggarwal et al. 2011[17]
HDR	**CtIP**	DNA end resection	**MLN4924**	NAE inhibitor, inhibts neddylation of CtIP	Jimeno et al. 2015[18]
	RPA	Coating and stabilization of ssDNA	**NSC15520**	Inhibits binding of RPA to p53 and RAD9	Glanzer et al. 2011[19], 2013[20]
	RAD52	ssDNA annealing	**AICAR**	RAD52 inhibitor	Sullivan et al. 2016[21]

	RAD51	Strand invasion with the donor DNA	**RS-1**	RAD51 enhancer	Song et al. 2016*[8]
			B02	RAD51 inhibitor	Huang et al. 2011[22]
DDS	**ATM**	Phosphorylates many DNA repair proteins	**Resveratrol**	Direct stimulatory effects on purified ATM	Lee et al. 2014[23]
			Trichostatin A	Histone deacetlyase inhibitor, induces phosphorylation of Ser1981 in ATM	Lee 2007[24]
?	**β3-adrenergic receptor**	Involved in activation of adenylate cyclase	**L755507**	β3-adrenergic receptor agonist	Yu et al. 2015*[15]

Supplementary Table 3: Oligonucleotides used in this study. gRNA (crRNA target) and single stranded DNA donors (ssODNs) for editing of *CALD1*, *KATNA1*, *SLITRK1*, *HPRT*, *DNMT1,* and AAVS1(BFP) as well as primers for analysis and Q5 site-directed-mutagenesis of the Cas9 iCRISPR donor plasmid are shown. Mutations are in bold letters and ancestral mutations are underlined as well.

gRNAs	*CALD1* t1	TGGAGACTATTGCTGCTTGA
	CALD1 t2	GCAGTATACCAGTGCAATTG
	KATNA1 t1	AAATGATGACCCTTCCAAAA
	KATNA1 t2	CAACACCTAAAATAAGGGTA
	SLITRK1 t1	GCTAACAGTTTACCCTGCCC
	SLITRK1 t1	ACCCGTCGCTATCGCTGCTG
	HPRT t1	GGTTAAAGATGGTTAAATGAT
	DNMT1 t1	CTGATGGTCCATGTCTGTTAC
	iCRISPR BFP insertion t1	TGTCGGCTGCTGGGACTCCG
	iCRISPR BFP insertion t2	TACAGCATCGGCCTGGCTAT
ssODNs	*CALD1* Cas9	GTATACTGCTCCAGTCTGCTGTCAATCTTGGAGACTA**C**TGCTGCTTGATGGGTCGATTTGA CACCACTGCTAAAAAAGTAAACACATACA
	CALD1 Cas9n	TTATATGTATGTGTTTACTTTTTTAGCAGTGGTGTCAAATCGACCCATCAAGC**T**GCA**G**TAG TCTCCAAGATTGACAGCAGACTGGAGCAGTATACCAGTGC**T**ATTGAGGTGAGAATTGTCCT CAGCGTTATGGTCCTGCTGAACAGAAATAGA
	KATNA1 Cas9	GAAGGGTCATCATTTTCAGAAG**C**ACCTCCAACACCTAAAATAAGGG**A**AAGGGGAGAGTGAA AAAGATATTAAGTTGGATTATACCAAATG
	KATNA1 Cas9n	CTCATCTATATCCCAGGGAAAATTAGTAGCTGCCAGAACCATAACCATTTT**A**GAAGGGTCA TCATTTTCAGA**G**G**CG**CCTCCAACACCTAAAATAA**C**GGTAAGGGGAGAGTGAAAAAGATATT AAGTTGGATTATACCAAATGAAGCT
	SLITRK1 Cas9	TGTTAGCTAAGGGTTTGTTCCTGG**C**GCTACCCGTCGCTATCGCTGC**G**GTGGGTCTGATTTT GATCTGCCAGTTGCCTGGGATCTTTGTAC
	SLITRK1 Cas9n	TCATCTTTAAACCCGACCCTGGGATGTGGTCGCAGCTGCAGCCCCCAGG**A**CAGGGTAAACT GTTAGCTAAGGGTTTGTTCCTGG**CA**CT**G**CCCGTCGCTATCGCTGC**G**GTGGGTCTGATTTTG ATCTGCCAGTTGCCTGGGATCTTTGTACCTCCG
	HPRT Cpf1	GCCATTTCACATAAAACTCTTTTAGGTTA**T**AGATGGTTAAATGA**A**TGACAAAAAAAGTAAT TCACTTACAGTCTGGCTTATATCCAACAC
	DNMT1 Cpf1	TTAACATCAGTACGTTAATGTTTCCTGAT**C**GTCCATGTCTGTTA**G**TCGCCTGTCAAGTGGC GTGACACCGGGCGTGTTCCCCAGAGTGAC

	mtagBFP-iCRISPR-Cas9n	AAAGACGATGACGATAAGATGGCCCCAAAGAAGAAGCGGAAGGTCGGTATCCACGGAGTCC CAGCAGCC**GTGAGCAAGGGCGAGGAGCTGATCAAGGAGAACATGCACATGAAGCTGTACAT** **GGAGGGCACCGTGGACAACCACCACTTCAAGTGCACCAGCGAGGGCGAGGGCAAGCCCTAC** **GAGGGCACCCAGACCATGCGCATCAAGGTGGTGGAGGGCGGCCCCCTGCCCTTCGCCTTCG** **ACATCCTGGCCACCAGCTTCCTGTACGGCAGCAAGACCTTCATCAACCACACCCAGGGCAT** **CCCCGACTTCTTCAAGCAGAGCTTCCCCGAGGGCTTCACCTGGGAGCGCGTGACCACCTAC** **GAGGACGGCGGCGTGCTGACCGCCACCCAGGACACCAGCCTGCAGGACGGCTGCCTGATCT** **ACAACGTGAAGATCCGCGGCGTGAACTTCACCAGTAATGGGCCTGTGATGCAGAAGAAGAC** **TCTGGGCTGGGAGGCATTCACCGAGACCCTCTATCCGGCTGATGGTGGGCTCGAGGGTCGC** **AACGATATGGCTTTGAAACTCGTCGGAGGAAGTCACCTCATCGCAAACGCTAAAACAACCT** **ATAGGTCTAAGAAGCCCGCCAAGAACTTGAAAATGCCAGGGGTCTACTATGTAGATTACCG** **CTTGGAACGAATTAAAGAGGCTAATAATGAGACTTACGTAGAACAACACGAGGTAGCAGTC** **GCTCGATATTGCGACTTGCCGAGTAAGCTCGGACATAAGCTGAACGGCAGTGGAGAAGGTC** **GGGGATCACTCCTGACGTGTGGAGATGTTGAAGAGAACCCCGGCCCC**GACAAGAAGTACAG CATCGGCCTGGCCATCGGCACCAACTCTGTGGGCTGGGCCGTGATCACCGACGAGTACAAG GTGCCCA
Primers	*CALD1* forward	ACACTCTTTCCCTACACGACGCTCTTCCGATCTGCTAATCAGCTAGCATATGTATGAGAA
	CALD1 reverse	GTGACTGGAGTTCAGACGTGTGCTCTTCCGATCTTTGGACTTGATTATTGTCCTAAGTG
	KATNA1 forward	ACACTCTTTCCCTACACGACGCTCTTCCGATCTCCTGACGGCAAAGGAATATAG
	KATNA1 reverse	GTGACTGGAGTTCAGACGTGTGCTCTTCCGATCTACTGTGCTTCCTTGTATTGTTGT
	SLITRK1 forward	ACACTCTTTCCCTACACGACGCTCTTCCGATCTGGGCTTCAAATCAGCCAAG
	SLITRK1 reverse	GTGACTGGAGTTCAGACGTGTGCTCTTCCGATCTTTTCAAGACAAATGGGCAAG
	HPRT forward	ACACTCTTTCCCTACACGACGCTCTTCCGATCTGGTGAAAAGGACCCCACGAA
	HPRT reverse	GTGACTGGAGTTCAGACGTGTGCTCTTCCGATCTTGGCAAATGTGCCTCTCTACAAAT
	DNMT1 forward	ACACTCTTTCCCTACACGACGCTCTTCCGATCTTGAACGTTCCCTTAGCACTCTG
	DNMT1 reverse	GTGACTGGAGTTCAGACGTGTGCTCTTCCGATCTCCTTAGCAGCTTCCTCCTCC
	Q5 D10A forward	TGGTGCCGAT**AG**CCAGGCCGATG
	Q5 D10A reverse	ACTCTGTGGGCTGGGCCG
	qPCR Cas9 forward	CCGAAGAGGTCGTGAAGAAG
	qPCR Cas9 reverse	GCCTTATCCAGTTCGCTCAG
	qPCR GAPDH forward	GGAGCCAAACGGGTCATCATCTC
	qPCR GAPDH reverse	GAGGGGCCATCCACAGTCTTCT
	ddPCR control forward	AATCTACTCCCAGGAGCAG
	ddPCR control reverse	GTCTGTTTGAGGTTGCTAGTG
	ddPCR control probe	[HEX]TCAGGGCAGAGCCATCTATTGCT[BHQ1]
	ddPCR Cas9 insert forward	CTGAACGCCAAGCTGATTAC
	ddPCR Cas9 insert reverse	TTTCCACCAGCTGTCTCTT
	ddPCR Cas9 insert probe	[6FAM]TTCGACAATCTGACCAAGGCCGAG[BHQ1]
	ddPCR Puro backb forward	GGGTTACATCGAACTGGATCTC
	ddPCR Puro backb reverse	CGGCGTCAATACGGGATAAT
	ddPCR Puro backb probe	[6FAM]TAAAGTTCTGCTATGTGGCGCGGT[BHQ1]
	ddPCR M2rtTA insert forward	GCATAGAATCGGTGGTAGGT
	ddPCR M2rtTA insert reverse	TACACTGGGCTGCGTATT
	ddPCR M2rtTA insert probe	[6FAM]TTGCTACTTGATGCTCCTGTTCCTCC[BHQ1]
	ddPCR Neo backb forward	GCGCCTTATCCGGTAACTAT
	ddPCR Neo backb reverse	ACATACCTCGCTCTGCTAATC
	ddPCR Neo backb probe	[6FAM]AAGACACGACTTATCGCCACTGGC[BHQ1]

Supplementary Table 4: Effects of small molecules on Targeted Nucleotide Substitution (TNS) efficiency in *CALD1*, *KATNA1* and *SLITRK1* with Cas9n and Cas9. Shown are the cleavage enzyme, small molecules, loci, the mean absolute percentages of TNS and indels of all technical replicates from n independent experiments, and the mean fold change of TNS when using the respective small molecule compared to the control (as also shown in Fig. 2). Concentrations used were 20µM NU7026, 0.01µM Trichostatin A, 0.5µM MLN4924, 1µM NSC 19630, 5µM NSC 15520, 20µM AICAR, 1µM RS-1, 1µM Resveratrol, 1µM SCR7, 5µM L755507, 5µM STL127685 and 20µM B02.

			Control		Small molecule			
			Indel	TNS	Indel	TNS		mean fold
Cleavage enzyme	Small molecule	Locus	[%]	[%]	[%]	[%]	n	change of TNS
iCRISPR Cas9n	NU7026	*CALD1*	40,7	8,1	34,6	11,7	4	1,5
		KATNA1	63,5	8,5	49,7	18,7	4	2,6
		SLITRK1	81,7	5,2	68,7	11,9	3	2,5
	Trichostatin A	*CALD1*	34,2	6,8	31,7	10,1	5	1,5
		KATNA1	63,5	8,5	53,4	17,6	4	2,2
		SLITRK1	81,7	5,2	77,3	8,7	3	1,8
	MNL4924	*CALD1*	34,0	6,8	32,4	7,7	5	1,2
		KATNA1	63,5	8,5	63,5	8,5	4	1,1
		SLITRK1	81,7	5,2	76,2	6,6	3	1,3
	NSC 19630	*CALD1*	47,6	9,1	47,6	9,4	3	1,1
		KATNA1	63,5	8,5	60,2	8,7	4	1,0
		SLITRK1	81,7	5,2	79,4	5,5	3	1,0
	NSC 15520	*CALD1*	34,2	6,8	36,7	7,5	5	1,4
		KATNA1	63,5	8,5	62,9	8,1	4	1,0
		SLITRK1	81,7	5,2	82,2	4,8	3	1,0
	AICAR	*CALD1*	34,2	6,8	36,8	6,9	5	1,1
		KATNA1	63,5	8,5	63,4	8,0	4	1,1
		SLITRK1	81,7	5,2	81,0	5,2	3	1,0
	RS-1	*CALD1*	47,6	9,2	48,6	8,5	3	1,1
		KATNA1	63,5	8,5	62,0	8,0	4	1,2
		SLITRK1	81,7	5,2	79,0	5,3	3	1,0
	Resveratrol	*CALD1*	35,8	7,1	37,3	7,1	3	1,1
		KATNA1	62,2	7,0	63,6	8,0	3	1,0
		SLITRK1	75,8	6,4	76,0	6,2	2	1,1
	SCR7	*CALD1*	35,8	7,1	35,6	7,4	3	1,1
		KATNA1	57,9	6,3	59,1	6,3	2	1,0
		SLITRK1	80,0	5,5	77,2	5,9	2	1,0
	L755507	*CALD1*	28,8	5,8	29,3	5,5	4	1,0
		KATNA1	57,9	6,3	55,2	5,6	2	1,0
		SLITRK1	80,0	5,5	80,4	4,6	2	0,9
	STL127685	*CALD1*	43,6	8,4	42,0	7,4	2	0,9
		KATNA1	62,2	7,0	59,8	6,4	3	1,1
		SLITRK1	80,0	5,5	78,8	4,9	2	0,9
	B02	*CALD1*	32,1	10,7	29,3	6,5	1	0,6
		KATNA1	35,4	8,3	37,7	3,9	1	0,5
		SLITRK1	70,6	7,7	71,1	4,6	1	0,6
iCRISPR Cas9	NU7026	*CALD1*	31,2	15,9	18,2	25,5	2	1,5
		KATNA1	30,5	3,2	18,6	5,2	2	1,6
		SLITRK1	18,7	4,9	8,3	6,2	2	1,2
	Trichostatin A	*CALD1*	31,2	13,1	26,3	12,3	2	0,8
		KATNA1	30,5	3,2	27,8	3,4	2	1,0
		SLITRK1	18,7	4,9	15,5	5,0	2	1,0
	MNL4924	*CALD1*	31,2	13,1	25,5	10,5	2	0,7
		KATNA1	30,5	3,2	32,8	2,7	2	0,8
		SLITRK1	18,7	4,9	18,5	4,1	2	0,8
	NSC 19630	*CALD1*	45,8	21,2	44,8	21,2	1	1,0
		KATNA1	30,5	3,2	31,0	2,8	2	0,9
		SLITRK1	18,7	4,9	18,0	5,0	2	1,0
	NSC 15520	*CALD1*	31,2	13,1	31,2	15,7	2	1,3
		KATNA1	30,5	3,2	31,7	3,3	2	1,1
		SLITRK1	18,7	4,9	18,9	5,4	2	1,1
	AICAR	*CALD1*	31,2	13,1	31,8	13,7	2	1,1
		KATNA1	30,5	3,2	29,6	2,9	2	0,9
		SLITRK1	18,7	4,9	18,6	5,1	2	1,0
	RS-1	*CALD1*	45,8	21,2	43,9	22,2	1	1,0
		KATNA1	30,5	3,2	30,1	2,5	2	0,8
		SLITRK1	18,7	4,9	17,5	4,4	2	0,9
	Resveratrol	*CALD1*	31,2	13,1	31,6	13,3	2	1,1
		KATNA1	30,5	3,2	24,7	2,7	2	0,8

	SLITRK1	18,7	4,9	17,9	4,3	2	0,9
SCR7	*CALD1*	31,2	13,1	31,2	12,5	2	0,9
	KATNA1	30,5	3,2	29,8	2,8	2	0,8
	SLITRK1	18,7	4,9	18,7	4,7	2	0,9
L755507	*CALD1*	31,2	13,1	31,4	11,6	2	0,9
	KATNA1	30,5	3,2	30,4	3,4	2	0,9
	SLITRK1	18,7	4,9	18,2	3,9	2	0,7
STL127685	*CALD1*	31,2	13,1	30,3	12,8	2	1,0
	KATNA1	30,5	3,2	29,6	2,7	2	0,8
	SLITRK1	18,7	4,9	18,8	4,9	2	1,0
B02	*CALD1*	45,8	21,2	41,5	13,1	1	0,6
	KATNA1	30,5	3,2	31,1	2,0	2	0,5
	SLITRK1	18,7	4,9	16,5	2,2	2	0,4

Supplementary data references

1. Pinello L, *et al.* Analyzing CRISPR genome-editing experiments with CRISPResso. *Nat Biotechnol* **34**, 695-697 (2016).
2. Chari R, Mali P, Moosburner M, Church GM. Unraveling CRISPR-Cas9 genome engineering parameters via a library-on-library approach. *Nat Methods* **12**, 823-826 (2015).
3. O'Brien J, Wilson I, Orton T, Pognan F. Investigation of the Alamar Blue (resazurin) fluorescent dye for the assessment of mammalian cell cytotoxicity. *Eur J Biochem* **267**, 5421-5426 (2000).
4. Maruyama T, Dougan SK, Truttmann MC, Bilate AM, Ingram JR, Ploegh HL. Increasing the efficiency of precise genome editing with CRISPR-Cas9 by inhibition of nonhomologous end joining. *Nat Biotechnol* **33**, 538-542 (2015).
5. Pinder J, Salsman J, Dellaire G. Nuclear domain 'knock-in' screen for the evaluation and identification of small molecule enhancers of CRISPR-based genome editing. *Nucleic Acids Res* **43**, 9379-9392 (2015).
6. Chu VT, *et al.* Increasing the efficiency of homology-directed repair for CRISPR-Cas9-induced precise gene editing in mammalian cells. *Nat Biotechnol* **33**, 543-548 (2015).
7. Singh P, Schimenti JC, Bolcun-Filas E. A mouse geneticist's practical guide to CRISPR applications. *Genetics* **199**, 1-15 (2015).
8. Song J, Yang D, Xu J, Zhu T, Chen YE, Zhang J. RS-1 enhances CRISPR/Cas9- and TALEN-mediated knock-in efficiency. *Nat Commun* **7**, 10548 (2016).
9. Yang D, Scavuzzo MA, Chmielowiec J, Sharp R, Bajic A, Borowiak M. Enrichment of G2/M cell cycle phase in human pluripotent stem cells enhances HDR-mediated gene repair with customizable endonucleases. *Sci Rep* **6**, 21264 (2016).
10. Greco GE, Matsumoto Y, Brooks RC, Lu Z, Lieber MR, Tomkinson AE. SCR7 is neither a selective nor a potent inhibitor of human DNA ligase IV. *DNA Repair (Amst)* **43**, 18-23 (2016).
11. Zhang JP, *et al.* Efficient precise knockin with a double cut HDR donor after CRISPR/Cas9-mediated double-stranded DNA cleavage. *Genome Biol* **18**, 35 (2017).
12. Suzuki K, *et al.* In vivo genome editing via CRISPR/Cas9 mediated homology-independent targeted integration. *Nature* **540**, 144-149 (2016).
13. Robert F, Barbeau M, Ethier S, Dostie J, Pelletier J. Pharmacological inhibition of DNA-PK stimulates Cas9-mediated genome editing. *Genome Med* **7**, 93 (2015).
14. Wang K, *et al.* Efficient Generation of Orthologous Point Mutations in Pigs via CRISPR-assisted ssODN-mediated Homology-directed Repair. *Mol Ther Nucleic Acids* **5**, e396 (2016).
15. Yu C, *et al.* Small molecules enhance CRISPR genome editing in pluripotent stem cells. *Cell Stem Cell* **16**, 142-147 (2015).
16. Weterings E, *et al.* A novel small molecule inhibitor of the DNA repair protein Ku70/80. *DNA Repair (Amst)* **43**, 98-106 (2016).
17. Aggarwal M, Sommers JA, Shoemaker RH, Brosh RM, Jr. Inhibition of helicase activity by a small molecule impairs Werner syndrome helicase (WRN) function in the cellular response to DNA damage or replication stress. *Proc Natl Acad Sci U S A* **108**, 1525-1530 (2011).
18. Jimeno S, Fernandez-Avila MJ, Cruz-Garcia A, Cepeda-Garcia C, Gomez-Cabello D, Huertas P. Neddylation inhibits CtIP-mediated resection and regulates DNA double strand break repair pathway choice. *Nucleic Acids Res* **43**, 987-999 (2015).

19. Glanzer JG, Liu S, Oakley GG. Small molecule inhibitor of the RPA70 N-terminal protein interaction domain discovered using in silico and in vitro methods. *Bioorg Med Chem* **19**, 2589-2595 (2011).

20. Glanzer JG, Carnes KA, Soto P, Liu S, Parkhurst LJ, Oakley GG. A small molecule directly inhibits the p53 transactivation domain from binding to replication protein A. *Nucleic Acids Res* **41**, 2047-2059 (2013).

21. Sullivan K*, et al.* Identification of a Small Molecule Inhibitor of RAD52 by Structure-Based Selection. *PLoS One* **11**, e0147230 (2016).

22. Huang F, Motlekar NA, Burgwin CM, Napper AD, Diamond SL, Mazin AV. Identification of specific inhibitors of human RAD51 recombinase using high-throughput screening. *ACS Chem Biol* **6**, 628-635 (2011).

23. Lee JH, Guo Z, Myler LR, Zheng S, Paull TT. Direct activation of ATM by resveratrol under oxidizing conditions. *PLoS One* **9**, e97969 (2014).

24. Lee JS. Activation of ATM-dependent DNA damage signal pathway by a histone deacetylase inhibitor, trichostatin A. *Cancer Res Treat* **39**, 125-130 (2007).

CHAPTER 2

Simultaneous precise editing of multiple genes in human cells

S. Riesenberg (corresponding), M. Chintalapati, D. Macak, P. Kanis, T. Maricic, and S. Pääbo

Nucleic Acids Research (2019)

Published online 8 August 2019

Nucleic Acids Research, 2019, Vol. 47, No. 19 ***e116***
doi: 10.1093/nar/gkz669

Simultaneous precise editing of multiple genes in human cells

Stephan Riesenberg*, Manjusha Chintalapati, Dominik Macak, Philipp Kanis, Tomislav Maricic† and Svante Pääbo†

Department of Evolutionary Genetics, Max Planck Institute for Evolutionary Anthropology

Received March 04, 2019; Revised June 26, 2019; Editorial Decision July 21, 2019; Accepted July 24, 2019

ABSTRACT

When double-strand breaks are introduced in a genome by CRISPR they are repaired either by non-homologous end joining (NHEJ), which often results in insertions or deletions (indels), or by homology-directed repair (HDR), which allows precise nucleotide substitutions to be introduced if a donor oligonucleotide is provided. Because NHEJ is more efficient than HDR, the frequency with which precise genome editing can be achieved is so low that simultaneous editing of more than one gene has hitherto not been possible. Here, we introduced a mutation in the human *PRKDC* gene that eliminates the kinase activity of the DNA-dependent protein kinase catalytic subunit (DNA-PKcs). This results in an increase in HDR irrespective of cell type and CRISPR enzyme used, sometimes allowing 87% of chromosomes in a population of cells to be precisely edited. It also allows for precise editing of up to four genes simultaneously (8 chromosomes) in the same cell. Transient inhibition of DNA-PKcs by the kinase inhibitor M3814 is similarly able to enhance precise genome editing.

INTRODUCTION

When CRISPR nucleases and guide RNAs (gRNAs) are used to introduce double-stranded breaks (DSBs) in a genome, the two DNA ends are covered by DNA-dependent protein kinase (DNA-PK) complexes, which consist of Ku70/80 and DNA-PKcs (1). DNA-PKcs then undergoes conformational changes induced in part by autophosphorylation (2,3) as well as by other kinases (4,5) at >60 phosphorylation sites (6–8). This allows it to recruit NHEJ repair proteins and inhibit HDR proteins, for example ataxia telangiectasia mutated kinase (ATM), by phosphorylation (6,9,10). DNA ends can also be bound by the MRN (Mre11, Rad50 and Nbs1) complex, which results in 5′-3′ resection of DNA ends and HDR or microhomology-mediated end joining (MMEJ), also referred to as alternative NHEJ (11,12). In the case of HDR, end resection is followed by RAD51-nucleoprotein filament generation, annealing of homologous DNA, and DNA synthesis (1,13). In case of MMEJ repair, identical sequences of 1–16 nucleotide in the single-stranded ends align to each other, followed by removal of unaligned parts of the single-stranded ends, gap filling DNA synthesis and ligation, resulting in a deletion at the DSB site (12).

Because NHEJ introduce indels that can lead to frameshift mutations it is often used to inactivate genes. In contrast, HDR normally uses a sister chromatid to repair the chromosome carrying a DNA break. If exogenous 'donor' DNA carrying desired mutations is provided, it is possible to perform precise genome editing (PGE), i.e. introduce desired nucleotide substitutions at specific positions in a genome. Typically, NHEJ is more efficient than HDR and has been used to knock out multiple target genes in cells, for example five genes in mouse embryonic stem cells (14) and 62 copies of one endogenous retrovirus in a porcine cell line (15). In contrast, although several studies have tried to inhibit NHEJ or enhance HDR in order to increase the efficiencies of PGE (16–20), simultaneous PGE of more than one desired target in animal cells has not been reported, although methods for co-selection of one desired edit by simultaneous introduction of a selectable modification at a different locus have been developed (21,22). However, this allows only a single desired target to be edited together with the selectable marker.

Because simultaneous knockouts of several genes by NHEJ is possible, DNA cleavage by the CRISPR enzymes is not rate limiting for genome editing. Rather, it seems that the higher efficiency of NHEJ relative to HDR limits the ability to introduce precise edits. In 2008, it was shown that a lysine to arginine mutation at position 3753 near the ATP binding site in the DNA-PKcs protein (KR) abolishes its kinase activity (13,23) in Chinese hamster ovary cells and that this increases homologous recombination to levels 2- to 3-fold above those seen when DNA-PKcs was completely knocked down (23). Inactive but structurally intact DNA-PKcs may increase homologous recombination be-

*To whom correspondence should be addressed. Tel: +49 341 3550519; Email: stephan_riesenberg@eva.mpg.de
†The authors wish it to be known that, in their opinion, the last two authors should be regarded as joint Last Authors.

cause phosphorylation of downstream NHEJ proteins as well as phosphorylation-induced inhibition of ATM kinase activity (9) is blocked, while ATM levels needed for efficient HDR are maintained (23). In contrast, in the absence of DNA-PKcs protein, levels of ATM and thus HDR are reduced (13,24). Knock down of the DNA-PKcs protein by siRNA (25), or in DNA-PKcs (-/-) cell line (26), could only moderately increase homologous recombination efficiencies.

METHODS

Cell culture

We recently created an iCRISPR-Cas9n line from human induced pluripotent stem cells (hiPSCs) (17) (409-B2, female, Riken BioResource Center) as described by Gonzalez *et al.* (17,27) (GMO permit AZ 54-8452/26). For this study, we further used HEK293 cells (ECACC, 85120602) with Dulbecco's modified Eagle's medium/F-12 (Gibco, 31330-038) supplemented with 10% fetal bovine serum (FBS) (SIGMA, F2442) and 1% NEAA (SIGMA, M7145); as well as K562 cells (ECACC, 89121407) with Iscove's modified Dulbecco's media (ThermoFisher, 12440053) supplemented with 10% FBS. 409-B2 hiPSCs were grown on Matrigel Matrix (Corning, 35248) in mTeSR1 medium (StemCell Technologies, 05851) with supplement (StemCell Technologies, 05852) that was replaced daily. Medium for HEK293 and K562 was replaced every second day. At ∼80% confluency, adherent cells were dissociated using EDTA (VWR, 437012C) and split 1:6 to 1:10 in medium supplemented with 10 μM Rho-associated protein kinase (ROCK) inhibitor Y-27632 (Calbiochem, 688000) for 1 day after replating. K562 cells were split 1:6 to 1:10 dilution after 1 week. All cells were grown at 37°C in a humidified incubator with 5% CO_2.

Lipofection of oligonucleotides

409-B2 iCRISPR-Cas9n hiPSCs were incubated in medium containing 2 μg/ml doxycycline (Clontech, 631311) three to 4 days prior to lipofection. Lipofection was done using the alt-CRISPR protocol (IDT) at a final concentration of 7.5 nM of each gRNA (crRNA/tracR duplex) and 10 nM of the DNA donors. In brief, 0.75 μl RNAiMAX (Invitrogen, 13778075) and the respective oligonucleotides were separately diluted in 25 μl OPTI-MEM (Gibco, 1985-062) and incubated at room temperature for 5 min. Both dilutions were mixed to yield 50 μl of OPTI-MEM including RNAiMAX, gRNAs and single stranded DNA donors (ssODNs). The lipofection mix was incubated for 20–30 min at room temperature. Cells were dissociated using EDTA for 5min and counted using the Countess Automated Cell Counter (Invitrogen). The lipofection mix, 100 μl containing 25 000 dissociated cells in mTeSR1 supplemented with Y-27632, and 2 μg/ml doxycycline were put in one well of a 96-well covered with Matrigel Matrix (Corning, 35248). Media was exchanged to regular mTeSR1 media after 24 h. *KATNA1, SLITRK1,* and *CALD1* were edited using lipofection (Figure 1A and B). We also attempted multiplexed editing of three genes simultaneously using lipofection, but achieved 3–10% HDR for a gene at best.

Oligonucleotide and ribonucleoprotein electroporation

The recombinant *Streptococcus pyogenes* Cas9 protein, *Acidaminococcus* sp. *BV3L6* Cpf1 protein and respective electroporation enhancer were from IDT (Coralville, USA) and electroporation was done using the manufacturer's protocol, except for the following alterations. Nucleofection was done using the B-16 program of the Nucleofector 2b Device (Lonza) in cuvettes for 100 μl Human Stem Cell nucleofection buffer (Lonza, VVPH-5022), containing 1 million cells, 78pmol electroporation enhancer, 160 pmol of each gRNA (crRNA/tracR duplex for Cas9 and crRNA for Cpf1), 200 pmol of each single stranded DNA donor (ssODN), and 252 pmol Cas9 or Cpf1. Cells were counted using the Countess Automated Cell Counter (Invitrogen). For multiplexing, only gRNAs and ssODNs were electroporated, since a Cas9n expressing iCRISPR-Cas9n hiPSC line was used. 409-B2 iCRISPR-Cas9n hiPSCs were incubated in medium containing 2 μg/ml doxycycline (Clontech, 631311) three to four days prior to editing. For multiplexed precise genome editing, this medium was exchanged to StemFlex with supplement (Gibco, A3349401), CloneR (StemCell Technologies, 05888), and doxycycline one day before electroporation. 90% of the electroporated cells were plated for bulk genotype analysis and for hiPSCs 10 percent were plated in a separate 6well to give rise to colonies derived from a single cell (clones) for which the media was supplemented with ROCK inhibitor Y-27632 for 2 days post-electroporation. After at least 7 days colonies were picked for following propagation and DNA isolation. Single cell colonies of HEK293 and K562 cells were acquired by sorting single cells in wells of a 96-well plate using a single-cell printer (Cytena).

Illumina library preparation and sequencing

At least 3 days after transfection cells were dissociated using Accutase (SIGMA, A6964), pelleted, and resuspended in 15 μl QuickExtract (Epicentre, QE0905T). Incubation at 65°C for 10 min, 68°C for 5 min and finally 98°C for 5 min was performed to yield single stranded DNA as a PCR template. Primers for each targeted loci containing adapters for Illumina sequencing were from IDT (Coralville, USA) (see Supplementary Table S1). PCR was done in a T100 Thermal Cycler (Bio-Rad) using the KAPA2G Robust PCR Kit (SIGMA, KK5024) with supplied buffer B and 3 μl of cell extract in a total volume of 25 μl. The thermal cycling profile of the PCR was: 95°C 3 min; 34× (95°C 15 s, 65°C 15 s, 72°C 15 s); 72°C 60 s. P5 and P7 Illumina adapters with sample specific indices were added in a second PCR reaction (28) using Phusion HF MasterMix (Thermo Scientific, F-531L) and 0.3 μl of the first PCR product. The thermal cycling profile of the PCR was: 98°C 30 s; 25× (98°C 10 s, 58°C, 10 s, 72°C 20 s); 72°C 5 min. Amplifications were verified by size separating agarose gel electrophoresis using 2% EX gels (Invitrogen, G4010–11). The indexed amplicons were purified using Solid Phase Reversible Immobilization (SPRI) beads in a 1:1 ratio of beads to PCR solution (29). Double-indexed libraries were sequenced on a MiSeq (Illumina) giving paired-end sequences of 2 × 150 bp (+7 bp index). After base calling using Bustard (Illumina) adapters were trimmed using leeHom (30).

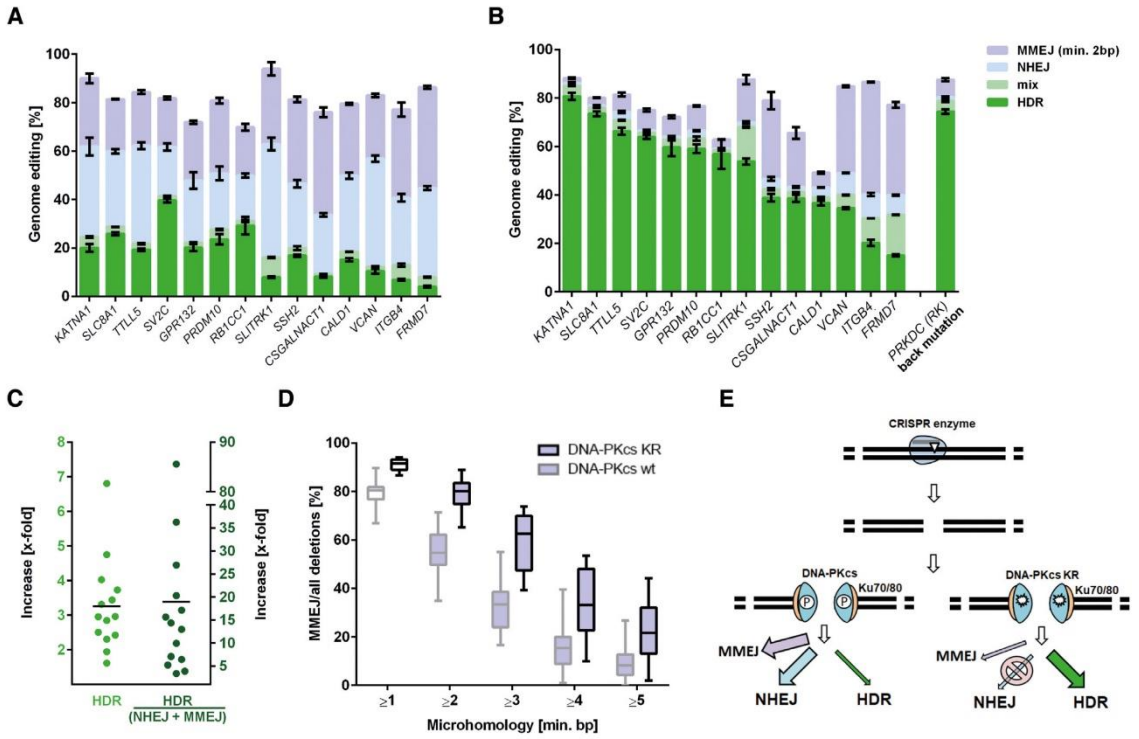

Figure 1. Catalytically inactive DNA-PKcs promotes homology-directed repair (HDR). (**A**) The genome editing frequencies with Cas9n and single stranded DNA donors for 14 genes in the DNA-PKcs WT cell line; and (**B**) in the DNA-PKcs KR cell line. HDR, 'mix' (HDR with indels), NHEJ, and MMEJ (≥2 bp microhomology) are indicated in green, light green, light blue and light purple, respectively. Error bars show the SEM of at least four replicate experiments. (**C**) Increase in frequency of HDR (left) and relative to NHEJ and MMEJ (right). Each dot corresponds to one gene and the black line shows the mean. (**D**) Percent of all deletions resulting from MMEJ for the 14 genes as a function of microhomology length in KR and WT cells. Boxes extend from the 25th to 75th percentile, show the median as a line and have whiskers from minimum to maximum values. (**E**) Schematic illustration of the repair of DSBs. After a DSB induced, e.g. by a CRISPR enzyme, DNA ends are covered by Ku70/80 (orange), followed by binding of DNA-PKcs (cyan blue), both constituting a DNA-PK complex. Autophosphorylation of DNA-PKcs leads to recruitment and activation of downstream NHEJ proteins. If DNA-PKcs is catalytically inactivated (e.g. by the K3753R mutation), the NHEJ pathway is blocked and only MMEJ can compete with HDR.

Amplicon sequence analysis

Bam-files were demultiplexed and converted into fastq files using SAMtools (31). CRISPResso (32) was used to analyse fastq files for percentage of wildtype, any targeted nucleotide substitution (HDR), indels (called as non-homologous end joining NHEJ), and mix of both. Analysis was restricted to amplicons with a minimum of 70% similarity to the wildtype sequence and to a window of 20 bp from each gRNA. Sequence homology for an HDR occurrence was set to 95%. Unexpected substitutions were ignored as putative sequencing errors. Since CRISPResso cannot distinguish reads with indels from NHEJ or microhomology-mediated end joining (MMEJ), we wrote a python script to call MMEJ events. Sequencing data from colonies derived from single cell seeding (Figure 2D) was analyzed using SAMtools and colonies were regarded as clones if the clear majority of reads consisted of a single sequence (homozygous) or of two sequences of similar read counts (heterozygous) and blocking mutations, ancient mutations, as well as indels for each chromosome of the cells of a clone were noted (Supplementary Tables S2–S5).

Whole genome sequencing

The 409-B2 iCRISPR-Cas9n hiPSCs WT line, KR clone and KR-KSC line were expanded and two million cells of the respective lines were harvested and DNA was isolated. DNA was sonicated three times with a Bioruptor (Diogenode), with the output selector switched to (H)igh to yield fragments of ∼0.15 to 0.8 kb. Shearing was checked by agarose gel electrophoresis using EX gels (Invitrogen, G4010–11) and a Typhoon 9410 imager (Amersham, Biosciences). Fragment ends were made blunt for 30 min at room temperature with the Quick Blunting Kit (New England Biolabs, E1201L), purified with SPRI beads (28), adapter-ligated for 30 min at room temperature with the Quick Ligation Kit (New England Biolabs, M2200L), purified with SPRI beads, double indexed by PCR-amplification and purified with SPRI beads. Double-indexed libraries

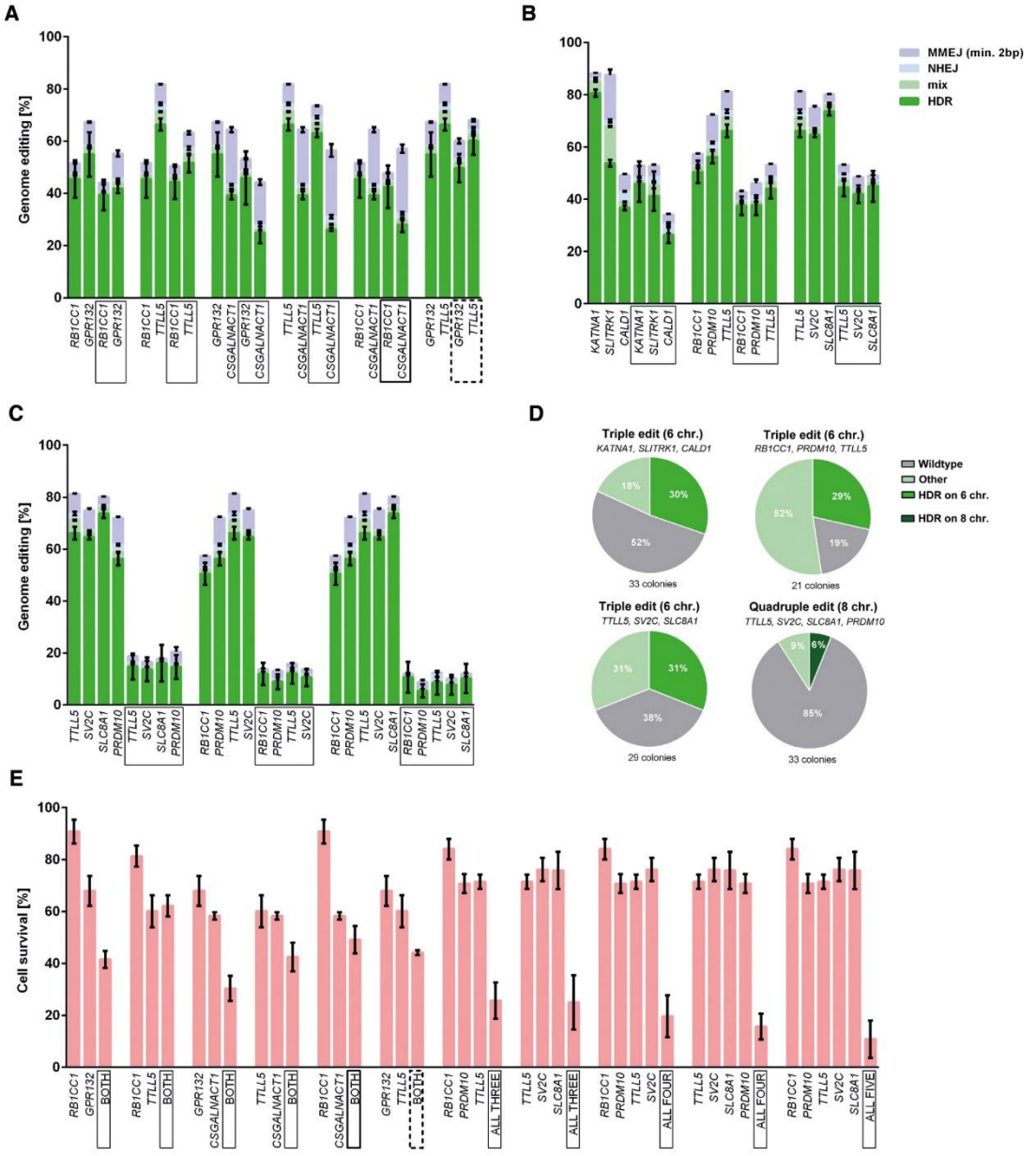

Figure 2. Multiplexed precise genome editing using catalytically inactive DNA-PKcs. (**A**) Editing frequencies for single genes and combinations of two out of four genes (framed). HDR, mix (HDR with indels), NHEJ, and MMEJ are indicated in green, light green, light blue and light purple, respectively. (**B**) Editing frequencies for single genes and combinations of three genes (framed). (**C**) Editing frequencies for single genes and combinations of four or five genes (framed). (**D**) Pie charts of the genotypes from single cell derived colonies after multiplexed editing of three combinations of three genes and one of four genes. See Supplementary Tables S2–S5 for details. (**E**) Cell survival after editing of one to five genes. Resazurin assays were performed three days after editing. Error bars show the SEM of four replicate experiments for A, B, C and D.The bold frame and bold dashed frame indicate that the targeted genes are on the same chromosome and are divided by a centromere (distance 34Mb) or are on the same chromosome arm (distance 29 Mb), respectively.

were sequenced on a HiSeq (Illumina) 2 × 75 bp (+7 bp index) (Figure 3C and Supplementary Figure S3).

Mapping and genotyping

Reads were mapped to the human reference (hg19) using Burrows-Wheeler Aligner (BWA) (33) default parameters. Genotyping was carried out using Genome Analysis Toolkit (GATK) (34) (version 3.3-0-g37228af). We indel realigned the BWA mapped bam files using GATK IndelRealigner with default parameters. The variant calling was carried out on the realigned bam files by GATK HaplotypeCaller (java -jar GenomeAnalysisTK.jar -T HaplotypeCaller -R human_reference.fa -L chromosome_number –out output.vcf –I realigned.bam –emitRefConfidence BP_RESOLUTION –allSitePLs –output_mode EMIT_ALL_CONFIDENT_SITES).

Genomic coverage calculation

Coverage along the chromosomes was calculated with for 1Mb windows, using unique genomic regions (wgEncodeDukeMapabilityUniqueness35bp=1) and excluding blacklisted regions (wgEncodeDacMapabilityConsensusExcludable, wgEncodeDukeMapabilityRegionsExcludable) (35).

Genotype variant filtering

The variants called by GATK were filtered by removing positions that overlap repeats annotated by the UCSC genome browser and that might lead to ambiguous alignments (map35_100% filter from reference (36)). Genomic positions with 30–50-fold coverage in all three lines were used for downstream analysis. We required the absolute difference between the maximum and minimum alternate allele frequency of a genotype in all three clones to be at least 30%. Finally, we inspected each genotype differences between lines using the Integrated Genome Viewer (IGV) (37) and excluded obvious genotyping artefacts.

Resazurin assay

409B2-iCRISPR hiPSCs expressing DNA-PKcs wildtype (WT), catalytically inactive DNA-PKcs (K3753R), or K562 cells were plated (50 000/100 000 cells per well in a 24-well plate). HiPSCs were grown for two days before treatment with different Bleomycin (Sigma, B8416) concentrations for 1 h. Afterwards cells were washed three times. After recovery for 72 h, 100 μl fresh media together with 10 μl resazurin solution (Cell Signaling, 11884) was added. Resazurin is converted into fluorescent resorfin by cellular dehydrogenases and fluorescence (exitation: 530–570 nm, emission: 590–620 nm) reflects the amount of living cells (38). Cells were incubated with resazurin at 37°C for 5 h before fluorescence readings using a Typhoon 9410 imager (Amershamn Biosciences) and quantification using ImageJ and the 'ReadPlate' plugin. Wells with media and resazurin, but without cells, were used a blank.

Karyotyping

Karyotyping by trypsin induced Giemsa staining (GTG) or spectral karyotyping (SKY) were carried out according to international quality guidelines (ISCN 2016: An International System for Human Cytogenetic Nomenclature (39)) by the 'Sächsischer Inkubator für klinische Translation' (Leipzig, Germany).

Cellular clone genotype and target gene copy number analysis

409-B2 hiPSCs were edited in the *FRMD7* gene using Cas9 ribonucleoprotein and DNA donor electroporation and cells were treated with or without 2 μM M3814 for 3 days. After recovery for three days cells were sorted using a single-cell printer (Cytena) with hydrophobic cartridges to establish cellular clones. DNA extracts were used for target amplification with PCR from which Illumina libraries were made and sequenced. Amplicon sequence analysis was carried out as described above. To determine *FRMD7* copy number, a TaqMan assay was done (ThermoFisher, 4400294, reporter target sequence: FAM-TTGCAGTGGGCTCTACATAGC-NFQ; human RNAse P copy number reference, ThermoFisher, 4403328; TaqMan genotyping master mix, ThermoFisher, 4371355). Quantitative PCR was carried out in a Stratagene MX3005P (Agilent Technologies). Long range PCR (~3 kb) of the *FRMD7* locus was done in a T100 Thermal Cycler (Bio-Rad) using the KAPA2G Robust PCR Kit (SIGMA, KK5024) with buffer B and 3 μl of DNA extract in a total volume of 25 μl. The thermal cycling profile of the PCR was: 95°C 3 min; 30× (95° 15 s, 65°C 15 s, 72°C 60 s); 72°C 60 s. Primers are stated in Supplementary Table S1.

Statistical analysis

Bar graphs in figures were plotted and SEM error bars were calculated using GraphPad Prism 6 software. The number of replicates is stated in the respective figure legends.

RESULTS

Catalytically inactive DNA-PKcs promotes homology-directed repair across cell types and CRISPR enzymes

To achieve high efficiency of targeted DSBs and reduce off-target DSBs we previously generated a human induced pluripotent stem cell (hiPSC) line carrying a doxycycline-inducible Cas9 with the D10A mutation (iCRISPR-Cas9n) causing it to generate nicks rather than double-stranded cuts in DNA targets (17). In this line, we now introduced the K3753R mutation in the *PRKDC* gene that encodes DNA-PKcs protein. We compared the efficiency with which nucleotide substitutions can be introduced in DNA-PKcs K3753R (KR) and DNA-PKcs wildtype (WT) cells. To do this, we designed gRNAs (40) and single-stranded oligodeoxynucleotide donors (ssODNs) to revert 14 substitutions that are fixed or almost fixed among present-day humans but occur in the ancestral, ape-like states in the Neandertal and Denisovan genomes (36) back to the ancestral states. When necessary, the ssODNs carried additional silent non-coding mutations to prevent repeated cutting of

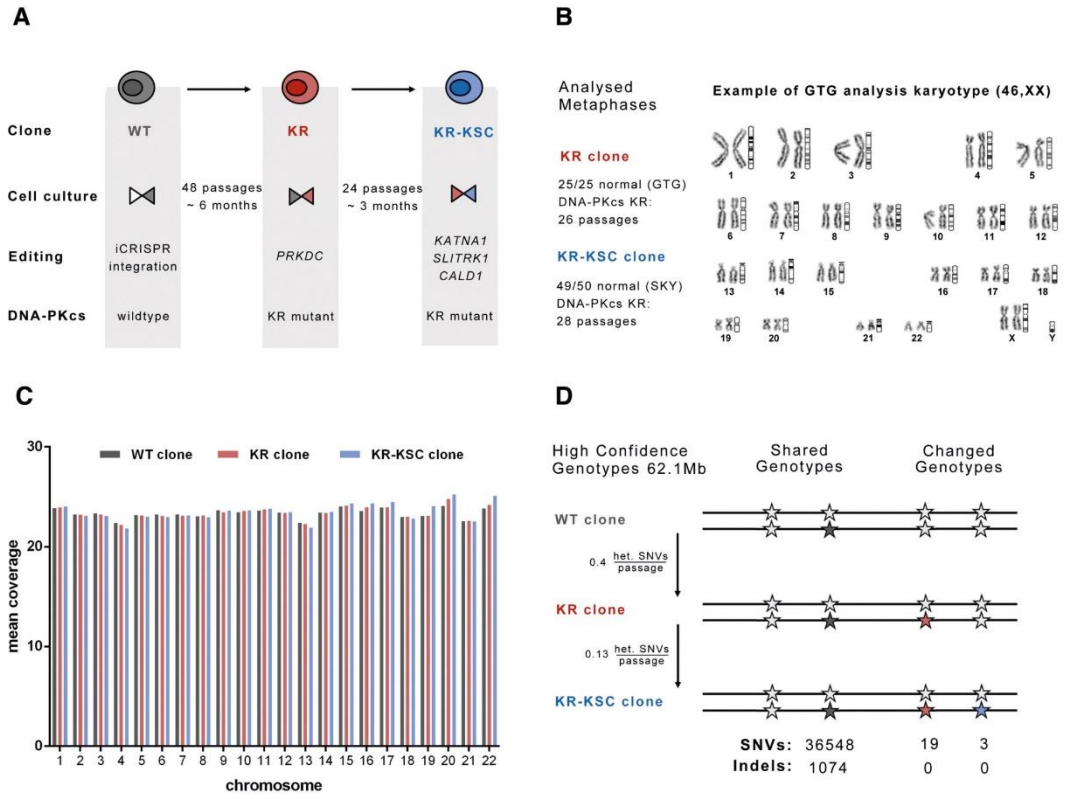

Figure 3. Genome stability of DNA-PKcs K3753R cells. (**A**) Schematic illustration of the cell lines used. A 409B2-iCRISPR iPSC line (gray) was edited to express the DNA-PKcs KR (red) which was in turn used to edit three genes *KATNA1, SLITRK1*, and *CALD1* to yield the KR-KSC line (blue). The editing scheme and passaging times between clonal bottlenecks are shown. (**B**) Karyotypes analyzed by Giemsa staining (GTG) spectral karyotyping (SKY) passage numbers are indicated. One polyploid metaphase was observed in the KR-KCS clone. (**C**) Genomic sequence coverage per chromosome in the three cell lines. (**D**) Numbers of SNVs and indels in high-confidence genotypes (62.1Mb) of the three cell lines are given. Novel genotypes that appeared first in the KR line (19) and KR-KSC (3) line, are colored red or blue, respectively.

the DNA once the targeted substitutions have been introduced (Supplementary Table S1).

Following induction of expression of Cas9n by doxycycline, cells were transfected gRNAs and ssODNs and cultured for three days. DNA was isolated, PCR amplicons of the targeted regions were sequenced and HDR scored as the presence of the ssODN-derived mutations in the target genes, which could have been introduced by classical homologous recombination or single-strand template repair. When editing each gene independently, HDR frequencies in the WT cells varied between 4% and 40% among the 14 genes (average 18%). In the KR cells, frequencies varied between 15% and 81% (average 51%) (Figure 1A and B). Across the genes, HDR is increased between 1.6-fold and 6.8-fold (average 3.3-fold) in KR cells (Figure 1C).

When deletions occurred at sites where the sequence on one end of the deletion was identical to the undeleted sequence on the other end and was at least two nucleotides long we classified this as MMEJ while other indels were considered to be the result of NHEJ. When compared to DNA-PKcs WT cells, NHEJ and MMEJ decreased in KR cells from an average of 31% to 4% (8.5-fold) and 29% to 17% (1.7-fold), respectively (Figure 1A and B). The average ratio of HDR to the sum of NHEJ and MMEJ was 0.3 in WT cells and 6.5 in KR cells (Figure 1C). For all genes tested, MMEJ is increased relatively to NHEJ in KR cells, regardless of the length of microhomology involved (Figure 1D). Thus, in KR cells, NHEJ is inhibited, resulting in a drastic increase of HDR, as schematically illustrated in Figure 1E.

For the three genes with the lowest HDR frequencies in KR cells, MMEJ is the predominant editing event. To increase HDR in those genes, we tried to use Cas9 instead of Cas9n to induce chromosomal breaks. This increased HDR for two genes from 35% and 20% to 73% and 87%, respectively, while the MMEJ decreased for all three genes (Supplementary Figure S1A). Thus, for some targets where MMEJ predominates, PGE can be 'rescued' by using a different CRISPR enzyme, which uses different cleavage sites and therefore possibly results in different tendencies for MMEJ (Supplementary Figure S1B).

To test if the increase in HDR seen in the hiPSCs was dependent on the cell type or enzyme used, we introduced

the DNA-PKcs KR mutation in human embryonic kidney cells (HEK293) and human immortalized myelogenous leukemia cells (K562). When gRNAs and ssODNs (selected from Figure 1 and a previous study (17)) are transfected together with Cas9 nickase, Cas9 or Cpf1 protein HDR increased in all cell lines regardless of the enzyme used (Supplementary Figure S1C), and regardless of if the enzyme was transfected or endogenously produced by the cell (Figure 1A, B and Supplementary Figure S1A–C).

Simultaneous precise genome editing of multiple genes in the same cell

We next electroporated gRNAs and the corresponding donor DNAs (selected from Figure 1) for all pairwise combinations of four different genes into KR cells after induction of Cas9n expression. The HDR frequency of double edits were similar or slightly lower than single edits of the corresponding genes, regardless if both genes were located on different chromosomes, on different chromosome arms, or on the same chromosome arm (Figure 2A). We next tried to simultaneously edit three, four and five genes. For three different combinations of three genes, the HDR efficiency was on average one third lower than for the single edits leading to average editing frequencies of 40% per targeted site (Figure 2B). For four or five genes, average HDR frequencies decreased to 13% and 8%, respectively (Figure 2C). Additionally, cell survival decreased from 30–68% for two edits to 11% for five edits (Figure 2E).

We isolated single cell-derived colonies (SCCs) from the pools of edited cells. For triple edits, approximately a third of SCCs carried the edited nucleotide in a homozygous form at all genes targeted (six chromosomes) while this was the case for 6% of SCCs for quadruple edits (eight chromosomes) (Figure 2D, Supplementary Tables S2–S5). Notably, the percentage of cellular clones homozygous for all four intended amino acid-changing substitutions (6%) is 1000-fold higher than would be expected by chance if edits of the different genes would be independent of each other (0.006%), suggesting that cells that are 'editing competent' will tend to be efficiently edited at multiple sites.

Genome stability of cells expressing catalytically inactive DNA-PKcs is not compromised

One concern is that inactivation of the catalytic activity of DNA-PKcs may lead to genomic instability because spontaneously occurring DSBs cannot be repaired by NHEJ. We therefore analyzed the karyotypes of hiPSCs that had expressed DNA-PKcs KR for three months by trypsin-Giemsa banding (GTG) and spectral karyotyping (SKY), which is able to detect smaller translocations. All 25 metaphases analyzed by GTG and 49 out of 50 analyzed by SKY had normal karyotypes (Figure 3B). Furthermore, we treated cells expressing either DNA-PKcs WT or KR with the DSB-inducing drug bleomycin to mimic the effect of the accumulation of DSBs over long times. As expected, bleomycin reduced cell survival. This effect was twice as strong in DNA-PKcs KR expressing cells as in WT cells (Supplementary Figure S2A). After bleomycin treatment, 4 out of 50 metaphases analyzed in DNA-PKcs WT cells contained unbalanced translocations with gain or loss of chromosomal fragments, while 2 out of 50 metaphases in DNA-PKcs KR cells contained balanced translocations (Supplementary Figure S2B–E). In conclusion, we observe no increase in aneuploidy or chromosomal rearrangements in KR cells compared to WT cells.

To asses other types of genetic instability we sequenced the genomes of three cellular clones: DNA-PKcs WT, its descendent KR clone, and KR's descendent triple-edited KR-KSC clone (*KATNA1-SLITRK1-CALD1* edited) (Figure 3A) to ∼24-fold genomic coverage. WT cells were passaged 48 times before the KR clone was generated and KR cells were passaged 24 times before the triple-edited clone was generated (Figure 3A). Genotypes that appear in both the KR clone and the KR-KSC clone and are different from the WT clone are likely to be due to mutations that occurred while DNA-PKcs WT was expressed, whereas genotypes that appear only in the KR-KSC clone are likely to be due to mutations that happened while DNA-PKcs KR was expressed. To find big deletions and duplications we compared genomic coverage per chromosome (Figure 3C) and in 1 Mb windows along the chromosomes (Supplementary Figure S3). The only difference found was a drop in coverage in one window on chromosome 9 in both KR and KR-KSC clones compared to the WT indicating a heterozygous deletion. After filtering for high-confidence genotypes (see Methods) we looked for single nucleotide variants (SNVs) and indels among clones. Surprisingly, the telomeric 41 Mb on the short arm of chromosome 5 are devoid of heterozygote positions in the KR and KR-KSC cells whereas it contains 431 high-confidence heterozygous positions in the WT cells. This is not due to a heterozygous deletion since there is no drop in coverage and the karyotypes of chromosome 5 are normal. We speculate that this is due to a break-induced repair event, which is described in yeast and has recently been proposed to occur also in mammalian cells (41). Excluding the 41Mb on chromosome 5, we found 19 novel heterozygous SNVs shared between the KR and KR-KSC cells and three novel heterozygous SNVs in the KR-KSC cells (Figure 3D). We found no indels that differed among the three cell lines, even though we find indels shared among them. Extrapolated to the whole genome, the rate of mutation fixation per passage is 21 in WT cells and 7 in KR cells.

Transient inactivation of DNA-PKcs by small molecule M3814

We note that the efficiency with which nucleotide substitutions can be introduced in KR cells makes it possible to restore the normal DNA-PKcs function once desired changes have been introduced in the genome. We demonstrated this by editing the *PRKDC* gene back to its wildtype state and find that this 'back mutation' can be introduced in 74% of chromosomes (Figure 1B). An alternative way to increase HDR may be to transiently inhibit the kinase activity of DNA-PKcs. Indeed, several small molecule inhibitors of DNA-PK have been described to moderately increase HDR (17,25). We tested this approach using M3814 (42), a novel more efficient DNA-PKcs inhibitor which has not previously been used in genome editing. After a Cas9-induced

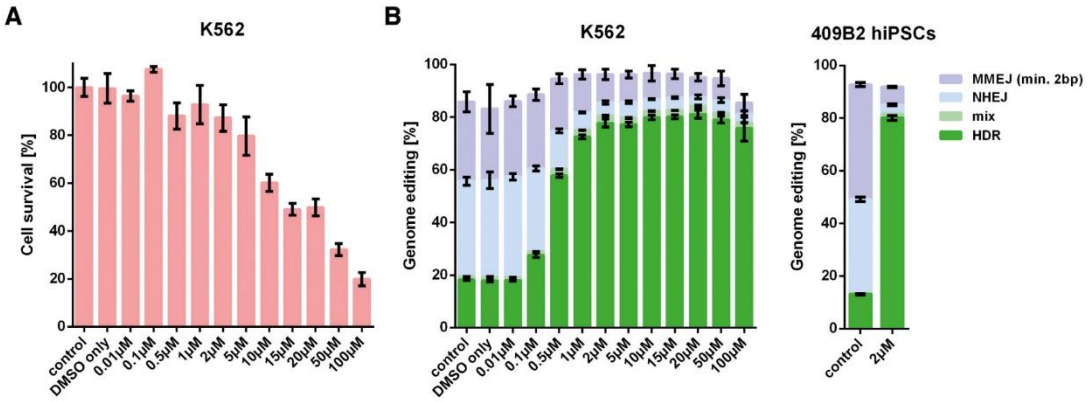

Figure 4. Effects of transient inactivation of DNA-PKcs by the small molecule M3814. (**A**) Resazurin assay for cell survival in K562 cells 3 days after editing of *FRMD7* with Cas9 protein and treatment with different concentrations of M3814. (**B**) Genome editing efficiencies of *FRMD7* with Cas9 protein in K562 cells treated with different concentrations of M3814, and in 409B2 hiPSCs with 2 μM M3814. M3814 was added for 3 days after editing. HDR, mix (HDR with indels), NHEJ, and MMEJ are indicated in green, light green, light blue and light purple, respectively. Error bars show the SEM of six replicates for A, three replicates for K562 cells for B, and two replicates for 409B2 hiPSCs for B.

DSB in K562 cells expressing wildtype DNA-PKcs M3814 increased HDR from 18% to 81% while exhibiting moderate toxicity. A comparable increase of HDR is seen in 409B2 hiPSCs (Figure 4A and B). The HDR increase when using M3814 is stronger than when using the previously described DNA-PK inhibitor NU7026 (4- versus 1.7-fold) (Supplementary Figure S4A).

To explore if this apparent high editing efficiency might be due to induction of large deletions of the target DNA sequences (43), we isolated cellular clones by single-cell printing after editing without and with M3814. By amplicon sequencing, we find that 10% of clones have homozygously incorporated the desired nucleotide substitution in an apparent diploid state when M3814 is not used whereas 76% have done so when M3814 is used (Supplementary Figure S5A and B). By long-range and quantitative PCR we found CRISPR-induced deletions in 2% of clones and apparent gains of one copy of the target locus in 6% of clones. The latter cases could be due to the duplication of the entire chromosome X, one of the most frequent aneuploidies in stem cells (44), or to erroneous repair of CRISPR-induced DSBs.

M3814 similarly increased HDR in several other genes and allowed for simultaneous multiple editing (data not shown). Thus, inhibition of the kinase activity of DNA-PKcs either by the reversible K3753R mutation or by the kinase inhibitor M3814 substantially increases PGE and allows the introduction of multiple nucleotide substitutions in human cells.

DISCUSSION

The approach described here makes it possible to simultaneously edit multiple target genes in a single cell much more efficiently than is currently possible. This will facilitate the testing and potentially the correction of multiple interacting disease-related genetic variants as well as the analyses of interacting variants of physiological or evolutionary interest. In fact, PGE as described here can presumably be made even more efficient by combining it with other approaches that increase PGE, for example with combinations of small molecules (Supplementary Figure S4B and C) (17). It is likely to be applicable not only in humans but also other vertebrates because the lysine residue at position 3753 in DNA-PKcs is conserved among vertebrates (45).

It is interesting that we find no evidence that the K3753R mutation decreases genome stability. In fact, we find fewer translocations after bleomycin treatment, and fewer mutations per passage, in the mutant cells than in the DNA-PKcs WT cells. Although this could be due to unknown differences among the cell lines, it is tempting to speculate that the impairment of the error-prone NHEJ may cause the cells to more frequently repair DSBs by the less error-prone HDR. If this fails, cells may undergo apoptosis, resulting in that surviving cells maintain their genome in a more accurate form.

The fact that the DNA-PKcs inhibitor M3814 is able to increase HDR to an extent comparable to what is achievable by the *PRKDC* mutation (Figure 4) is encouraging because M3814 can be used to transiently inhibit NHEJ and thus make the modification of *PRKDC* unnecessary. It is also encouraging for work in whole organisms because permanent DNA-PKcs inactivation results in severe combined immunodeficiency in mammals due to inability to carry out V(D)J recombination (24). Indeed, M3814 is in phase Ib/II clinical trials for treatment of various cancers, for example small cell lung cancer (NCT03116971) and rectal cancer (NCT03770689). If safe in humans, M3814 could therefore find use in gene therapy applications where high HDR efficiencies may be needed to achieve therapeutic goals.

DATA AVAILABILITY

All data are available from the corresponding author upon request. Genome sequencing data are deposited in the SRA database under accession number PRJNA543747.

SUPPLEMENTARY DATA

Supplementary Data are available at NAR Online.

ACKNOWLEDGEMENTS

Author contributions: S.R. conceived the idea and performed the experiments. D.M. and P.K. helped with experiments. S.R. and T.M. and S.P. planned the experiments and wrote the paper. M.C. and T.M. analyzed genome sequencing data. We thank Antje Weihmann and Barbara Schellbach for DNA sequencing, Heidrun Holland for karyotyping, Janet Kelso for help with DNA sequence analyses and Karin Mörl and Nelly Helmbrecht for helpful discussions.

FUNDING

Max-Planck Society and by the NOMIS foundation. Funding for open access charge: Max-Planck-Institute for Evolutionary Anthropology, Department of Evolutionary Genetics.
Conflict of interest statement. Related patent applications have been filed by the Max Planck Society (inventors S.R. and T.M.).

REFERENCES

1. Dueva,R. and Iliakis,G. (2013) Alternative pathways of non-homologous end joining (NHEJ) in genomic instability and cancer. *Transl Cancer Res.*, **2**, 163–177.
2. Meek,K., Lees-Miller,S.P. and Modesti,M. (2012) N-terminal constraint activates the catalytic subunit of the DNA-dependent protein kinase in the absence of DNA or Ku. *Nucleic Acids Res.*, **40**, 2964–2973.
3. Sibanda,B.L., Chirgadze,D.Y., Ascher,D.B. and Blundell,T.L. (2017) DNA-PKcs structure suggests an allosteric mechanism modulating DNA double-strand break repair. *Science*, **355**, 520–524.
4. Chen,B.P., Uematsu,N., Kobayashi,J., Lerenthal,Y., Krempler,A., Yajima,H., Lobrich,M., Shiloh,Y. and Chen,D.J. (2007) Ataxia telangiectasia mutated (ATM) is essential for DNA-PKcs phosphorylations at the Thr-2609 cluster upon DNA double strand break. *J. Biol. Chem.*, **282**, 6582–6587.
5. Yajima,H., Lee,K.J. and Chen,B.P. (2006) ATR-dependent phosphorylation of DNA-dependent protein kinase catalytic subunit in response to UV-induced replication stress. *Mol. Cell Biol.*, **26**, 7520–7528.
6. Neal,J.A., Sugiman-Marangos,S., VanderVere-Carozza,P., Wagner,M., Turchi,J., Lees-Miller,S.P., Junop,M.S. and Meek,K. (2014) Unraveling the complexities of DNA-dependent protein kinase autophosphorylation. *Mol. Cell Biol.*, **34**, 2162–2175.
7. Dobbs,T.A., Tainer,J.A. and Lees-Miller,S.P. (2010) A structural model for regulation of NHEJ by DNA-PKcs autophosphorylation. *DNA Repair (Amst.)*, **9**, 1307–1314.
8. Hornbeck,P.V., Kornhauser,J.M., Tkachev,S., Zhang,B., Skrzypek,E., Murray,B., Latham,V. and Sullivan,M. (2012) PhosphoSitePlus: a comprehensive resource for investigating the structure and function of experimentally determined post-translational modifications in man and mouse. *Nucleic Acids Res.*, **40**, D261–D270.
9. Zhou,Y., Lee,J.H., Jiang,W., Crowe,J.L., Zha,S. and Paull,T.T. (2017) Regulation of the DNA damage response by DNA-PKcs inhibitory phosphorylation of ATM. *Mol. Cell*, **65**, 91–104.
10. Neal,J.A., Dang,V., Douglas,P., Wold,M.S., Lees-Miller,S.P. and Meek,K. (2011) Inhibition of homologous recombination by DNA-dependent protein kinase requires kinase activity, is titratable, and is modulated by autophosphorylation. *Mol. Cell Biol.*, **31**, 1719–1733.
11. Iliakis,G., Wang,H., Perrault,A.R., Boecker,W., Rosidi,B., Windhofer,F., Wu,W., Guan,J., Terzoudi,G. and Pantelias,G. (2004) Mechanisms of DNA double strand break repair and chromosome
12. Sfeir,A. and Symington,L.S. (2015) Microhomology-mediated end joining: a back-up survival mechanism or dedicated pathway? *Trends Biochem. Sci.*, **40**, 701–714.
13. Shrivastav,M., De Haro,L.P. and Nickoloff,J.A. (2008) Regulation of DNA double-strand break repair pathway choice. *Cell Res.*, **18**, 134–147.
14. Wang,H., Yang,H., Shivalila,C.S., Dawlaty,M.M., Cheng,A.W., Zhang,F. and Jaenisch,R. (2013) One-step generation of mice carrying mutations in multiple genes by CRISPR/Cas-mediated genome engineering. *Cell*, **153**, 910–918.
15. Yang,L., Guell,M., Niu,D., George,H., Lesha,E., Grishin,D., Aach,J., Shrock,E., Xu,W., Poci,J. *et al.* (2015) Genome-wide inactivation of porcine endogenous retroviruses (PERVs). *Science*, **350**, 1101–1104.
16. Chu,V.T., Weber,T., Wefers,B., Wurst,W., Sander,S., Rajewsky,K. and Kuhn,R. (2015) Increasing the efficiency of homology-directed repair for CRISPR-Cas9-induced precise gene editing in mammalian cells. *Nat. Biotechnol.*, **33**, 543–548.
17. Riesenberg,S. and Maricic,T. (2018) Targeting repair pathways with small molecules increases precise genome editing in pluripotent stem cells. *Nat. Commun.*, **9**, 2164.
18. Lin,S., Staahl,B.T., Alla,R.K. and Doudna,J.A. (2014) Enhanced homology-directed human genome engineering by controlled timing of CRISPR/Cas9 delivery. *Elife*, **3**, e04766.
19. Richardson,C.D., Ray,G.J., DeWitt,M.A., Curie,G.L. and Corn,J.E. (2016) Enhancing homology-directed genome editing by catalytically active and inactive CRISPR-Cas9 using asymmetric donor DNA. *Nat. Biotechnol.*, **34**, 339–344.
20. Canny,M.D., Moatti,N., Wan,L.C.K., Fradet-Turcotte,A., Krasner,D., Mateos-Gomez,P.A., Zimmermann,M., Orthwein,A., Juang,Y.C., Zhang,W. *et al.* (2018) Inhibition of 53BP1 favors homology-dependent DNA repair and increases CRISPR-Cas9 genome-editing efficiency. *Nat. Biotechnol.*, **36**, 95–102.
21. Shy,B.R., MacDougall,M.S., Clarke,R. and Merrill,B.J. (2016) Co-incident insertion enables high efficiency genome engineering in mouse embryonic stem cells. *Nucleic Acids Res.*, **44**, 7997–8010.
22. Agudelo,D., Duringer,A., Bozoyan,L., Huard,C.C., Carter,S., Loehr,J., Synodinou,D., Drouin,M., Salsman,J., Dellaire,G. *et al.* (2017) Marker-free coselection for CRISPR-driven genome editing in human cells. *Nat. Methods*, **14**, 615–620.
23. Shrivastav,M., Miller,C.A., De Haro,L.P., Durant,S.T., Chen,B.P., Chen,D.J. and Nickoloff,J.A. (2009) DNA-PKcs and ATM co-regulate DNA double-strand break repair. *DNA Repair (Amst.)*, **8**, 920–929.
24. Neal,J.A., Xu,Y., Abe,M., Hendrickson,E. and Meek,K. (2016) Restoration of ATM expression in DNA-PKcs-deficient cells inhibits signal end joining. *J. Immunol.*, **196**, 3032–3042.
25. Robert,F., Barbeau,M., Ethier,S., Dostie,J. and Pelletier,J. (2015) Pharmacological inhibition of DNA-PK stimulates Cas9-mediated genome editing. *Genome Med.*, **7**, 93.
26. Pierce,A.J., Hu,P., Han,M.G., Ellis,N. and Jasin,M. (2001) Ku DNA end-binding protein modulates homologous repair of double-strand breaks in mammalian cells. *Gene Dev.*, **15**, 3237–3242.
27. Gonzalez,F., Zhu,Z., Shi,Z.D., Lelli,K., Verma,N., Li,Q.V. and Huangfu,D. (2014) An iCRISPR platform for rapid, multiplexable, and inducible genome editing in human pluripotent stem cells. *Cell Stem Cell*, **15**, 215–226.
28. Kircher,M., Sawyer,S. and Meyer,M. (2012) Double indexing overcomes inaccuracies in multiplex sequencing on the Illumina platform. *Nucleic Acids Res.*, **40**, e3.
29. Meyer,M. and Kircher,M. (2010) Illumina sequencing library preparation for highly multiplexed target capture and sequencing. *Cold Spring Harb. Protoc.*, **2010**, pdb prot5448.
30. Renaud,G., Stenzel,U. and Kelso,J. (2014) leeHom: adaptor trimming and merging for Illumina sequencing reads. *Nucleic Acids Res.*, **42**, e141.
31. Li,H., Handsaker,B., Wysoker,A., Fennell,T., Ruan,J., Homer,N., Marth,G., Abecasis,G., Durbin,R. and Genome Project Data Processing, S. (2009) The sequence Alignment/Map format and SAMtools. *Bioinformatics*, **25**, 2078–2079.
32. Pinello,L., Canver,M.C., Hoban,M.D., Orkin,S.H., Kohn,D.B., Bauer,D.E. and Yuan,G.C. (2016) Analyzing CRISPR genome-editing experiments with CRISPResso. *Nat. Biotechnol.*, **34**, 695–697.

33. Li,H. and Durbin,R. (2009) Fast and accurate short read alignment with Burrows-Wheeler transform. *Bioinformatics*, **25**, 1754–1760.
34. McKenna,A., Hanna,M., Banks,E., Sivachenko,A., Cibulskis,K., Kernytsky,A., Garimella,K., Altshuler,D., Gabriel,S., Daly,M. *et al.* (2010) The Genome Analysis Toolkit: a MapReduce framework for analyzing next-generation DNA sequencing data. *Genome Res.*, **20**, 1297–1303.
35. Pedersen,B.S. and Quilan,A.R. (2018) Mosdepth: quick coverage calculation for genomes and exomes. *Bioinformatics*, **34**, 867–868.
36. Prufer,K., Racimo,F., Patterson,N., Jay,F., Sankararaman,S., Sawyer,S., Heinze,A., Renaud,G., Sudmant,P.H., de Filippo,C. *et al.* (2014) The complete genome sequence of a Neanderthal from the Altai mountains. *Nature*, **505**, 43–49.
37. Robinson,J.T., Thorvaldsdottir,H., Winckler,W., Guttman,M., Lander,E.S., Getz,G. and Mesirov,J.P. (2011) Integrative genomics viewer. *Nat. Biotechnol.*, **29**, 24–26.
38. O'Brien,J., Wilson,I., Orton,T. and Pognan,F. (2000) Investigation of the Alamar Blue (resazurin) fluorescent dye for the assessment of mammalian cell cytotoxicity. *Eur. J. Biochem.*, **267**, 5421–5426.
39. International Standing Committee on Human Cytogenomic Nomenclature, McGowan-Jordan,J., Simons,A. and Schmid,M. (2016) *ISCN: An International System For Human Cytogenomic Nomenclature (2016)*. Karger, Basel.
40. Shen,B., Zhang,W., Zhang,J., Zhou,J., Wang,J., Chen,L., Wang,L., Hodgkins,A., Iyer,V., Huang,X. *et al.* (2014) Efficient genome modification by CRISPR-Cas9 nickase with minimal off-target effects. *Nat. Methods*, **11**, 399–402.
41. Costantino,L., Sotiriou,S.K., Rantala,J.K., Magin,S., Mladenov,E., Helleday,T., Haber,J.E., Iliakis,G., Kallioniemi,O.P. and Halazonetis,T.D. (2014) Break-induced replication repair of damaged forks induces genomic duplications in human cells. *Science*, **343**, 88–91.
42. Harnor,S.J., Brennan,A. and Cano,C. (2017) Targeting DNA-Dependent protein kinase for cancer therapy. *ChemMedChem*, **12**, 895–900.
43. Adikusuma,F., Piltz,S., Corbett,M.A., Turvey,M., McColl,S.R., Helbig,K.J., Beard,M.R., Hughes,J., Pomerantz,R.T. and Thomas,P.Q. (2018) Large deletions induced by Cas9 cleavage. *Nature*, **560**, E8–E9.
44. Rebuzzini,P., Zuccotti,M., Redi,C.A. and Garagna,S. (2015) Chromosomal abnormalities in embryonic and somatic stem cells. *Cytogenet. Genome Res.*, **147**, 1–9.
45. Kent,W.J., Sugnet,C.W., Furey,T.S., Roskin,K.M., Pringle,T.H., Zahler,A.M. and Haussler,D. (2002) The human genome browser at UCSC. *Genome Res.*, **12**, 996–1006.

Supplementary Data

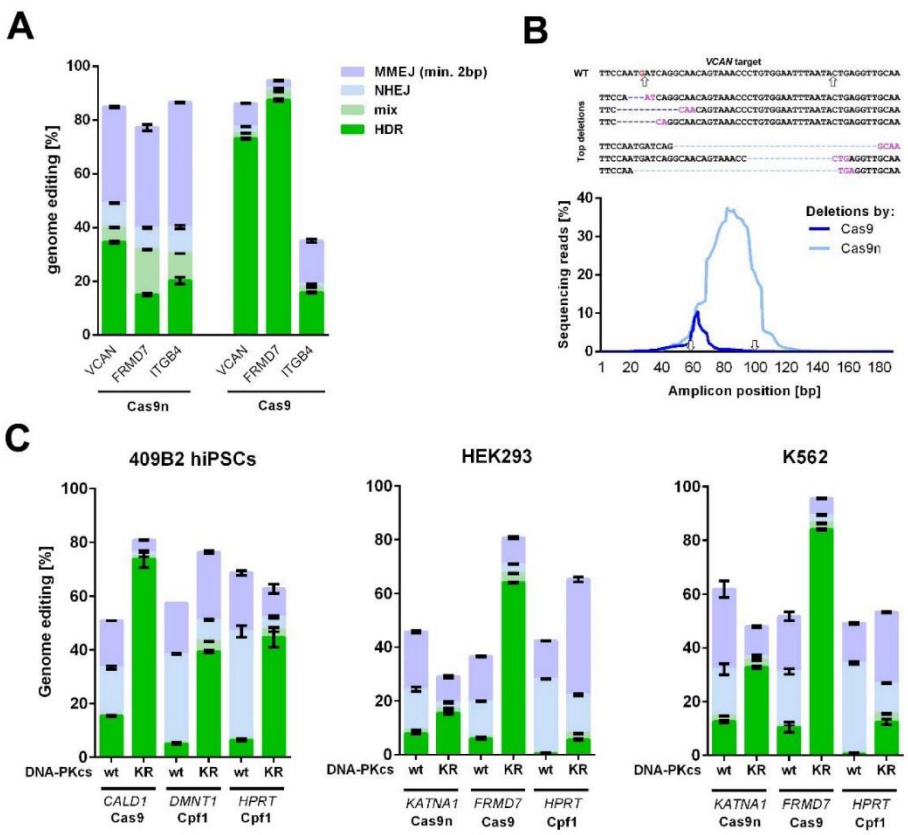

Supplementary Fig. 1. Frequency of genome editing in different DNA-PKcs K3753R cell lines using different CRISPR enzymes. (**A**) Genome editing of three genes with Cas9n (iCRISPR) and with Cas9 protein in 409B2 hiPSCs. (**B**) Patterns of deletions after editing with Cas9n and Cas9 in the gene *VCAN* as an example. Both nicking sites are indicated by arrows, the left one was used also for Cas9. The three most abundant deletions are shown for Cas9 (dark blue) and the bottom three for Cas9n (light blue). Microhomologies are indicated in pink. (**C**) The genome editing frequencies in cells expressing the DNA-PKcs wildtype (WT) or DNA-PKcs KR mutant for different recombinant CRISPR enzymes in 409B2 hiPSCs, HEK293 cells, and K562 cells. HDR, HDR with indels, NHEJ, and MMEJ are indicated in green, light green, light blue, and light purple, respectively. Error bars show the SEM of two replicates for A and four replicates for C.

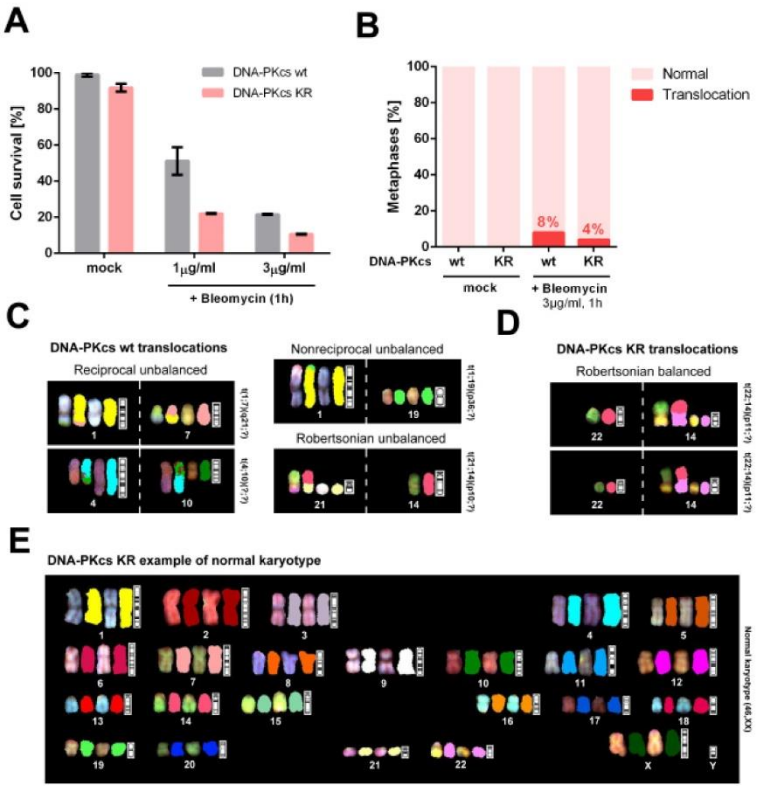

Supplementary Fig. 2. Impact of bleomycin treatment on DNA-PKcs wildtype (WT) and DNA-PKcs KR cells. (**A**) Cell survival as measured by the resazurin assay after bleomycin treatment. Error bars show the SEM of two replicates. **(B)** Spectral karyotyping (SKY) of cells after treatment with 3µg/ml bleomycin. (**C**) The translocations observed for DNA-PKcs WT cells; and **(D)** DNA-PKcs KR cells. (**E**) An example of the majority of normal metaphases observed.

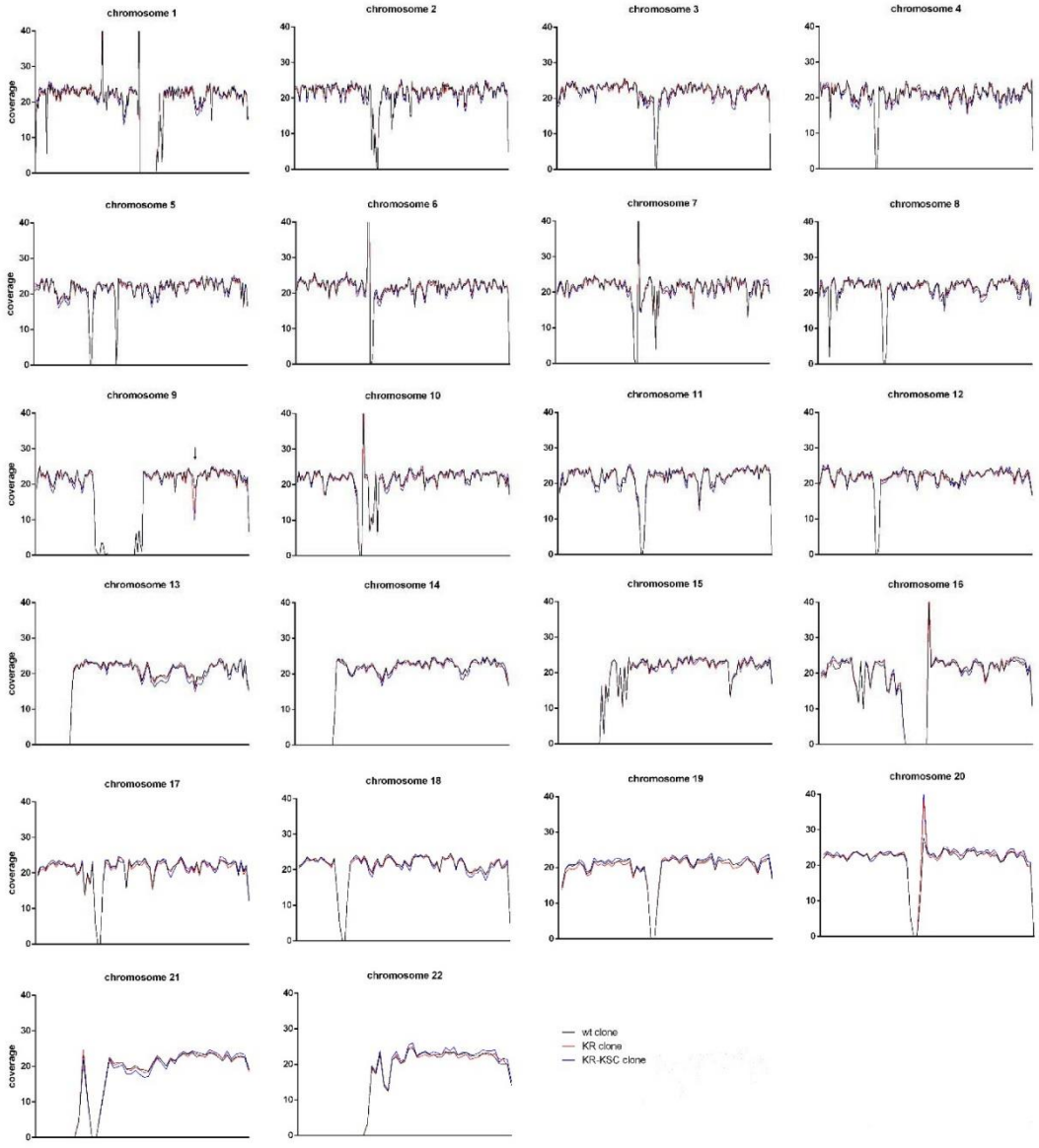

Supplementary Fig. 3. Base coverage along the chromosomes for the WT, KR, and KR-KSC hiPSC lines. Coverage was calculated for 1Mb windows, using unique genomic regions. WT, KR, and KR-KSC are indicated as a grey, red, and blue lines, respectively. A 1Mb region on chromosome 9 (arrow) carries a heterozygous deletion in the KR and KR-KSC lines.

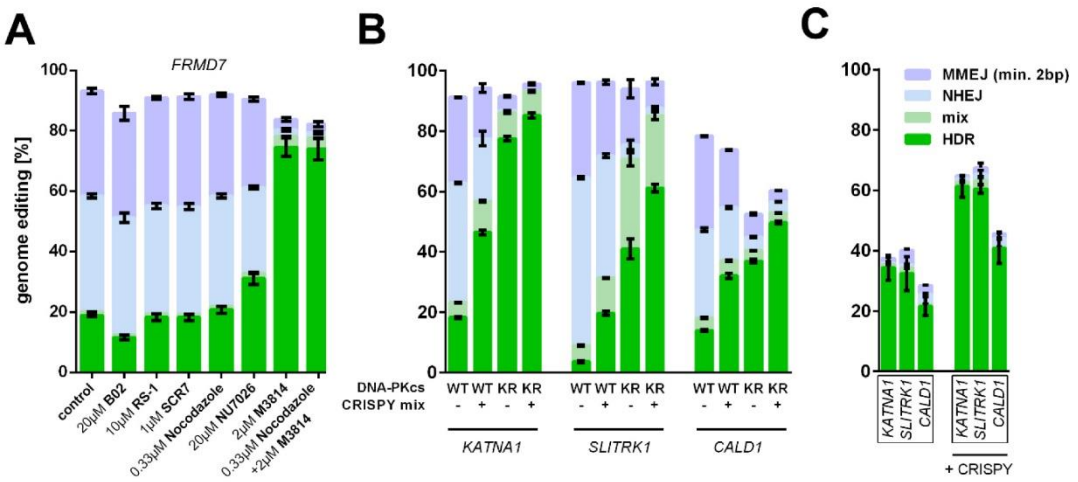

Supplementary Fig. 4. Effect of small molecules and the CRISPY mix (17) **on genome editing efficiency in 409B2 hiPSCs. (A)** Effect of RAD51 inhibitor B02, RAD51 enhancer RS-1, disputed DNA ligase IV inhibitor SCR7, cell cycle inhibitor Nocodazole (removed after 16h to achieve cell cycle synchronization), and DNA-PK inhibitors NU7026 and M3814, on genome editing of *FRMD7* with Cas9 RNP. **(B)** Genome editing of *KATNA1, SLITRK1,* and *CALD1* in DNA-PKcs WT and KR cells with or without CRISPY small molecule mix using doxycycline inducible Cas9n (iCRISPR). **(C)** Simultaneous editing of the three genes (framed) with and without the CRISPY mix. Histogram designations as in Suppl. Fig. 1. Error bars show the SEM of four replicates for A, three replicates for B and two replicates for C.

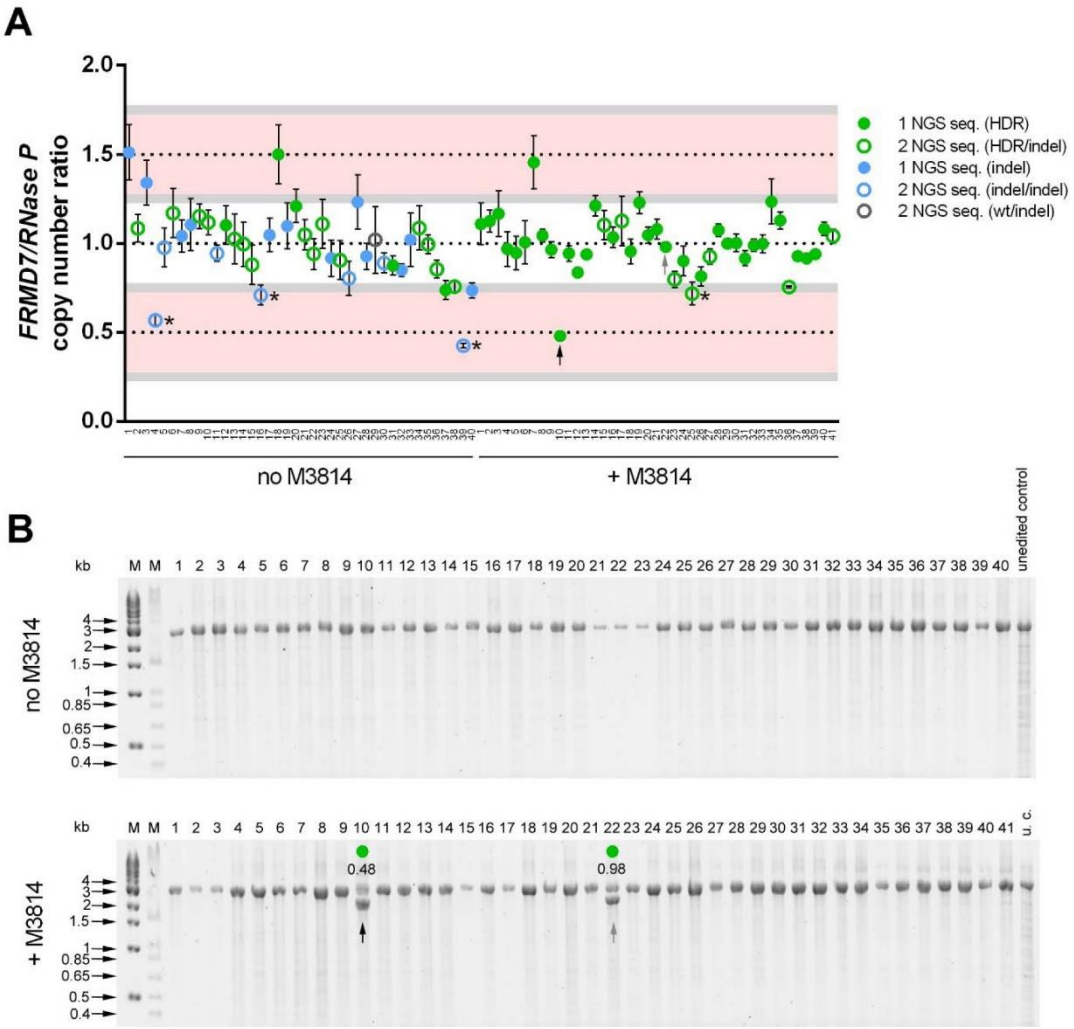

Supplementary Fig. 5 *FRMD7* gene copy number analysis in 409B2-hiPSCs edited with or without M3814. **(A)** Copy number ratio between *FRMD7* and the control gene *RNAse P* based on a TaqMan quantitative PCR assay. Each circle represents a cellular clone. Closed circles represent clones where amplicon sequencing yields a single DNA sequence (HDR: green; indels: blue), open circles indicate two DNA sequences of similar read number (HDR/indel mix: green; indel/indel: blue; wildtype/indel: grey). Asterisks indicate clones where a heterozygous deletion identified by DNA sequencing is expected to interfere with binding of the TaqMan probe (min. 5nt mismatch), resulting in copy number ratios below the expectation of the diploid state. Error bars show the SEM of at least four technical replicates. **(B)** Long range PCR of the *FRMD7* target locus for each clone. Arrows indicate two clones carrying heterozygous big deletions and the respective TaqMan assay copy number ratio is stated. The +M3814 clone 22 has a deletion and a copy number ratio of 0.98, suggesting a gain of one copy of the target locus in this clone as well.

Supplementary Table 1. Oligonucleotides used in this study. gRNA (gRNA 20mer target) and single stranded DNA donors (ssODNs) for editing, as well as primers for analysis are shown. Mutations are in bold letters and ancestral mutations are underlined. The gRNAs with an asterisk were used for Cas9 cleavage.

gRNAs	*KATNA1* t1	AAATGATGACCCTTCCAAAA
	KATNA1 t2	CAACACCTAAAATAAGGGTA
	SLC8A1 t1	GAGTCTCTTATTTTCCCATG
	SLC8A1 t2	CAGATGAAATCCCATTGAAA
	TTLL5 t1	CGTGGCAGGCCAGTAGGGCT
	TTLL5 t2	CGATCAGGAAGTCACACCAT
	SV2C t1	GCAGAGGTTTAATGACATCA
	SV2C t2	TGCATTGCTAACCAGAAATG
	GPR132 t1	CCATGAAGACAGACGTCACC
	GPR132 t2	TTTCCACCCCTTATGGATTC
	PRDM10 t1	TCATCACCACCACCACCAAC
	PRDM10 t2	TCTGCTGTTGGCTGTTGGTC
	RB1CC1 t1	TGAGAAAGACAGACAAAAAT
	RB1CC1 t2	CTTCGTATTTCTCTTCTTGT
	SLITRK1 t1	GCTAACAGTTTACCCTGCCC
	SLITRK1 t2	ACCCGTCGCTATCGCTGCTG
	SSH2 t1	CAGATCCTCAGGAGGGCCCA
	SSH2 t2	GTGGTCAAACTCCAGCACCT
	CSGALNACT1 t1	CTCATCTTATTTCGACCATT
	CSGALNACT1 t2	GCCGTTTGAATTCGTGTTTG
	CALD1 t1*	TGGAGACTATTGCTGCTTGA
	CALD1 t2	GCAGTATACCAGTGCAATTG
	VCAN t1*	GTTTACTGTTGCCTGATCAT
	VCAN t2	CCCTGTGGAATTTAATACTG
	ITGB4 t1	GGGTCCTGGGGTGGGCAGAT
	ITGB4 t2*	CCGCAGCTGGGCAGCCGTGC
	FRMD7 t1	AGCCAGCTGAAAGAAGCCCA
	FRMD7 t2*	GTGGGCTCTACATAGCTATG
	PRKDC t1	GGTCCTCGCCACCCTTCACC
	PRKDC t2	GCGCGTGGAGCAGCTCTTCC
	PRKDC t1back	GGTCCTCGCCACCTCTCACC
	DNMT1 t1 (Cpf1)	CTGATGGTCCATGTCTGTTAC
	HPRT t1 (Cpf1)	GGTTAAAGATGGTTAAATGAT
ssODNs	*KATNA1* Cas9n	CTCATCTATATCCCAGGGAAAATTAGTAGCTGCCAGAACCATAACCATTTT**A**GAAGGGTCA TCATTTTCAGAAG**C**ACCTCCAACACCTAAAATAA**C**GGTAAGGGGAGAGTGAAAAAGATATT AAGTTGGATTATACCAAATGAAGCT
	SLC8A1 Cas9n	TTCATTTCCTTCTCCTTCCATTTCTGTCTCAGCAATTACATGGTCCACATG**A**GAAAATAAGA GACTCACA**A**TAACTAACAGATGAAATCCCAT**A**GAAAAGGTGGGTGAAAGACTTAATCGCC GCATGTTGTACATGACACTTCCA
	TTLL5 Cas9n	CTGCCAGTGCTTCTCCCTGCCTACATCCCGGGGCACAGAACATCCCAAGCCCT**G**CTGGC CTGCCACGCTGTCGATCAGGAAGTCACACCATTGGTCCCTTTTCTTC
	SV2C Cas9n	ACATTTCTTTGTCTTTGCAGGTACTATGGATTATCCGTTTGGTTCCCTGA**C**GTCATTAAAC**A** TCTGCAGTCCGATGAATATGCATTGCTAACCAGAAATGTGGAGAGAGATAAAT
	GPR132 Cas9n	GCCACGGGCGACTGCAGCTCCTCGGTGTCCCTGCTGTGGGTGAGCCTGGT**A**ACGTCTGT CTTCATGGACCACT**G**TTTCCACCCCTTATG**A**ATTCTGGACACTTCTTGGCGGGAATGGTC CGTGGCCAGCACGTAGATAATG
	PRDM10 Cas9n	GGAGTCCAGGTCGAGCCACCTGCACACAGTGACTCCCTGGACCCCCAGACC**C**ACAGCCA ACAGCAGACCACACAGTACATCATCACCACCACCACCAACGGGAACGGAAGCAGC
	RB1CC1 Cas9n	AAGCTTCTGAATTAACTGTTCTCTGTCTTGCTCCTGGCTGCTGACCAATTT**G**TGT**T**TGTCTT TCTCAAGGTTCTGGATAATAGCTTCGTATTTCTCTTCTTGTTGGGTAATTTTTTCATCTTTTT GTCTTTCAAGAGCACTCAATTCTGA

	SLITRK1 Cas9n	TCATCTTTAAACCCGACCCTGGGATGTGGTCGCAGCTGCAGCCCCCAGGGCA**T**GGTAAA CTGTTAGCTAAGGGTTTGTTCCTGG**C**GCTACCCGTCGCTATCGC**A**GCTGTGGGTCTGATT TTGATCTGCCAGTTGCCTGGGATCTTTGTACCTCCG
	SSH2 Cas9n	ATCTGACCCTGGGCCCTCCTGAGGATCTGGCAAGTGGTCAAACTCCAGCACC**T**TGGGAG CTGGAACAGTGGCATTCTGCTCAGAATGGGACAGTGAGCCAGCCTCA
	CSGALNACT1 Cas9n	GTTGGCCATGTTGAGCTTTTCATTTTTCACTTTCATGATGGGGCCGAATGG**A**CGAAATAAG A**C**GAGCCGTTTGAATTCGTGTTTGTGGTCCCCTTTGAAGGTGAGCTCATACA
	CALD1 Cas9n	TTATATGTATGTGTTTACTTTTTTAGCAGTGGTGTCAAATCGACCCATCAAGC**T**GCA**G**TAGT CTCCAAGATTGACAGCAGACTGGAGCAGTATACCAGTGC**T**ATTGAGGTGAGAATTGTCCT CAGCGTTATGGTCCTGCTGAACAGAAATAGA
	CALD1 Cas9	GTATACTGCTCCAGTCTGCTGTCAATCTTGGAGACTA**C**TGCTGCTTGATGGGTCGATTTGA CACCACTGCTAAAAAAGTAAACACATACA
	VCAN Cas9n	GATAGCAGCATCAGAACAGCAAGTGGCAGCGAGAATTCTTGATTCCAAT**A**ATCAGGCAAC AGTAAACCCTGTGGAATTTAATACTGAGGTTGCAACACCAC
	VCAN Cas9	CCTGAAACTCAAGCAGCTTTAATCAGAGGGCAGGATTCCACGATAGCAGCATCAGAACAG CAAGTGGCAGCGAGAATTCTTGATTCCAAT**A**ATCAGGCAACAGTAAACCCTGTGGAATTTA ATACTG
	ITGB4 Cas9n	TGGTGATGCTGCTGTACTCGCTTTGCAGCGGGTGCTGGAAGAGCCCGGCA**T**GGCTGCCC AGCTGCGGGAAGGGTCCTGGGGTGGGCAGATAGGCCAGTCAGAGGG
	ITGB4 Cas9	CTCACCCACTAGGAAGGGCTCGGTGGCGCTGGTGTGGGTGGTGGTGATGCTGCTGTACT CGCTTTGCAGCGGGTGCTGGAAGAGCCCGGCA**T**GGCTGCCCAGCTGCGGGAAGGGTCC TGGGGTGGGC
	FRMD7 Cas9n	AGGTGCCCAGATGGTCCCCAATTAGAGCAGAGGAAAGGACAAGTCCA**G**ATAGCTATGTA GAGCCCACTGCAATGAAGCCAGCTGAAAGAAGCCCAAGGAATATCAGAATG
	FRMD7 Cas9	TATGCCTCCCCAGGTCTTTTTTTATGTGGACAAGCCACCCCAGGTGCCCAGATGGTCCCC AATTAGAGCAGAGGAAAGGACAAGTCCA**G**ATAGCTATGTAGAGCCCACTGCAATGAAGCC AGCTGAA
	PRKDC Cas9n	GCGAAGGCCCAAGCGCATCATCATCCGTGGCCATGACGAGAGGGAACACCCTTTCCTGG TGA**GA**GGTGGCGAGGACCTGCGGCAGGACCAGCGCGTGGAGCAGCTCTTCCAGGTCAT GAATGGGATCCTGGCCCAAG
	PRKDC back mutation Cas9n	GCGAAGGCCCAAGCGCATCATCATCCGTGGCCATGACGAGAGGGAACACCCTTTCCTGG TGA**AG**GGTGGCGAGGACCTGCGGCAGGACCAGCGCGTGGAGCAGCTCTTCCAGGTCAT GAATGGGATCCTGGCCCAAG
	DNMT1 Cpf1	TTAACATCAGTACGTTAATGTTTCCTGAT**C**GTCCATGTCTGTTA**G**TCGCCTGTCAAGTGGC GTGACACCGGGCGTGTTCCCCAGAGTGAC
	HPRT Cpf1	GCCATTTCACATAAAACTCTTTTAGGTTA**T**AGATGGTTAAATGA**A**TGACAAAAAAAGTAATT CACTTACAGTCTGGCTTATATCCAACAC
Primers	*KATNA1* forward	CCTGACGGCAAAGGAATATAG
	KATNA1 reverse	ACTGTGCTTCCTTGTATTGTTGT
	SLC8A1 forward	AAGAAGGGTCTTGGGGTTCC
	SLC8A1 reverse	TGCCCTCTCCCCCATCTTAT
	TTLL5 forward	CCTTGCCACCATTCTTCTTT
	TTLL5 reverse	CTTTGCTGAAGAGGGACGAG
	SV2C forward	GGGAGTTGCTCATTGCCTCT
	SV2C reverse	ACCTGCCATTGTCGTATTCCA
	GPR132 forward	GCCTGGAGAAGGTGTAGTGG
	GPR132 reverse	CAGCCTCTGTGGTGTTTCTG
	PRDM10 forward	ACAGACATGAGGTGGGTGCT
	PRDM10 reverse	TCAGAATTGGAAGAAAAGCAAA
	RB1CC1 forward	GGGCAGTCTGAATAGCTTCATC
	RB1CC1 reverse	TTTGCATAACCAAGCATTTGA
	SLITRK1 forward	GGGCTTCAAATCAGCCAAG
	SLITRK1 reverse	TTTCAAGACAAATGGGCAAG
	SSH2 forward	TCAGGACTCCTTCCTGCTGT
	SSH2 reverse	GCACCAAAAGGGAAAAGTGA
	CSGALNACT1 forward	GATGCTGTCAGTGGTCAGGA
	CSGALNACT1 reverse	TCTTACCGTGCAAAGAAGGAG
	CALD1 forward	GCTAATCAGCTAGCATATGTATGAGAA
	CALD1 reverse	TTGGACTTGATTATTGTCCTAAGTG
	VCAN forward	GGCAGGATTCCACGATAGCA
	VCAN reverse	CGTGCCTTCCACTGACTCTT
	ITGB4 forward	CCATAGAGTCCCAGGATGGA
	ITGB4 reverse	GTGCTCACCCACTAGGAAGG

FRMD7 forward	TGCTCCTACCGCTAGTCCTG
FRMD7 reverse	GGTATTATGCCTCCCCAGGT
PRKDC forward	CTAGCCTGTGCCCTGAGATG
PRKDC reverse	GCACAACGCTATAGGTCCTCA
DNMT1 forward	TGAACGTTCCCTTAGCACTCTG
DNMT1 reverse	CCTTAGCAGCTTCCTCCTCC
HPRT forward	GGTGAAAAGGACCCCACGAA
HPRT reverse	TGGCAAATGTGCCTCTCTACAAAT
Illumina adapter forward 5'	ACACTCTTTCCCTACACGACGCTCTTCCGATCT
Illumina adapter reverse 5'	GTGACTGGAGTTCAGACGTGTGCTCTTCCGATCT
FRMD7 for. (long range)	AGGCCAGAACCAATCACTTC
FRMD7 rev. (long range)	GTTAGCTTCCTGGGGAGGTC
FRMD7 for. TaqMan	GGCTTCTTTCAGCTGGCTTCA
FRMD7 rev TaqMan	CCAATTAGAGCAGAGGAAAGGACAA

Supplementary Table 2. Overview of mutations introduced in *KATNA1*, *SLITRK1, and* CALD1 in 33 single cell-derived colonies (SCCs) after multiplexed editing. Integration of targeted nucleotide substitutions (left blocking mutation, 'ancient' missense mutation, and right blocking mutation) and insertion/deletions (indels) is labelled with 'y', while absence of these mutations is labelled with 'n'. Homozygous (homo) or heterozygous (het) integration of the mutations is stated. Intended substitutions or indels are highlighted with green or gray, respectively. SSC 2 has an additional unintended substitution in *CALD1* and SSC 29 has an additional unintended substitution in *KATNA1*.

	KATNA1								*SLITRK1*								*CALD1*							
	Haplotype A				Haplotype B				Haplotype A				Haplotype B				Haplotype A				Haplotype B			
SSC	Left block	Ancient	Right block	Indel	Left block	Ancient	Right block	Indel	Left block	Ancient	Right block	Indel	Left block	Ancient	Right block	Indel	Left block	Ancient	Right block	Indel	Left block	Ancient	Right block	Indel
1	y (het)	y (homo)	y (homo)	n	n	y (homo)	y (homo)	n	y (het)	n	n	n	n	y (het)	y (het)	n	y (homo)	y (homo)	n	n	y (homo)	y (homo)	n	n
2	y (homo)	y (homo)	y (homo)	n	y (homo)	y (homo)	y (homo)	n	y (homo)	y (homo)	y (homo)	n	y (homo)	y (homo)	y (homo)	n	y (homo)	y (homo)	y (homo)	n	y (homo)	y (homo)	y (homo)	n
3	n	n	n	n	n	n	n	n	n	n	n	n	n	n	n	n	n	n	n	n	n	n	n	n
4	n	n	n	n	n	n	n	n	n	n	n	n	n	n	n	n	n	n	n	n	n	n	n	n
5	n	n	n	n	n	n	n	n	n	n	n	n	n	n	n	n	n	n	n	n	n	n	n	n
6	n	n	n	n	n	n	n	n	n	n	n	n	n	n	n	n	n	n	n	n	n	n	n	n
7	y (homo)	y (homo)	y (homo)	n	y (homo)	y (homo)	y (homo)	n	y (homo)	y (homo)	y (het)	n	y (homo)	y (homo)	n	n	y (homo)	y (homo)	y (homo)	n	y (homo)	y (homo)	y (homo)	n
8	n	n	n	n	n	n	n	n	n	n	n	n	n	n	n	n	n	n	n	n	n	n	n	n
9	n	n	n	n	n	n	n	n	n	n	n	n	n	n	n	n	n	n	n	n	n	n	n	n
10	n	n	n	n	n	n	n	n	n	n	n	n	n	n	n	n	n	n	n	n	n	n	n	n
11	n	n	n	n	n	n	n	n	n	n	n	n	n	n	n	n	n	n	n	n	n	n	n	n
12	n	n	n	n	n	n	n	n	n	n	n	n	n	n	n	n	n	n	n	n	n	n	n	n
13	n	n	n	n	n	n	n	n	n	n	n	n	n	n	n	n	n	n	n	n	n	n	n	n
14	n	n	n	n	n	n	n	n	n	n	n	n	n	n	n	n	n	n	n	n	n	n	n	n
15	y (homo)	y (homo)	y (homo)	n	y (homo)	y (homo)	y (homo)	n	y (het)	y (homo)	y (homo)	y (homo)	n	y (homo)	y (homo)	y (homo)	n	n	y (homo)	n	n	n	y (homo)	n
16	n	n	n	n	n	n	n	n	n	n	n	n	n	n	n	n	n	n	n	n	n	n	n	n
17	n	n	n	n	n	n	n	n	n	n	n	n	n	n	n	n	n	n	n	n	n	n	n	n
18	y (homo)	y (homo)	y (homo)	n	y (homo)	y (homo)	y (homo)	n	y (homo)	y (homo)	y (homo)	n	y (homo)	y (homo)	y (homo)	n	y (het)	y (het)	y (homo)	n	n	n	y (homo)	n
19	y (homo)	y (het)	y (het)	n	y (homo)	n	n	y (het)	y (homo)	y (homo)	y (homo)	n	y (homo)	y (homo)	y (homo)	n	y (het)	y (het)	n	n	n	n	y (het)	n
20	n	n	n	n	n	n	n	n	n	n	n	n	n	n	n	n	n	n	n	n	n	n	n	n
21	y (homo)	y (homo)	y (homo)	n	y (homo)	y (homo)	y (homo)	n	y (het)	y (het)	y (homo)	n	n	n	y (homo)	n	y (homo)	y (homo)	y (het)	n	y (homo)	y (homo)	n	n
22	y (homo)	y (homo)	y (homo)	n	y (homo)	y (homo)	y (homo)	n	y (homo)	n	n	y (het)	y (homo)	y (het)	y (het)	n	y (homo)	y (homo)	y (het)	n	y (homo)	y (homo)	n	n
23	n	y (homo)	y (homo)	n	n	y (homo)	y (homo)	n	y (homo)	y (homo)	y (homo)	n	y (homo)	y (homo)	y (homo)	n	y (homo)	y (homo)	y (het)	n	y (homo)	y (homo)	n	n
24	n	y (homo)	y (homo)	n	n	y (homo)	y (homo)	n	y (homo)	y (homo)	y (homo)	n	y (homo)	y (homo)	y (homo)	n	y (homo)	y (homo)	y (het)	n	y (homo)	y (homo)	n	n
25	y (homo)	y (homo)	y (het)	n	y (homo)	y (homo)	n	n	y (homo)	y (homo)	y (homo)	n	y (homo)	y (homo)	y (homo)	n	y (het)	y (het)	n	n	n	n	y (het)	n
26	y (het)	y (homo)	y (homo)	y (het)	n	y (homo)	y (homo)	n	y (het)	n	n	n	n	y (het)	y (het)	n	y (het)	y (het)	n	n	n	n	y (het)	n
27	y (homo)	y (homo)	y (homo)	n	y (homo)	y (homo)	y (homo)	n	y (homo)	y (homo)	y (homo)	n	y (homo)	y (homo)	y (homo)	n	y (homo)	y (homo)	y (het)	n	y (homo)	y (homo)	n	n
28	n	n	n	n	n	n	n	n	n	n	n	n	n	n	n	n	n	n	n	n	n	n	n	n
29	y (homo)	y (homo)	y (homo)	n	y (homo)	y (homo)	y (homo)	n	y (homo)	y (homo)	y (homo)	n	y (homo)	y (homo)	y (homo)	n	y (het)	y (het)	y (homo)	n	n	n	y (homo)	n
30	n	n	n	n	n	n	n	n	n	n	n	n	n	n	n	n	n	n	n	n	n	n	n	n
31	n	n	n	n	n	n	n	n	n	n	n	n	n	n	n	n	n	n	n	n	n	n	n	n
32	y (homo)	y (homo)	y (homo)	n	y (homo)	y (homo)	y (homo)	n	y (homo)	y (het)	y (het)	n	y (homo)	n	n	n	n	n	y (homo)	n	n	n	y (homo)	n
33	y (het)	y (het)	y (het)	y (homo)	n	n	n	y (homo)	y (homo)	y (het)	y (homo)	n	y (homo)	n	y (homo)	y (het)	y (homo)	y (homo)	n	n	y (homo)	y (homo)	n	n

Supplementary Table 3. Overview of mutations introduced in *RB1CC1, PRDM10* and *TTLL5* in 21 single cell-derived colonies (SCCs) after multiplexed precise genome editing. Integration of targeted nucleotide substitutions ('ancient' missense mutation and left blocking mutation – dependent on the editing design of the respective gene) and insertion/deletions (indels) is labelled with 'y', while absence of these mutations is labelled with 'n'. Homozygous (homo) or heterozygous (het) integration of the mutations is stated. Intended substitutions or indels are highlighted with green or gray, respectively. SSC 15 has an additional unintended substitution in *RB1CC1* and *TTLL5*.

	RB1CC1						***PRMD10***				***TTLL5***			
	Haplotype A			**Haplotype B**			**Haplotype A**		**Haplotype B**		**Haplotype A**		**Haplotype B**	
SSC	Left block	Ancient	Indel	Left block	Ancient	Indel	Ancient	Indel	Ancient	Indel	Ancient	Indel	Ancient	Indel
1	y (het)	y (het)	n	n	n	n	y (homo)	n	y (homo)	n	y (het)	n	n	y (het)
2	y (homo)	y (homo)	n	y (homo)	y (homo)	n	y (homo)	n	y (homo)	n	y (het)	n	n	y (het)
3	y (homo)	y (het)	n	y (homo)	n	n	y (homo)	n	y (homo)	n	y (homo)	n	y (homo)	n
4	y (homo)	y (homo)	n	y (homo)	y (homo)	n	y (homo)	n	y (homo)	n	y (het)	n	n	y (het)
5	n	n	n	n	n	n	n	n	n	n	n	n	n	n
6	y (het)	y (het)	n	n	n	n	y (homo)	n	y (homo)	n	y (homo)	n	y (homo)	n
7	n	n	n	n	n	n	n	n	n	n	y (het)	n	n	n
8	n	n	n	n	n	n	y (het)	n	n	n	y (homo)	n	y (homo)	n
9	y (het)	y (het)	n	n	n	n	y (het)	n	n	n	y (homo)	n	y (homo)	n
10	n	n	n	n	n	n	y (het)	n	n	n	y (homo)	n	y (homo)	n
11	y (homo)	y (homo)	n	y (homo)	y (homo)	n	y (homo)	n	y (homo)	n	y (homo)	n	y (homo)	n
12	y (homo)	y (homo)	n	y (homo)	y (homo)	n	y (homo)	n	y (homo)	n	y (homo)	n	y (homo)	n
13	y (het)	y (het)	n	n	n	n	y (het)	n	n	y (het)	y (het)	n	n	n
14	n	n	n	n	n	n	n	n	n	n	n	n	n	n
15	y (het)	n	n	n	n	n	y (het)	n	n	y (het)	y (het)	n	n	n
16	n	n	n	n	n	n	n	n	n	y (het)	y (het)	n		n
17	y (homo)	y (homo)	n	y (homo)	y (homo)	n	y (homo)	n	y (homo)	n	y (homo)	n	y (homo)	n
18	n	n	n	n	n	n	n	n	n	n	n	n	n	n
19	y (homo)	y (homo)	n	y (homo)	y (homo)	n	y (homo)	n	y (homo)	n	y (homo)	n	y (homo)	n
20	y (homo)	y (homo)	n	y (homo)	y (homo)	n	y (homo)	n	y (homo)	n	y (homo)	n	y (homo)	n
21	n	n	n	n	n	n	n	n	n	n	n	n	n	n

Supplementary Table 4. Overview of mutations introduced in *TTLL5, SV2C,* and *SLC8A1* in 29 single cell-derived colonies (SCCs) after multiplexed precise genome editing. Integration of targeted nucleotide substitutions ('ancient' missense mutation, left blocking mutation, and right blocking mutation – dependent on the editing design of the respective gene) and insertion/deletions (indels) is labelled with 'y', while absence of these mutations is labelled with 'n'. Homozygous (homo) or heterozygous (het) integration of the mutations is stated. Intended substitutions or indels are highlighted with green or gray, respectively. SSC 3 has an additional unintended substitution in *SLC8A1*.

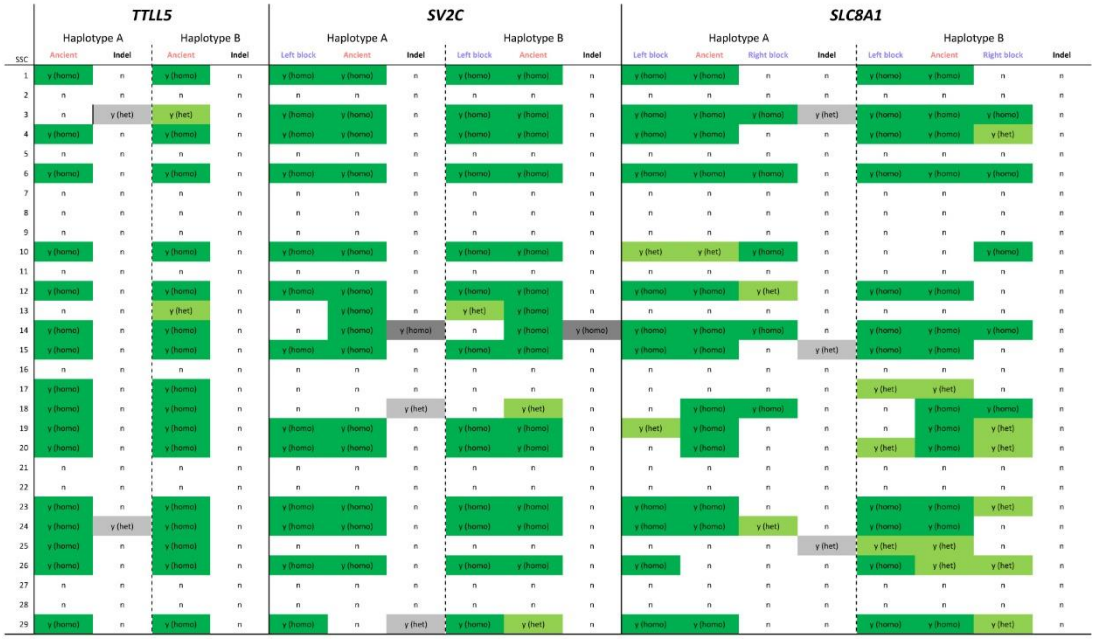

	TTLL5				*SV2C*						*SLC8A1*							
	Haplotype A		Haplotype B		Haplotype A			Haplotype B			Haplotype A				Haplotype B			
SSC	Ancient	Indel	Ancient	Indel	Left block	Ancient	Indel	Left block	Ancient	Indel	Left block	Ancient	Right block	Indel	Left block	Ancient	Right block	Indel
1	y (homo)	n	y (homo)	n	y (homo)	y (homo)	n	y (homo)	y (homo)	n	y (homo)	y (homo)	n	n	y (homo)	y (homo)	n	n
2	n	n	n	n	n	n	n	n	n	n	n	n	n	n	n	n	n	n
3	n	y (het)	y (het)	n	y (homo)	y (homo)	n	y (homo)	y (homo)	n	y (homo)	y (homo)	y (homo)	y (het)	y (homo)	y (homo)	y (homo)	n
4	y (homo)	n	y (homo)	n	y (homo)	y (homo)	n	y (homo)	y (homo)	n	y (homo)	y (homo)	n	n	y (homo)	y (homo)	y (het)	n
5	n	n	n	n	n	n	n	n	n	n	n	n	n	n	n	n	n	n
6	y (homo)	n	y (homo)	n	y (homo)	y (homo)	n	y (homo)	y (homo)	n	y (homo)	y (homo)	y (homo)	n	y (homo)	y (homo)	y (homo)	n
7	n	n	n	n	n	n	n	n	n	n	n	n	n	n	n	n	n	n
8	n	n	n	n	n	n	n	n	n	n	n	n	n	n	n	n	n	n
9	n	n	n	n	n	n	n	n	n	n	n	n	n	n	n	n	n	n
10	y (homo)	n	y (homo)	n	y (homo)	y (homo)	n	y (homo)	y (homo)	n	y (het)	y (het)	y (homo)	n	n	n	y (homo)	n
11	n	n	n	n	n	n	n	n	n	n	n	n	n	n	n	n	n	n
12	y (homo)	n	y (homo)	n	y (homo)	y (homo)	n	y (homo)	y (homo)	n	y (homo)	y (homo)	y (het)	n	y (homo)	y (homo)	n	n
13	n	n	y (het)	n	n	y (homo)	n	y (het)	y (homo)	n	n	n	n	n	n	n	n	n
14	y (homo)	n	y (homo)	n	n	y (homo)	y (homo)	n	y (homo)	y (homo)	y (homo)	y (homo)	y (homo)	n	y (homo)	y (homo)	y (homo)	n
15	y (homo)	n	y (homo)	n	y (homo)	y (homo)	n	y (homo)	y (homo)	n	y (homo)	y (homo)	n	y (het)	y (homo)	y (homo)	n	n
16	n	n	n	n	n	n	n	n	n	n	n	n	n	n	n	n	n	n
17	y (homo)	n	y (homo)	n	n	n	n	n	n	n	n	y (homo)	y (homo)	n	y (het)	y (het)	n	n
18	y (homo)	n	y (homo)	n	n	n	y (het)	n	y (het)	n	n	y (homo)	y (homo)	n	n	y (homo)	y (homo)	n
19	y (homo)	n	y (homo)	n	y (homo)	y (homo)	n	y (homo)	y (homo)	n	y (het)	y (homo)	n	n	n	y (homo)	y (het)	n
20	y (homo)	n	y (homo)	n	y (homo)	y (homo)	n	y (homo)	y (homo)	n	n	y (homo)	n	n	y (het)	y (homo)	y (het)	n
21	n	n	n	n	n	n	n	n	n	n	n	n	n	n	n	n	n	n
22	n	n	n	n	n	n	n	n	n	n	n	n	n	n	n	n	n	n
23	y (homo)	n	y (homo)	n	y (homo)	y (homo)	n	y (homo)	y (homo)	n	y (homo)	y (homo)	n	n	y (homo)	y (homo)	y (het)	n
24	y (homo)	y (het)	y (homo)	n	y (homo)	y (homo)	n	y (homo)	y (homo)	n	y (homo)	y (homo)	y (het)	n	y (homo)	y (homo)	n	n
25	y (homo)	n	y (homo)	n	n	n	n	n	n	n	n	n	n	y (het)	y (het)	y (het)	n	n
26	y (homo)	n	y (homo)	n	y (homo)	y (homo)	n	y (homo)	y (homo)	n	y (homo)	n	n	n	y (homo)	y (het)	y (het)	n
27	n	n	n	n	n	n	n	n	n	n	n	n	n	n	n	n	n	n
28	n	n	n	n	n	n	n	n	n	n	n	n	n	n	n	n	n	n
29	y (homo)	n	y (homo)	n	y (homo)	n	y (het)	y (homo)	y (het)	n	y (homo)	y (homo)	n	n	y (homo)	y (homo)	y (het)	n

Supplementary Table 5. Overview of mutations introduced in *TTLL5, SV2C, SLC8A1,* and *PRDM10* in 33 single cell-derived colonies (SCCs) after multiplexed precise genome editing. Integration of targeted nucleotide substitutions ('ancient' missense mutation, left blocking mutation, and right blocking mutation – dependent on the editing design of the respective gene) and insertion/deletions (indels) is labelled with 'y', while absence of these mutations is labelled with 'n'. Homozygous (homo) or heterozygous (het) integration of the mutations is stated. Intended substitutions or indels are highlighted with green or gray, respectively.

	TTLL5				***SV2C***						***SLC8A1***								***PRMD10***			
	Haplotype A		Haplotype B		Haplotype A			Haplotype B			Haplotype A				Haplotype B				Haplotype A		Haplotype B	
SSC	Ancient	Indel	Ancient	Indel	Left block	Ancient	Indel	Left block	Ancient	Indel	Left block	Ancient	Right block	Indel	Left block	Ancient	Right block	Indel	Ancient	Indel	Ancient	Indel
1	y (homo)	n	y (homo)	n	n	n	n	n	n	n	n	y (homo)	y (homo)	n	n	y (homo)	y (homo)	n	y (het)	n	n	n
2	n	n	n	n	n	n	n	n	n	n	n	n	n	n	n	n	n	n	n	n	n	n
3	n	n	n	n	n	n	n	n	n	n	n	n	n	n	n	n	n	n	n	n	n	n
4	y (homo)	n	y (homo)	n	y (homo)	y (homo)	n	y (homo)	y (homo)	n	n	y (homo)	y (homo)	n	n	y (homo)	y (homo)	n	y (homo)	n	y (homo)	n
5	n	n	n	n	n	n	n	n	n	n	n	n	n	n	n	n	n	n	n	n	n	n
6	n	n	n	n	n	n	n	n	n	n	n	n	n	n	n	n	n	n	n	n	n	n
7	n	n	n	n	n	n	n	n	n	n	n	n	n	n	n	n	n	n	n	n	n	n
8	n	n	n	n	n	n	n	n	n	n	n	n	n	n	n	n	n	n	n	n	n	n
9	n	n	n	n	n	n	n	n	n	n	n	n	n	n	n	n	n	n	n	n	n	n
10	n	n	n	n	n	n	n	n	n	n	n	n	n	n	n	n	n	n	n	n	n	n
11	n	n	n	n	n	n	n	n	n	n	n	n	n	n	n	n	n	n	n	n	n	n
12	n	n	n	n	n	n	n	n	n	n	n	n	n	n	n	n	n	n	n	n	n	n
13	n	n	n	n	n	n	n	n	n	n	n	n	n	n	n	n	n	n	n	n	n	n
14	n	n	n	n	n	n	n	n	n	n	n	n	n	n	n	n	n	n	n	n	n	n
15	n	n	n	n	n	n	n	n	n	n	n	n	n	n	n	n	n	n	n	n	n	n
16	n	n	n	n	n	n	n	n	n	n	n	n	n	n	n	n	n	n	n	n	n	n
17	n	n	n	n	n	n	n	n	n	n	n	n	n	n	n	n	n	n	n	n	n	n
18	n	n	n	n	n	n	n	n	n	n	n	n	n	n	n	n	n	n	n	n	n	n
19	n	n	n	n	n	n	n	n	n	n	n	n	n	n	n	n	n	n	n	n	n	n
20	n	n	n	n	n	n	n	n	n	n	n	n	n	n	n	n	n	n	n	n	n	n
21	n	n	n	n	n	n	n	n	n	n	n	n	n	n	n	n	n	n	n	n	n	n
22	y (homo)	n	y (homo)	n	y (homo)	y (homo)	n	y (homo)	y (homo)	n	y (homo)	y (homo)	n	n	y (homo)	y (homo)	n	n	y (homo)	n	y (homo)	n
23	n	n	n	n	n	n	n	n	n	n	n	n	n	n	n	n	n	n	n	n	n	n
24	n	n	n	n	n	n	n	n	n	n	n	n	n	n	n	n	n	n	n	n	n	n
25	n	y (het)	n	n	n	n	n	y (het)	y (het)	n	n	n	n	n	n	n	n	n	n	n	n	n
26	n	n	n	n	n	n	n	n	n	n	n	n	n	n	n	n	n	n	n	n	n	n
27	y (homo)	n	y (homo)	n	n	n	y (het)	y (het)	y (het)	n	y (homo)	n	n	n	y (homo)	y (het)	y (het)	n	y (homo)	n	y (homo)	n
28	n	n	n	n	n	n	n	n	n	n	n	n	n	n	n	n	n	n	n	n	n	n
29	n	n	n	n	n	n	n	n	n	n	n	n	n	n	n	n	n	n	n	n	n	n
30	n	n	n	n	n	n	n	n	n	n	n	n	n	n	n	n	n	n	n	n	n	n
31	n	n	n	n	n	n	n	n	n	n	n	n	n	n	n	n	n	n	n	n	n	n
32	n	n	n	n	n	n	n	n	n	n	n	n	n	n	n	n	n	n	n	n	n	n
33	n	n	n	n	n	n	n	n	n	n	n	n	n	n	n	n	n	n	n	n	n	n

REFERENCES

Adikusuma, F., Piltz, S., Corbett, M.A., Turvey, M., McColl, S.R., Helbig, K.J., Beard, M.R., Hughes, J., Pomerantz, R.T., and Thomas, P.Q. (2018). Large deletions induced by Cas9 cleavage. *Nature* **560**, E8-E9.

Aggarwal, M., Sommers, J.A., Shoemaker, R.H., and Brosh, R.M., Jr. (2011). Inhibition of helicase activity by a small molecule impairs Werner syndrome helicase (WRN) function in the cellular response to DNA damage or replication stress. *Proc Natl Acad Sci U S A* **108**, 1525-1530.

Agudelo, D., Duringer, A., Bozoyan, L., Huard, C.C., Carter, S., Loehr, J., Synodinou, D., Drouin, M., Salsman, J., Dellaire, G., et al. (2017). Marker-free coselection for CRISPR-driven genome editing in human cells. *Nat Methods* **14**, 615-620.

Bento, A.P., Gaulton, A., Hersey, A., Bellis, L.J., Chambers, J., Davies, M., Kruger, F.A., Light, Y., Mak, L., McGlinchey, S., et al. (2014). The ChEMBL bioactivity database: an update. *Nucleic Acids Res* **42**, D1083-1090.

Blanpain, C., Mohrin, M., Sotiropoulou, P.A., and Passegue, E. (2011). DNA-damage response in tissue-specific and cancer stem cells. *Cell Stem Cell* **8**, 16-29.

Bothmer, A., Phadke, T., Barrera, L.A., Margulies, C.M., Lee, C.S., Buquicchio, F., Moss, S., Abdulkerim, H.S., Selleck, W., Jayaram, H., et al. (2017). Characterization of the interplay between DNA repair and CRISPR/Cas9-induced DNA lesions at an endogenous locus. *Nature Communications* **8**, 13905.

Canny, M.D., Moatti, N., Wan, L.C.K., Fradet-Turcotte, A., Krasner, D., Mateos-Gomez, P.A., Zimmermann, M., Orthwein, A., Juang, Y.C., Zhang, W., et al. (2018). Inhibition of 53BP1 favors homology-dependent DNA repair and increases CRISPR-Cas9 genome-editing efficiency. *Nat Biotechnol* **36**, 95-102.

Chari, R., Mali, P., Moosburner, M., and Church, G.M. (2015). Unraveling CRISPR-Cas9 genome engineering parameters via a library-on-library approach. *Nat Methods* **12**, 823-826.

Chen, B.P., Uematsu, N., Kobayashi, J., Lerenthal, Y., Krempler, A., Yajima, H., Lobrich, M., Shiloh, Y., and Chen, D.J. (2007). Ataxia telangiectasia mutated (ATM) is essential for DNA-PKcs phosphorylations at the Thr-2609 cluster upon DNA double strand break. *J Biol Chem* **282**, 6582-6587.

Chu, V.T., Weber, T., Wefers, B., Wurst, W., Sander, S., Rajewsky, K., and Kuhn, R. (2015). Increasing the efficiency of homology-directed repair for CRISPR-Cas9-induced precise gene editing in mammalian cells. *Nat Biotechnol* **33**, 543-548.

Cong, L., Ran, F.A., Cox, D., Lin, S., Barretto, R., Habib, N., Hsu, P.D., Wu, X., Jiang, W., Marraffini, L.A., et al. (2013). Multiplex genome engineering using CRISPR/Cas systems. *Science* **339**, 819-823.

Costantino, L., Sotiriou, S.K., Rantala, J.K., Magin, S., Mladenov, E., Helleday, T., Haber, J.E., Iliakis, G., Kallioniemi, O.P., and Halazonetis, T.D. (2014). Break-induced replication repair of damaged forks induces genomic duplications in human cells. *Science* **343**, 88-91.

Dobbs, T.A., Tainer, J.A., and Lees-Miller, S.P. (2010). A structural model for regulation of NHEJ by DNA-PKcs autophosphorylation. *DNA Repair (Amst)* **9**, 1307-1314.

Dueva, R., and Iliakis, G. (2013). Alternative pathways of non-homologous end joining (NHEJ) in genomic instability and cancer. *Transl Cancer Res* **2**, 163-177.

Field, A. (2005). Discovering Statistics using SPSS (London: Sage Publications).

Fu, Y., Foden, J.A., Khayter, C., Maeder, M.L., Reyon, D., Joung, J.K., and Sander, J.D. (2013). High-frequency off-target mutagenesis induced by CRISPR-Cas nucleases in human cells. *Nat Biotechnol* **31**, 822-826.

Glanzer, J.G., Carnes, K.A., Soto, P., Liu, S., Parkhurst, L.J., and Oakley, G.G. (2013). A small molecule directly inhibits the p53 transactivation domain from binding to replication protein A. *Nucleic Acids Res* **41**, 2047-2059.

Glanzer, J.G., Liu, S., and Oakley, G.G. (2011). Small molecule inhibitor of the RPA70 N-terminal protein interaction domain discovered using in silico and in vitro methods. *Bioorg Med Chem* **19**, 2589-2595.

Gomez-Cabello, D., Checa-Rodriguez, C., Abad, M., Serrano, M., and Huertas, P. (2017). CtIP-Specific Roles during Cell Reprogramming Have Long-Term Consequences in the Survival and Fitness of Induced Pluripotent Stem Cells. *Stem Cell Reports* **8**, 432-445.

Gonzalez, F., Zhu, Z., Shi, Z.D., Lelli, K., Verma, N., Li, Q.V., and Huangfu, D. (2014). An iCRISPR platform for rapid, multiplexable, and inducible genome editing in human pluripotent stem cells. *Cell Stem Cell* **15**, 215-226.

Greco, G.E., Matsumoto, Y., Brooks, R.C., Lu, Z., Lieber, M.R., and Tomkinson, A.E. (2016). SCR7 is neither a selective nor a potent inhibitor of human DNA ligase IV. *DNA Repair (Amst)* **43**, 18-23.

Grimme, J.M., Honda, M., Wright, R., Okuno, Y., Rothenberg, E., Mazin, A.V., Ha, T., and Spies, M. (2010). Human Rad52 binds and wraps single-stranded DNA and mediates annealing via two hRad52-ssDNA complexes. *Nucleic Acids Res* **38**, 2917-2930.

Harnor, S.J., Brennan, A., and Cano, C. (2017). Targeting DNA-Dependent Protein Kinase for Cancer Therapy. *ChemMedChem* **12**, 895-900.

Hornbeck, P.V., Kornhauser, J.M., Tkachev, S., Zhang, B., Skrzypek, E., Murray, B., Latham, V., and Sullivan, M. (2012). PhosphoSitePlus: a comprehensive resource for investigating the structure and function of experimentally determined post-translational modifications in man and mouse. *Nucleic Acids Res* **40**, D261-270.

Hsu, P.D., Scott, D.A., Weinstein, J.A., Ran, F.A., Konermann, S., Agarwala, V., Li, Y., Fine, E.J., Wu, X., Shalem, O., et al. (2013). DNA targeting specificity of RNA-guided Cas9 nucleases. *Nat Biotechnol* **31**, 827-832.

Huang, F., Motlekar, N.A., Burgwin, C.M., Napper, A.D., Diamond, S.L., and Mazin, A.V. (2011). Identification of specific inhibitors of human RAD51 recombinase using high-throughput screening. *ACS Chem Biol* **6**, 628-635.

Iliakis, G., Wang, H., Perrault, A.R., Boecker, W., Rosidi, B., Windhofer, F., Wu, W., Guan, J., Terzoudi, G., and Pantelias, G. (2004). Mechanisms of DNA double strand break repair and chromosome aberration formation. *Cytogenet Genome Res* **104**, 14-20.

International Standing Committee on Human Cytogenomic Nomenclature, McGowan-Jordan, J., Simons, A., and Schmid, M. (2016). ISCN : an international system for human cytogenomic nomenclature (2016) (Basel ; New York: Karger).

Jiang, W., and Marraffini, L.A. (2015). CRISPR-Cas: New Tools for Genetic Manipulations from Bacterial Immunity Systems. *Annu Rev Microbiol* **69**, 209-228.

Jimeno, S., Fernandez-Avila, M.J., Cruz-Garcia, A., Cepeda-Garcia, C., Gomez-Cabello, D., and Huertas, P. (2015). Neddylation inhibits CtIP-mediated resection and regulates DNA double strand break repair pathway choice. *Nucleic Acids Res* **43**, 987-999.

Kaushik, G., Ponnusamy, M.P., and Batra, S.K. (2018). Concise Review: Current Status of Three-Dimensional Organoids as Preclinical Models. *Stem Cells* **36**, 1329-1340.

Kent, W.J., Sugnet, C.W., Furey, T.S., Roskin, K.M., Pringle, T.H., Zahler, A.M., and Haussler, D. (2002). The human genome browser at UCSC. *Genome Res* **12**, 996-1006.

Khatodia, S., Bhatotia, K., Passricha, N., Khurana, S.M., and Tuteja, N. (2016). The CRISPR/Cas Genome-Editing Tool: Application in Improvement of Crops. *Front Plant Sci* **7**, 506.

Kim, D., Kim, J., Hur, J.K., Been, K.W., Yoon, S.H., and Kim, J.S. (2016). Genome-wide analysis reveals specificities of Cpf1 endonucleases in human cells. *Nat Biotechnol* **34**, 863-868.

Kircher, M., Sawyer, S., and Meyer, M. (2012). Double indexing overcomes inaccuracies in multiplex sequencing on the Illumina platform. *Nucleic Acids Res* **40**, e3.

Kleinstiver, B.P., Tsai, S.Q., Prew, M.S., Nguyen, N.T., Welch, M.M., Lopez, J.M., McCaw, Z.R., Aryee, M.J., and Joung, J.K. (2016). Genome-wide specificities of CRISPR-Cas Cpf1 nucleases in human cells. *Nat Biotechnol* **34**, 869-874.

LaFountaine, J.S., Fathe, K., and Smyth, H.D. (2015). Delivery and therapeutic applications of gene editing technologies ZFNs, TALENs, and CRISPR/Cas9. *Int J Pharm* **494**, 180-194.

Lee, J.H., Guo, Z., Myler, L.R., Zheng, S., and Paull, T.T. (2014). Direct activation of ATM by resveratrol under oxidizing conditions. *PLoS One* **9**, e97969.

Lee, J.S. (2007). Activation of ATM-dependent DNA damage signal pathway by a histone deacetylase inhibitor, trichostatin A. *Cancer Res Treat* **39**, 125-130.

Li, H., and Durbin, R. (2009). Fast and accurate short read alignment with Burrows-Wheeler transform. *Bioinformatics* **25**, 1754-1760.

Li, H., Handsaker, B., Wysoker, A., Fennell, T., Ruan, J., Homer, N., Marth, G., Abecasis, G., Durbin, R., and Genome Project Data Processing, S. (2009). The Sequence Alignment/Map format and SAMtools. *Bioinformatics* **25**, 2078-2079.

Lin, S., Staahl, B.T., Alla, R.K., and Doudna, J.A. (2014). Enhanced homology-directed human genome engineering by controlled timing of CRISPR/Cas9 delivery. *Elife* **3**, e04766.

Makarova, K.S., Wolf, Y.I., and Koonin, E.V. (2018). Classification and Nomenclature of CRISPR-Cas Systems: Where from Here? *CRISPR J* **1**, 325-336.

Mandai, M., Kurimoto, Y., and Takahashi, M. (2017). Autologous Induced Stem-Cell-Derived Retinal Cells for Macular Degeneration. *N Engl J Med* **377**, 792-793.

Maruyama, T., Dougan, S.K., Truttmann, M.C., Bilate, A.M., Ingram, J.R., and Ploegh, H.L. (2015). Increasing the efficiency of precise genome editing with CRISPR-Cas9 by inhibition of nonhomologous end joining. *Nat Biotechnol* **33**, 538-542.

McKenna, A., Hanna, M., Banks, E., Sivachenko, A., Cibulskis, K., Kernytsky, A., Garimella, K., Altshuler, D., Gabriel, S., Daly, M., et al. (2010). The Genome Analysis Toolkit: a MapReduce framework for analyzing next-generation DNA sequencing data. *Genome Res* **20**, 1297-1303.

Meek, K., Lees-Miller, S.P., and Modesti, M. (2012). N-terminal constraint activates the catalytic subunit of the DNA-dependent protein kinase in the absence of DNA or Ku. *Nucleic Acids Res* **40**, 2964-2973.

Meyer, M., and Kircher, M. (2010). Illumina sequencing library preparation for highly multiplexed target capture and sequencing. *Cold Spring Harb Protoc* **2010**, pdb prot5448.

Milanowska, K., Krwawicz, J., Papaj, G., Kosinski, J., Poleszak, K., Lesiak, J., Osinska, E., Rother, K., and Bujnicki, J.M. (2011). REPAIRtoire--a database of DNA repair pathways. *Nucleic Acids Res* **39**, D788-792.

Mora-Bermudez, F., Badsha, F., Kanton, S., Camp, J.G., Vernot, B., Kohler, K., Voigt, B., Okita, K., Maricic, T., He, Z., et al. (2016). Differences and similarities between human and chimpanzee neural progenitors during cerebral cortex development. *Elife* **5**, e18683.

Murry, C.E., and Keller, G. (2008). Differentiation of embryonic stem cells to clinically relevant populations: lessons from embryonic development. *Cell* **132**, 661-680.

Neal, J.A., Dang, V., Douglas, P., Wold, M.S., Lees-Miller, S.P., and Meek, K. (2011). Inhibition of homologous recombination by DNA-dependent protein kinase requires kinase activity, is titratable, and is modulated by autophosphorylation. *Mol Cell Biol* **31**, 1719-1733.

Neal, J.A., Sugiman-Marangos, S., VanderVere-Carozza, P., Wagner, M., Turchi, J., Lees-Miller, S.P., Junop, M.S., and Meek, K. (2014). Unraveling the complexities of DNA-dependent protein kinase autophosphorylation. *Mol Cell Biol* **34**, 2162-2175.

Neal, J.A., Xu, Y., Abe, M., Hendrickson, E., and Meek, K. (2016). Restoration of ATM Expression in DNA-PKcs-Deficient Cells Inhibits Signal End Joining. *J Immunol* **196**, 3032-3042.

Nussenzweig, A., and Nussenzweig, M.C. (2007). A backup DNA repair pathway moves to the forefront. *Cell* **131**, 223-225.

O'Brien, J., Wilson, I., Orton, T., and Pognan, F. (2000). Investigation of the Alamar Blue (resazurin) fluorescent dye for the assessment of mammalian cell cytotoxicity. *Eur J Biochem* **267**, 5421-5426.

Pedersen, B.S., and Quilan, A.R. (2018). Mosdepth: quick coverage calculation for genomes and exomes. *Bioinformatics* **34**, 867-868.

Pierce, A.J., Hu, P., Han, M.G., Ellis, N., and Jasin, M. (2001). Ku DNA end-binding protein modulates homologous repair of double-strand breaks in mammalian cells. *Gene Dev* **15**, 3237-3242.

Pinder, J., Salsman, J., and Dellaire, G. (2015). Nuclear domain 'knock-in' screen for the evaluation and identification of small molecule enhancers of CRISPR-based genome editing. *Nucleic Acids Res* **43**, 9379-9392.

Pinello, L., Canver, M.C., Hoban, M.D., Orkin, S.H., Kohn, D.B., Bauer, D.E., and Yuan, G.C. (2016). Analyzing CRISPR genome-editing experiments with CRISPResso. *Nat Biotechnol* **34**, 695-697.

Prüfer, K., Racimo, F., Patterson, N., Jay, F., Sankararaman, S., Sawyer, S., Heinze, A., Renaud, G., Sudmant, P.H., de Filippo, C., et al. (2014). The complete genome sequence of a Neanderthal from the Altai Mountains. *Nature* **505**, 43-49.

Quinn, G.P.K., M.J. (2002). Experimental Designs and Data Analysis for Biologists (Cambridge: Cambridge University Press).

Ran, F.A., Hsu, P.D., Wright, J., Agarwala, V., Scott, D.A., and Zhang, F. (2013). Genome engineering using the CRISPR-Cas9 system. *Nat Protoc* **8**, 2281-2308.

Rebuzzini, P., Zuccotti, M., Redi, C.A., and Garagna, S. (2015). Chromosomal Abnormalities in Embryonic and Somatic Stem Cells. *Cytogenet Genome Res* **147**, 1-9.

Renaud, G., Stenzel, U., and Kelso, J. (2014). leeHom: adaptor trimming and merging for Illumina sequencing reads. *Nucleic Acids Res* **42**, e141.

Richardson, C.D., Ray, G.J., DeWitt, M.A., Curie, G.L., and Corn, J.E. (2016). Enhancing homology-directed genome editing by catalytically active and inactive CRISPR-Cas9 using asymmetric donor DNA. *Nat Biotechnol* **34**, 339-344.

Riesenberg, S., and Maricic, T. (2018). Targeting repair pathways with small molecules increases precise genome editing in pluripotent stem cells. *Nat Commun* **9**, 2164.

Robert, F., Barbeau, M., Ethier, S., Dostie, J., and Pelletier, J. (2015). Pharmacological inhibition of DNA-PK stimulates Cas9-mediated genome editing. *Genome Med* **7**, 93.

Robinson, J.T., Thorvaldsdottir, H., Winckler, W., Guttman, M., Lander, E.S., Getz, G., and Mesirov, J.P. (2011). Integrative genomics viewer. *Nat Biotechnol* **29**, 24-26.

Robinton, D.A., and Daley, G.Q. (2012). The promise of induced pluripotent stem cells in research and therapy. *Nature* **481**, 295-305.

Rocha, C.R., Lerner, L.K., Okamoto, O.K., Marchetto, M.C., and Menck, C.F. (2013). The role of DNA repair in the pluripotency and differentiation of human stem cells. *Mutat Res* **752**, 25-35.

Sapranauskas, R., Gasiunas, G., Fremaux, C., Barrangou, R., Horvath, P., and Siksnys, V. (2011). The Streptococcus thermophilus CRISPR/Cas system provides immunity in Escherichia coli. *Nucleic Acids Res* **39**, 9275-9282.

Sfeir, A., and Symington, L.S. (2015). Microhomology-Mediated End Joining: A Back-up Survival Mechanism or Dedicated Pathway? *Trends Biochem Sci* **40**, 701-714.

Shen, B., Zhang, W., Zhang, J., Zhou, J., Wang, J., Chen, L., Wang, L., Hodgkins, A., Iyer, V., Huang, X., et al. (2014). Efficient genome modification by CRISPR-Cas9 nickase with minimal off-target effects. *Nat Methods* **11**, 399-402.

Shrivastav, M., De Haro, L.P., and Nickoloff, J.A. (2008). Regulation of DNA double-strand break repair pathway choice. *Cell Res* **18**, 134-147.

Shrivastav, M., Miller, C.A., De Haro, L.P., Durant, S.T., Chen, B.P., Chen, D.J., and Nickoloff, J.A. (2009). DNA-PKcs and ATM co-regulate DNA double-strand break repair. *DNA Repair (Amst)* **8**, 920-929.

Shy, B.R., MacDougall, M.S., Clarke, R., and Merrill, B.J. (2016). Co-incident insertion enables high efficiency genome engineering in mouse embryonic stem cells. *Nucleic Acids Res* **44**, 7997-8010.

Sibanda, B.L., Chirgadze, D.Y., Ascher, D.B., and Blundell, T.L. (2017). DNA-PKcs structure suggests an allosteric mechanism modulating DNA double-strand break repair. *Science* **355**, 520-524.

Singh, P., Schimenti, J.C., and Bolcun-Filas, E. (2015). A mouse geneticist's practical guide to CRISPR applications. *Genetics* **199**, 1-15.

Song, J., Yang, D., Xu, J., Zhu, T., Chen, Y.E., and Zhang, J. (2016). RS-1 enhances CRISPR/Cas9- and TALEN-mediated knock-in efficiency. *Nat Commun* **7**, 10548.

Subach, O.M., Cranfill, P.J., Davidson, M.W., and Verkhusha, V.V. (2011). An enhanced monomeric blue fluorescent protein with the high chemical stability of the chromophore. *PLoS One* **6**, e28674.

Sullivan, K., Cramer-Morales, K., McElroy, D.L., Ostrov, D.A., Haas, K., Childers, W., Hromas, R., and Skorski, T. (2016). Identification of a Small Molecule Inhibitor of RAD52 by Structure-Based Selection. *PLoS One* **11**, e0147230.

Suzuki, K., Tsunekawa, Y., Hernandez-Benitez, R., Wu, J., Zhu, J., Kim, E.J., Hatanaka, F., Yamamoto, M., Araoka, T., Li, Z., et al. (2016). In vivo genome editing via CRISPR/Cas9 mediated homology-independent targeted integration. *Nature* **540**, 144-149.

Takahashi, K., and Yamanaka, S. (2006). Induction of pluripotent stem cells from mouse embryonic and adult fibroblast cultures by defined factors. *Cell* **126**, 663-676.

Wang, H., Yang, H., Shivalila, C.S., Dawlaty, M.M., Cheng, A.W., Zhang, F., and Jaenisch, R. (2013). One-step generation of mice carrying mutations in multiple genes by CRISPR/Cas-mediated genome engineering. *Cell* **153**, 910-918.

Wang, K., Tang, X., Liu, Y., Xie, Z., Zou, X., Li, M., Yuan, H., Ouyang, H., Jiao, H., and Pang, D. (2016). Efficient Generation of Orthologous Point Mutations in Pigs via CRISPR-assisted ssODN-mediated Homology-directed Repair. *Mol Ther Nucleic Acids* **5**, e396.

Weterings, E., Gallegos, A.C., Dominick, L.N., Cooke, L.S., Bartels, T.N., Vagner, J., Matsunaga, T.O., and Mahadevan, D. (2016). A novel small molecule inhibitor of the DNA repair protein Ku70/80. *DNA Repair (Amst)* **43**, 98-106.

Williams, A.B., and Schumacher, B. (2016). p53 in the DNA-Damage-Repair Process. *Cold Spring Harb Perspect Med* **6**, a026070.

Yajima, H., Lee, K.J., and Chen, B.P. (2006). ATR-dependent phosphorylation of DNA-dependent protein kinase catalytic subunit in response to UV-induced replication stress. *Mol Cell Biol* **26**, 7520-7528.

Yang, D., Scavuzzo, M.A., Chmielowiec, J., Sharp, R., Bajic, A., and Borowiak, M. (2016). Enrichment of G2/M cell cycle phase in human pluripotent stem cells enhances HDR-mediated gene repair with customizable endonucleases. *Sci Rep* **6**, 21264.

Yang, L., Guell, M., Niu, D., George, H., Lesha, E., Grishin, D., Aach, J., Shrock, E., Xu, W., Poci, J., et al. (2015). Genome-wide inactivation of porcine endogenous retroviruses (PERVs). *Science* **350**, 1101-1104.

Yu, C., Liu, Y., Ma, T., Liu, K., Xu, S., Zhang, Y., Liu, H., La Russa, M., Xie, M., Ding, S., et al. (2015). Small molecules enhance CRISPR genome editing in pluripotent stem cells. *Cell Stem Cell* **16**, 142-147.

Zar, J.H. (1999). Biostatistical Analysis (New Jersey: Prentice Hall).

Zetsche, B., Gootenberg, J.S., Abudayyeh, O.O., Slaymaker, I.M., Makarova, K.S., Essletzbichler, P., Volz, S.E., Joung, J., van der Oost, J., Regev, A., et al. (2015). Cpf1 is a single RNA-guided endonuclease of a class 2 CRISPR-Cas system. *Cell* **163**, 759-771.

Zhang, J.P., Li, X.L., Li, G.H., Chen, W., Arakaki, C., Botimer, G.D., Baylink, D., Zhang, L., Wen, W., Fu, Y.W., et al. (2017). Efficient precise knockin with a double cut HDR donor after CRISPR/Cas9-mediated double-stranded DNA cleavage. *Genome Biol* **18**, 35.

Zhou, Y., Lee, J.H., Jiang, W., Crowe, J.L., Zha, S., and Paull, T.T. (2017). Regulation of the DNA Damage Response by DNA-PKcs Inhibitory Phosphorylation of ATM. *Mol Cell* **65**, 91-104.

ACKNOWLEDGEMENTS

I am endlessly grateful for the opportunity to do my PhD at the Max Planck Institute for Evolutionary Anthropology in the group of Svante Pääbo. He was a great supervisor, who gave me the chance and confidence to work independently on own ideas while helping me stay focused on the main projects of the lab. I am equally indebted to my mentor Tomislav Maricic. He started the genome editing in the lab and showed me many techniques, but most importantly he always had an open ear to discuss ideas and problems, which he evaluated with great interest and sharp logic. I would like to extent my gratitude to Dominik Macak, Philipp Kanis, and Nelly Helmbrecht, who are the best genome editing colleagues one can think of. Those and the rest of the 'Functional group' Maria Schörnig, Michael Boyle, Wulf Hevers, Elena Taverna, Damian Wollny, Sabina Kanton and Xiang-Chun Ju provided an excellent atmosphere to work in and always gave valuable input during our meetings. I would further like to thank Antje Weihmann and Barbara Schellbach for sequencing many libraries, Janet Kelso and Johann Visagie for help with sequencing pipeline problems, Ines Bünger and Rigo Schultz for the continuous IT-support, and the awesome secretary Viola Mittag. Marie-Theres Gansauge and Tobias Gerber were always kind to offer help on many questions regarding small problems in the lab. All the people at the Department of Evolutionary Genetics made it a pleasure to work and socialize at this place.

I am happy for the support of my family and especially my mother throughout my life and during this thesis. My beloved father is one of the main reasons I am pursuing an academic career in life sciences and he will always be in my heart. I would further like to thank my love Friederike Scharlau, who was a great partner to overcome temporary setbacks and celebrate success of my PhD projects.

DECLARATION OF INDEPENDENCE

I hereby declare that I have written and conceived this thesis without any inadmissible help and without using materials other than those explicitly stated. I have not previously attempted to complete this or any other doctorate degree.

Leipzig, 23.06.20

_____

Stephan Riesenberg

AUTHOR CONTRIBUTION STATEMENT

Title: **Targeting repair pathways with small molecules increases precise genome editing efficiency in pluripotent stem cells**

Journal: Nature Communications

Authors: Stephan Riesenberg and Tomislav Maricic

Contribution Stephan Riesenberg

- Project idea
- Project design
- Generation and analysis of data
- Wrote the manuscript

Contribution Tomislav Maricic

- Project design
- Wrote the manuscript

_____	_____
Stephan Riesenberg	Tomislav Maricic

AUTHOR CONTRIBUTION STATEMENT

Title: **Simultaneous precise editing of multiple genes in human cells**

Journal: Nucleic Acids Research

Authors: Stephan Riesenberg, Manjusha Chintalapati, Dominik Macak, Philipp Kanis, Tomislav Maricic and Svante Pääbo

---

Contribution Stephan Riesenberg

- Project idea
- Project design
- Generation and analysis of data
- Wrote the manuscript

Contribution Manjusha Chintalapati

- Analysis of whole-genome-sequencing data

Contribution Dominik Macak

- Generation of data

Contribution Philipp Kanis

- Generation of data

Contribution Tomislav Maricic

- Project design
- Analysis of whole-genome-sequencing data
- Wrote the manuscript

Contribution Svante Pääbo

- Project design
- Wrote the manuscript

_____	_____
Stephan Riesenberg	Svante Pääbo